

*Investigating the role of the base mismatches within the hairpin ends of
vaccinia virus genome in viral life cycle*

by

Mira Maged Michael Shenouda

A thesis submitted in partial fulfillment of the requirements for the degree of

Doctor of Philosophy

in

Virology

Department of Medical Microbiology and Immunology

University of Alberta

© Mira Maged Michael Shenouda, 2023

Abstract:

The genome of poxviruses consists of a double-stranded DNA that is flanked by two AT-rich hairpin ends encoding mismatched nucleotides. These mismatched structures are composed of incompletely base paired regions forming extra-helical loops. Though the functionality of these mismatches has not yet been firmly established, their presence is conserved among all completely sequenced poxviruses. Thus, the focus of this project has been to study the function(s) of the hairpin ends and the mismatches within them.

These ends of the poxvirus genome have been very difficult to study using conventional recombination-based genome editing methods. Using synthetic genome assembly methods, I have modified these ends to remove some of the mismatches. We showed that simply altering the sequence of the 70bp hairpin ends attenuates the virus. Specifically, our results showed that removing most of these mismatches suppressed the growth of the virus. However, these modifications do not affect viral genome replication nor the resolution reactions that generate monomeric genomes. The most penetrant of these telomeric mutations caused about a 12-fold increase in the proportion of defective viral particles. However, these defective particles still packaged DNA. Finally, our microscopy data suggests that altering the hairpin ends affects virion maturation, causing the accumulation of defective immature virions in infected cells. We also showed that these forms of mutant viruses exhibited decreased virulence in immunocompromised mice. However, these attenuated strains can still be used as vaccines to protect against a lethal challenge in immunocompetent animals.

Preface:

The research project, of which this thesis is a part, received research ethics approval from the University of Alberta Research Ethics Board, Project Name “Vaccinia Virulence”, No AUP00000506. Animal studies were carried out at the University of Alberta, Edmonton Alberta, and conducted in accordance with the Canadian Council on Animal Care Guidelines and Policies with approval from the Cross Cancer Institute’s Animal Care Committee and the Animal Care and Use Committee: Health Sciences for the University of Alberta.

Portions of this thesis have been published as “Mira M. Shenouda, Ryan S. Noyce, Stephen Z. Lee, Jun L. Wang, Yi-Chan Lin, Nicole A. Favis, Megan A. Desaulniers, David H. Evans, The mismatched nucleotides encoded in vaccinia virus flip-and-flop hairpin telomeres serve an essential role in virion maturation. *PLoS Pathog.* 18 (2022), doi:10.1371/JOURNAL.PPAT.1010392.”

Acknowledgements:

First I would like to thank my supervisor, Dr. David Evans, for taking me on as a graduate student with limited knowledge in virology and giving me the chance to grow into the virologist I am today. I thank you for allowing me to grow into a better scientist and for supporting my interest in virology and oncolytic viruses. You have given me the chance to get involved in all projects carried out in the laboratory. I appreciate all the support you have given me to excel as a scientist and as active member of the department.

I would like to also thank my wonderful committee members Dr. James Smiley and Dr. Troy Baldwin, for the endless support, encouragement and thought provoking conversations. I was truly lucky to have such brilliant scientists guide me during my degree. I have always enjoyed my committee meetings, your questions, suggestions, guidance and encouragement. For that and much more, I thank you very much.

I truly appreciate the support of everyone in the Evans' Laboratory. You have all been my collogues, friends, and a second family. I appreciate all your help and I consider myself very lucky to have worked with you all. I would first like to send a special thanks to Dr. Ryan Noyce! You have been a great support during my degree, I cannot thank you enough for the countless times you have been there to offer help, guidance, and advice. Thank you Dr. James Lin for all your support with electron microscopy and with your guidance with those experiments. Thank you Drs. Les Nagata, Sid Biswas, and Chad Irwin, I am happy to have met you all and work alongside you. Thank you to the amazing, kind and wonderful Nicole Favis and Megan Desaulniers for all your technical help and for your wonderful friendship. To my fellow graduate students who have shared with me this whole journey, Dr. Brittany Umer and Quinten Kieser, you both mean so much to me and I cherish our friendship. Finally, I would like to thank Patrick Paszkowski, Greg Vallee, Suzy Wang and Stephen Lee I truly appreciate all your help.

To everyone within the department of MMI, thank you for six wonderful years and for making our department a great supportive place to work in. I would like to thank our departmental staff, Debbie Doudiet, Tabitha Nguyen, Michelle Zadunayski and Melissa Northmore. Especial thanks to Debbie and Tabitha, I believe our department is a great place to work in because you make everything run so smoothly. It all seems to happen so effortlessly, but the work you put in to make our lives as graduate students

easier is tremendous. I cannot thank you both enough for all your advice, help and support from the very first day I came to interview in the department, where you have shown me such kindness and encouragement, till the last day as I defended my thesis, where you have been there supporting me and making sure everything is in order.

To all my fellow graduate students and friends. Thank you for being there to lend a helping hand and for being there to celebrate each other's accomplishments. Special thanks to few friends that I consider myself a better scientist and friend for sharing with you this fantastic journey, Drs. Farah Elawar, Brittany Umer, and Connie Le, and for the very soon to be Drs. Quinten Keiser, Quinn Storozynsky, and Francisca Cristi Munoz. I would like to acknowledge a very special and lovely friend, Dr. Farah Elawar, who though is no longer with us, has made her mark in our department and lives. Her friendship meant so much to me and to everyone who knew her. Her smile and positive energy was contagious, her dedication to science was inspiring and her care for all her friends was uplifting. I am truly lucky to have known you, and to call you my friend, you have inspired me and encouraged me to reach new potentials every day and for that and much more I thank you and love you. Your memory will forever live in my heart.

Last but not least, I would like to thank my very loving and caring family, my parents, Mervat Banoub and Maged Beshara, my brother and my sister-in-law, Beshoy Shenouda and Mirna Sobhy and my loving and supportive husband, David Botros and our beautiful lovely daughter Sophia Allegra Botros. You have been my backbone, support and help during it all. Thank you for supporting and encouraging me, and for believing in me even during times when I didn't believe I could do it. Thank you for being there for me through the thick and thin of it all and for all your unconditional love. I could not have gotten through to this stage without you all. I would also like to thank my grandmother, Allegra Farag, who is no longer with us, for being the source of my inspiration and love for science and knowledge. She taught me the meaning of perseverance and determination through her dedication to science and thrive for knowledge. I love you all!

Above all, thanks and glory be to God who is always leading us triumphantly. I thank my Lord Jesus Christ for giving me the strength to face all the challenges, the blessings to excel in my professional career and the chance to meet brilliant people along this wonderful journey. Thank you all!

Table of Contents

Chapter 1: 1

1. Chapter 1: Introduction..... 2

1.1. Poxviruses 2

1.1.1. Poxvirus taxonomy 2

1.1.2. Orthopoxviruses 3

1.1.2.1. Variola virus 4

1.1.2.1.1. Vaccination history..... 4

1.1.2.2. Vaccinia virus 5

1.1.2.2.1. VACV origins 5

1.1.2.2.2. Modern VACV strains..... 6

1.2. VACV genome structure..... 7

1.2.1. Central genome..... 7

1.2.2. Inverted terminal repeats 8

1.2.3. Tandem repeats 9

1.2.4. Concatemer resolution site and hairpin ends 9

1.3. VACV life cycle.....10

1.3.1. Viral entry10

1.3.2. Factory formation.....12

1.3.3. Genome replication.....12

1.3.3.1. Genetic recombination.....14

1.3.3.2. Poxvirus reactivation14

1.3.4. Genome resolution15

1.3.5. DNA packaging and morphogenesis.....16

1.3.5.1. Crescent formation16

1.3.5.2. Virus morphogenesis16

1.3.5.3. Telomere binding proteins.....17

1.3.5.4. Proteins involved in DNA encapsidation18

1.4. Project rationale18

Chapter 2: 21

2. Chapter 2: Materials and Methods 22

2.1. Cells and viruses22

| | | |
|--|--|-----------|
| 2.2. | Infecting cells with virus and calculating viral titres | 22 |
| 2.3. | Preparation of virus stocks | 23 |
| 2.4. | Virus growth | 24 |
| 2.5. | DNA isolation..... | 24 |
| 2.6. | Hairpin design and endonuclease digestion | 25 |
| 2.7. | Viral DNA replication and genome copy numbers | 26 |
| 2.8. | Concatemer resolution and Southern blot assays | 28 |
| 2.9. | Flow virometry | 29 |
| 2.10. | Super-resolution fluorescence microscopy..... | 29 |
| 2.11. | Electron microscopy | 31 |
| 2.12. | Animal Care..... | 32 |
| Chapter 3: | | 34 |
| 3. Chapter 3: Investigating the effects of deleting extra-helical loops from the VACV hairpin ends..... | | 35 |
| 3.1. | Reactivation of a synthetic chimeric Acambis 2000 virus (ScA2K) | 35 |
| 3.2. | Reactivation of ScA2K with either the flip or flop ends (F or S) | 38 |
| 3.3. | Reactivation of ScA2K with Shope fibroma virus hairpin ends | 41 |
| 3.4. | The telomeric repeats of A2K virus are not essential | 43 |
| 3.5. | Extra-helical loops are essential for viral viability and reactivation | 45 |
| 3.6. | Designing different hairpin ends by deleting extra-helical loops | 46 |
| 3.7. | Reactivating viruses using different hairpin ends..... | 46 |
| 3.8. | The number of extra-helical loops affect virus fitness and growth..... | 48 |
| 3.9. | Increasing the GC content of the hairpin end does not yield a viable virus..... | 49 |
| Chapter 4: | | 52 |
| 4. Chapter 4: Exploring the effects of hairpin mutations..... | | 53 |
| 4.1. | Tagging the virus with a fluorescent marker protein | 53 |
| 4.2. | The SΔ1Δ3-6 mutant virus has a decreased plaque size..... | 54 |
| 4.3. | The hairpin mutations cause no defect in DNA synthesis..... | 55 |
| 4.3.1. | Genome copy number determined using the E9L gene | 55 |
| 4.3.2. | Genome copy number based on the C23L gene..... | 55 |
| 4.4. | Telomere resolution is not affected by the mutant SΔ1Δ3-6 hairpin | 57 |
| 4.5. | Stocks of SΔ1Δ3-6 hairpin mutant viruses contain increased amounts of defective particles..... | 60 |

| | | |
|---|---|-----------|
| 4.5.1. | Using Flow virometry to detect difference in particle count..... | 60 |
| 4.5.2. | Using fluorescence microscopy to visualize difference in particle count | 63 |
| 4.6. | The defective particles in the hairpin mutant virus contain DNA | 64 |
| 4.6.1. | Using flow virometry to detect DNA packaging | 64 |
| 4.6.2. | Using qPCR to detect DNA packaged in viral particles | 66 |
| 4.7. | The formation and assembly of a D13 lattice is not affected by the hairpin mutations..... | 67 |
| 4.8. | Localization and expression of other viral proteins during an infection | 69 |
| 4.9. | The $\Delta 1\Delta 3$ -6 mutant virus exhibits a defect in a late maturation step | 72 |
| 4.9.1. | Presence of immature virions at viral entry | 72 |
| 4.9.2. | An abundance of immature viral particles are seen at 24 hours post infection | 74 |
| 4.9.3. | Mutant viral stocks contain mostly immature virions | 76 |
| Chapter 5: | | 79 |
| 5. Chapter 5: The effects of the hairpin end mutations on the virulence of the <i>ScA2K-S$\Delta 1\Delta 3$-6</i> virus in animal models..... | | 80 |
| 5.1. | Effect of extra-helical loop deletions on VACV virulence in immunocompromised mice | 81 |
| 5.1.1. | Virulence of the synthetic VACV A2K strain in Nu:Nu nude mice..... | 81 |
| 5.1.2. | Virulence of mutant and WT A2K viruses in SCID-NCr Mice | 84 |
| 5.1.3. | Comparison of the diseases caused by synthetic A2K and hairpin mutant viruses in SCID-NCr mice..... | 86 |
| 5.2. | Viruses recovered from the infection site showed potential mutations in the hairpin ends | 90 |
| 5.3. | The hairpin mutant virus still protects against a lethal VACV challenge in immunocompetent mice | 93 |
| Chapter 6: | | 95 |
| 6. Chapter 6: Discussion and future directions..... | | 96 |
| 6.1. | General conclusions and key findings..... | 96 |
| 6.2. | Recovering reactivated virus with different hairpin ends | 98 |
| 6.3. | Hairpin stability and structure | 98 |
| 6.4. | Interactions between the hairpin ends and telomere binding proteins | 99 |
| 6.5. | The role of the hairpin ends in genome packaging | 101 |
| 6.6. | The role of the hairpin ends in virion maturation | 102 |

6.7. The animal models103
6.8. Hairpin ends in other DNA viruses.....104
6.9. Using synthetic biology to study different genomic elements within the poxvirus genome105
References 106

List of Tables:

Table 1: Chordopoxviruses and their host range.3
Table 2: The sequences of synthesized oligonucleotides.26
Table 3: List of antibodies used and their dilutions.30

List of Figures:

Figure 1.1: Vaccinia virus genome structure.8

Figure 1.2: Vaccinia virus replication cycle.11

Figure 1.3: Genome replication and concatemer resolution.....13

Figure 3.1. The design of the synthetic chimeric VACV (ScA2K).37

Figure 3.2. Diagram showing the reactivation of a synthetic virus.....38

Figure 3.3. Resolution of the viral Holliday junction and hairpin rearrangement. 40

Figure 3.4. Substituting the SFV hairpin for the ScA2K hairpin does not affect
viral growth.42

Figure 3.5. Deleting the 125 and 54bp repeats does not affect viral growth.44

Figure 3.6. Design of a completely base-paired hairpin end.....45

Figure 3.7. Hairpin oligonucleotide secondary structure.....47

Figure 3.8. The number of extra-helical loops within the hairpin ends affects
ScA2K growth.48

Figure 3.9. The secondary structure of novel hairpins.....50

Figure 4.1: Mutant viruses exhibit a smaller plaque size phenotype.....54

Figure 4.2: Mutant and WT viruses replicate DNA equally well.....56

Figure 4.3. Sample preparation affects the measurement of genome copy number.
.....57

Figure 4.4. Concatemer resolution is unaffected by hairpin mutations.59

Figure 4.5: The hairpin mutant (SΔ1Δ3-6) virus exhibits a 12-fold higher
particle/PFU ratio compared to WT virus.62

Figure 4.6. Microscopy images showing the increased particle concentration in the
mutant viral stocks compared to WT.63

Figure 4.7. Greater than 98% of viral particles are stained with SYBR Gold.65

Figure 4.8. The mutant viral particles contain relatively more DNA when
normalized to PFU.....66

Figure 4.9. There is no alteration in D13 expression or lattice formation.....68

Figure 4.10. The behavior of the B5 envelope protein is unaffected by hairpin
mutations.69

| | |
|---|------------|
| Figure 4.11. The expression of I3 single stranded DNA binding protein is unaffected by the hairpin mutations. | 70 |
| Figure 4.12. The hairpin mutations cause formation of A5-YFP protein aggregates by 24 hours post infection. | 71 |
| Figure 4.13. Immature virions are seen during the entry stage of infection by hairpin mutant virus..... | 73 |
| Figure 4.14. Cells infected with mutant viruses contain a greater proportion of IV particles..... | 75 |
| Figure 4.15. Difference in morphology between mutant viral particles compared to WT virus. | 77 |
| Figure 5.1. Synthetic VACV strain A2K is not lethal in Nu:Nu nude mice. | 82 |
| Figure 5.2. Nu:Nu nude mice develop a prolonged infection at the inoculation site. | 83 |
| Figure 5.3. Tail lesions in different Nu:Nu nude mice..... | 84 |
| Figure 5.4. Dose escalation study comparing mutant and wildtype viruses using SCID-NCr mice. | 85 |
| Figure 5.5. Repair of the thymidine kinase gene (J2R) does not alter virus growth in vitro..... | 86 |
| Figure 5.6. The ScA2K-SΔ1Δ3-6 virus is less virulent in immunocompromised SCID-NCr mice..... | 88 |
| Figure 5.7. Some SCID-NCr mice developed a progressive pox lesion at the infection site..... | 89 |
| Figure 5.8. Weight change observed in individual SCID-NCr mice infected with the mutant ScA2K-Δ1Δ3-6 virus..... | 91 |
| Figure 5.9. Sequence of hairpin ends of viruses isolated from mice infected with ScA2K-Δ1Δ3-6 virus. | 92 |
| Figure 5.10. Mutant ScA2K-SΔ1Δ3-6 virus protects against a lethal challenge as well as the WT ScA2K-S virus..... | 93 |
| Figure 6.1: Schematic of key findings during infection with ScA2K-SΔ1Δ3-6 hairpin mutant virus..... | 97 |
| Figure 6.2: Proposed model for genome packaging. | 102 |

List of Abbreviations:

| | |
|-----------|--------------------------------------|
| A2K | Acambis 2000 |
| CMC | Carboxymethyl cellulose |
| CRS | Concatemer resolution site |
| DUP | Duplex piece of DNA |
| EM | Electron microscopy |
| ER | Endoplasmic reticulum |
| EV | Enveloped virion |
| F Hairpin | Fast hairpin |
| FBS | Fetal bovine serum |
| GAGs | glycosaminoglycans |
| GPT | guanosine phosphoribosyl transferase |
| HP | Hairpin |
| HPXV | Horsepox virus |
| ITR | Inverted terminal repeats |
| IV | Immature virion |
| LITR | Left inverted terminal repeats |
| mAb | Monoclonal antibodies |
| MEM | Minimum Essential Media |
| MOI | Multiplicity of infection |
| MV | Mature virion |
| MVA | modified vaccinia virus Ankara |
| NCLDV | NucleoCytoplasmic Large DNA Viruses |
| NK cells | Natural Killer cells |
| NR | Non-repeat regions |
| NYCBH | New York City Board of Health |
| ORF | Open reading frame |
| PBS | Phosphate-buffered saline |

| | |
|-----------|----------------------------------|
| PFA | Paraformaldehyde |
| PFU | Plaque forming units |
| RITR | Right inverted terminal repeats |
| S Hairpin | Slow hairpin |
| ScA2K | Synthetic chimeric Acambis 2000 |
| SCID | Severe combined immunodeficiency |
| SFV | Shope fibroma virus |
| TK | Thymidine kinase |
| VACV | Vaccinia Virus |
| WR | Western Reserve |
| WT | Wild type |
| WV | Wrapped virion |
| YFP | Yellow fluorescent protein |

Chapter 1:
Introduction

1. Chapter 1: Introduction

1.1. Poxviruses

1.1.1. Poxvirus taxonomy

Poxviruses are large double-stranded DNA viruses that, unlike most other DNA viruses, replicate within the cytoplasm. The genome size ranges from 135 to 360kbp (1, 2) and the family is divided into two subfamilies, the chordopoxvirinae which infect vertebrates, and the entomopoxvirinae that infect insects. Chordopoxviruses are further divided into more than 10 genera including: avipoxviruses, capripoxviruses, cervidpoxviruses, crocodylipoxviruses, leporipoxviruses, molluscipoxviruses, orthopoxviruses, parapoxviruses, suipoxviruses, and yatapoxviruses. These viruses infect a wide range of animals such as birds, cattle, deer, reptiles, rabbits, swine, rodents, non-human primates and humans (1, 2). Chordopoxviruses share approximately 90 conserved genes that are involved in replication, transcription, morphogenesis and assembly (1, 2). In most of these viruses, the conserved genes are present and arranged in a common order at the center of the genome, except for avipoxviruses and parapoxvirus (1, 3). The host range can vary greatly between viruses within the poxviridae family (Table 1). For example, both variola virus and cowpox virus are orthopoxviruses with the first virus infecting humans, with the potential ability to infect non-human primates (4, 5), whereas the latter has a broad range of hosts, including rodents, cattle, cats, dogs, non-human primates and humans (2) (Table 1). The host-range of poxviruses and virus virulence is determined by multiple gene families. These gene families include protease inhibitors, apoptosis inhibitors, tumor-necrosis-factor (TNF) like receptors, and protein kinase inhibitors (2, 6).

Table 1: Chordopoxviruses and their host range.

The table shows some of the chordopoxviruses genera and a few examples within each genus. The dots within the host range column indicates the extent of host range of the virus. A small circle indicates a limited host range, and a large circle indicates a broad range. Viruses that have been shown to cause infection in humans are noted by red circles. The table is an adaptation from a figure in Haller S. et al., 2014 (2).

| Genus | Virus | Host Range |
|------------------|-----------------------------|------------|
| Orthopoxviruses | Ectromelia virus | ● |
| | Cowpox virus | ● |
| | Monkeypox virus | ● |
| | Camelpox Virus | ● |
| | Variola Virus | ● |
| | Horsepox virus | ● |
| | Vaccinia Virus | ● |
| Parapoxviruses | Orf virus | ● |
| Leporipoxvirus | Shope fibroma virus | ● |
| | Myxoma virus | ● |
| Molluscipoxvirus | Molluscum contagiosum virus | ● |
| Avipoxvirus | Canarypox virus | ● |
| | Fowlpox virus | ● |

1.1.2. Orthopoxviruses

Of significant threat to, and impact on, humans are orthopoxviruses, many of which have been fully sequenced and extensively studied (2). Orthopoxviruses have a wide host range and can infect mammals including rodents and non-human primates (7, 8). Many of these viruses have also been reported to infect humans, including camelpox virus, buffalopox virus, monkeypox virus, cowpox virus, vaccinia virus (VACV) and of course

the causative agent of smallpox, variola virus (7, 8) (Table 1). The threat of zoonotic spread of viruses within the orthopoxvirus genus from animal reservoirs to the human population remains of significant concern.

1.1.2.1. Variola virus

The most infamous and deadly orthopoxvirus is variola virus, the causative agent of smallpox. Smallpox is a historic disease possibly dating back to more than 3000 years ago when discovery of Egyptian mummies showed skin lesions with some resemblance to smallpox lesions (9). However, those observations are not supported by molecular evidence since these authors were not able to isolate viral DNA (9). In recent years, however, multiple discoveries have shown evidence of smallpox infection that have been confirmed by sequencing data (10). The earliest sequencing-based evidence for variola virus dates to 600-1050 CE in Europe. Another study of a mummified child from the mid 17th century also showed DNA evidence of variola virus infection (11, 12). Thus, available molecular evidence suggests the variola virus lineages date back to at least the 7th century.

Smallpox was a devastating disease with fatality rates of up to 30%. Early attempts of protection against smallpox were done through a procedure called variolation. Variolation involved taking infectious crust/scab material from a lesion of a patient and inoculating another person via scarification in the hope that the patient would get a milder disease (13).

1.1.2.1.1. Vaccination history

It was not until 1796 that Edward Jenner demonstrated cross-protection from smallpox following vaccination of patients with material from livestock, infected with cowpox virus, which caused a milder disease in humans (14). One of his most famous cases was the vaccination and infection of an eight-year-old boy (the 17th case described in his publication) (14). Jenner took a sample from a lesion of a milkmaid, Sara Nelms, who had contracted cowpox disease and inoculated the boy, James Phipps, with material from that lesion (14). He then inoculated the boy with smallpox material on two different occasions, but he observed no visible smallpox disease symptoms, suggesting that the boy was protected from smallpox using material from cowpox-infected livestock (14). Edward

Jenner's work laid the foundations of vaccination against smallpox. In 1959 the World Health Organization (WHO) initiated an eradication program and declared smallpox eradicated in 1980 (15).

1.1.2.2. Vaccinia virus

1.1.2.2.1. VACV origins

One of the most studied poxviruses and the prototypic orthopoxvirus is VACV. The origin of VACV is unknown and there is controversy around whether it originated as a cowpox or horsepox. Jenner describes using cowpox lesions for his vaccination studies (14). He even termed the procedure “vaccine inoculation” referring to the cow, which is *vacca* in Latin. Thus, the relationship between the widely used VACV and cowpox virus stems from the observations Jenner made about how the cowpox lesions were able to protect people from smallpox. This led to the assumption that the smallpox vaccine is the same virus as cowpox virus and the two terms were used interchangeably for over a century. However, this idea was challenged in 1939 when immunological studies established a distinction between the infection caused by the human vaccine strain and that caused by spontaneous cowpox infections acquired from cattle (16–18).

The other hypothesis proposes that VACV was originally derived from horsepox. This was partly because “equination”, which is a term used for vaccination using horsepox (equine) material, was a common practice in Italy in the early 1800s (19–21). Even Jenner, in his *Inquiry*, states that he sometimes used material from the equine disease, termed grease, which he noted produced lesions in humans resembling smallpox lesions. He theorized that the horsepox disease could be transferred to cows and then cause disease in milkers (14, 22). This theory was complicated (and controversial) since inoculation with “horsepox” material did not always cause protection against smallpox. The situation could have arisen due to confusion between the horsepox disease “grease”, caused by a poxvirus, and a dermatitic disease also called “grease”, which would not have provided protection against smallpox (22).

Recent sequencing evidence suggest that VACV shares a common ancestor to the one known and since eradicated horsepox virus (HPXV) that was isolated in 1976 in Mongolia (23–25). However, the main difference between VACV strains and the one known HPXV

sequence is that all of the VACV strains have deletions within the telomeric ends of the viruses (23). Moreover, a smallpox vaccine manufactured in 1902 by the Mulford company, showed 99.7% similarity to horsepox virus (26), but interestingly still encodes the deletions found in VACV strains. Finally, a recent study of some viral materials recovered from an 1860's vaccination kit, from Philadelphia's Mütter Museum, showed these viruses also grouped closely to the Mulford 1902 vaccine and both clustered with the Mongolian HPXV strain in a phylogenetic analysis (27). This provides some evidence that VACV and horsepox virus share a common ancestor. It has been speculated that the horsepox virus isolated in the 1976 could have been an old strain of vaccinia virus that had escaped at some point and infected horses (27). However, this theory seems unlikely, since even the earliest known strains of VACV have deleted portions of the telomeres that are still present in HPXV (28). Using the sequences encoded within the central conserved portions of these viruses one can show that the closest common ancestor to the early VACV vaccines was a HPXV-like virus, but whether it was a horsepox virus will likely never be known.

1.1.2.2.2. Modern VACV strains

Multiple factors contributed to the development of different VACV strains, which are reviewed in (29). These factors include early arm-to-arm vaccination, the absence of clonal isolation, the co-culturing of strains, propagation on different hosts, and lack of proper quality control (29). The early vaccine strains were mostly named based on geographical or historical origins, such as Tian Tan, Copenhagen, Lister, and the New York City Board of Health (NYCBH) strains (30). The two strains of VACV used in my studies were the Western Reserve (WR) strain and the Acambis 2000 (A2K) strain, which both derive from the NYCBH strain (29, 31).

The development of the WR strain is not well documented. We know that a Dr. Rivers isolated a few attenuated strains, derived from NYCBH strain, by passaging the virus in chick embryonic tissue and rabbits in the early 1930s (32, 33). These strains, named CVII, CVI and CVI-78, showed decreased pathogenicity in humans, however, they also showed a decreased ability to protect against smallpox compared to the earlier NYCBH strain (34–37). It is thought that this strain was then distributed to other laboratories and acquired

many names such as WR, IHD, and LED-0 (29). Parker *et al.*, at Western Reserve University, describes passaging the WR strain in mice through intracerebral inoculation and comparing it to the CVI and CVII strains (38). Both WR and IHD strains showed increased virulence compared to the other two strains (38). The intracerebral passaging in mice could explain why the WR virus is highly neuropathogenic and virulent in mice and rabbits (39). Thus, compared to other second-generation vaccine strains, WR has an *increased* pathogenicity in animals.

Dryvax, was another vaccine that was cultured in cows by Wyeth Laboratories and its predecessors. It also derives from the NYCBH strain (30). Due to the passaging process, and like many other early smallpox vaccines, Dryvax is a quasispecies vaccine containing different sub-strains of VACV with different virulence properties (40). Thus, in the early 2000s, plaques were picked from a stock of Dryvax which led to the isolation of a clone that is less neurovirulent than the original polyclonal Dryvax vaccine (41). This strain was passaged and plaque purified through two different cell lines, MRC-5 (41) and then Vero cells, to give rise to a second-generation vaccine named Acambis 2000 (A2K) (42). The A2K was shown to be less virulent in animal models and as safe and effective in humans when compared to the Dryvax vaccine (42–45). Thus, the A2K strain was licensed and approved by the FDA in 2007 for use in humans as a smallpox vaccine replacing the Dryvax vaccine.

1.2. VACV genome structure

1.2.1. Central genome

The poxvirus genome comprises a single molecule of double-stranded DNA. The genome encodes all the genes encoding the proteins needed for DNA synthesis, transcription, and replication, giving the virus the ability to replicate outside of the nucleus. Most of those essential genes are arranged within the center of the genome (Figure 1.1) (1, 3). Given that the average size of these genes is 1Kbp, the ~190Kbp VACV genome encodes more than 200 genes. The open reading frames (ORFs) are arranged bidirectionally within the genome, and this directionality is denoted in the gene name by L (left) or R (right). The genes within the genome are tightly packed with little overlap between them and only a few areas of non-coding sequence (46). The naming of the genes within the virus was historically done based

on digestion of the Copenhagen VACV strain genome with the restriction enzyme, *Hind*III. After digestion, the largest fragment was named A and the smallest fragment took the letter O (47, 48). The genes within each fragment adopted a number representing its position within the fragment and a letter for the gene direction (46). The problem with this nomenclature is that the *Hind*III restriction sites are not distributed the same way between different orthopoxviruses, or even between VACV strains (49). Thus, with advances in sequencing, the genes are now usually numbered beginning from the left to the right end of the genome (48). However, some genes and homologs in other poxviruses, are still referred to by the original name based on Copenhagen nomenclature.

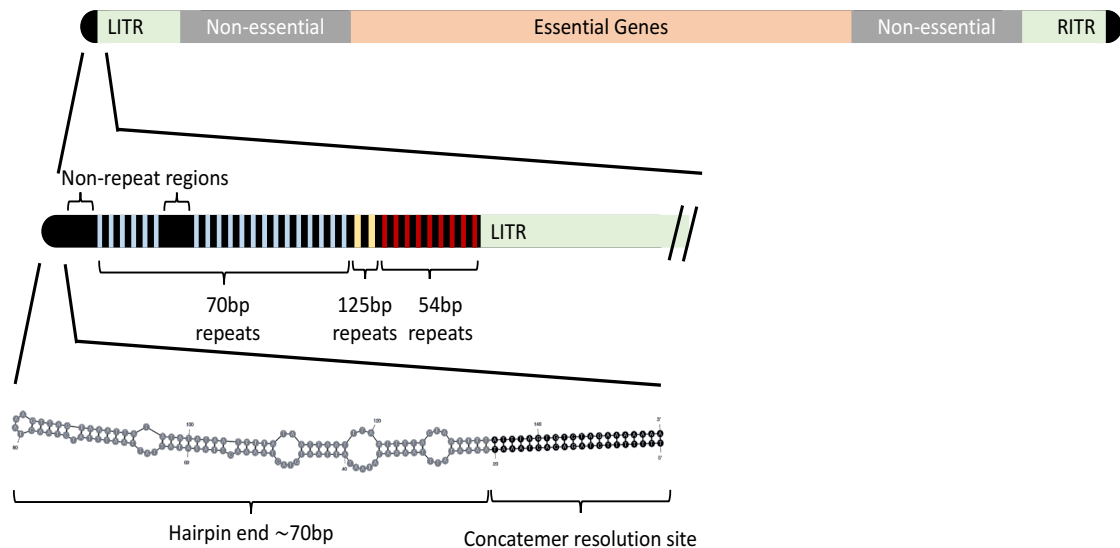


Figure 1.1: Vaccinia virus genome structure.

The figure shows a schematic of VACV genome structure. The central genome contains essential genes flanked by non-essential and host range genes and finally the inverted terminal repeats (ITR) at each end of the genome, left (LITR) and right (RITR). At each end, there are tandem repeats of 70bp, 125bp and 54bp repeats, and two non-repeat regions. Finally, the genome is enclosed in two hairpin ends which encode mismatched nucleotides and the concatemer resolution sites.

1.2.2. Inverted terminal repeats

The presence of inverted terminal repeats flanking the genomes of VACV and rabbitpox virus was discovered in the 1970s using restriction digests, DNA annealing and cross-hybridization experiments (50, 51). From DNA sequencing it is now known that all poxviruses encode inverted terminal repeat (ITR) regions (Figure 1.1). However, the size of these repeats varies greatly between different virus species and strains and ranges from

0.1Kbp to >16Kbp (2, 3). The size of the VACV ITRs also vary, ranging in size from 3.4 to 16Kbp in different strains (2, 3, 46) and even within stocks (40). Many of the genes found in the ITRs are not essential for viral replication, and they are mostly involved in host-range (2).

1.2.3. Tandem repeats

The ITRs of VACV also contain regions of non-coding tandem repeats at the ends of the genome (52, 53). The presence of these repeats in VACV genome was first suggested in 1977 (54) and were thought to be involved in genome replication (54, 55). The VACV genome has multiple sets of repeats, including at least 18 sets of 70bp repeats, two sets of 125bp repeats and 8 sets of 54 bp repeats (Figure 1.1) (56). These different sets of repeats in VACV have high sequence similarity suggesting they could have formed due to early cross-over events (56, 57). Tandem repeats have also been found in other poxviruses. However their sequence, length and number can vary, with some viruses having only a few copies of the repeats (23, 58–62). These repeat regions are typically flanked (on the core side of the genome) by two non-repeat regions, NR I and NR II, that seem to be conserved among poxviruses (23, 60–63). The role of these repeat and non-repeat regions within the genome is not well understood. They may just be selfish DNA.

1.2.4. Concatemer resolution site and hairpin ends

The VACV genome then terminates in two incompletely base-paired hairpin ends (HP) that are complementary on each end. Adjacent to the hairpin ends are found a conserved stretch of bases called the concatemer resolution site (CRS) (Figure 1.1) (53, 64). The CRS is essential for genome resolution which takes place following replication (see below).

Studies concerning the hairpin ends of poxviruses were first pursued in the early 1980s. The first report of the different forms of the hairpin ends was published by Baroudy *et al.* in 1982 (53). They show that the VACV hairpin ends consisted of two forms, named fast (F) and slow (S) based on their electrophoretic mobility through a non-denaturing polyacrylamide gel. Using a Maxam and Gilbert chemical sequencing protocol, they showed that F and S forms are complementary to each other and can be recovered in equimolar amounts (53). The most striking feature of these molecules is that because the hairpins appeared to have been formed from the refolding of imperfect inverted repeats, they encode miss-paired loops and extrahelical bases (53). A few years later, the Moss laboratory cloned the hairpin ends into a

bacterial plasmid (as a duplex imperfect inverted repeat) and these clones permitted many further studies designed to investigate the role of the CRS sites, the hairpin ends, and the mismatches within them in the life cycle of the virus (64–67). Dr. Grant McFadden's laboratory subsequently showed that the SFV hairpin ends also exhibit a similar structure including the extra-helical bases (63, 68, 69). However, the sequence of the SFV hairpin ends is not the same as the sequence of the VACV ends, though they are both AT-rich sequences. In recent years, many other poxviruses, including orthopoxviruses such as monkeypox (70) and cowpox (71), some capripoxviruses (72), and parapoxviruses (73), have also been shown to encode similar mismatched hairpin telomeres.

1.3. VACV life cycle

1.3.1. Viral entry

The two main infectious forms of VACV are mature virions and extracellular virions. The mature virion is formed within the infected cell where it can sometimes acquire two additional membranes and creating intracellular wrapped virions. These can then fuse with the outer cell membrane releasing the extracellular virion form (74, 75). Because of this process, the extracellular virion acquires one additional membrane compared to the mature virion (i.e., two lipid bilayers instead of just one). The way by which virions attach and enter the cell is not completely understood, partially because of the difference in the composition of proteins on the surface of these two virion forms. Especially since the fusion machinery is found on the mature virion (74, 76). There are two main ways by which VACV virions enter the cell, one is through binding to host glycosaminoglycans (GAGs) which facilitate membrane fusion and release of the core into the cell (77, 78). The other mechanism is through internalization by macropinocytosis (or fluid phase endocytosis) (79, 80) which through the acidity in the endosome activates viral fusion machinery (81, 82) (Figure 1.2).

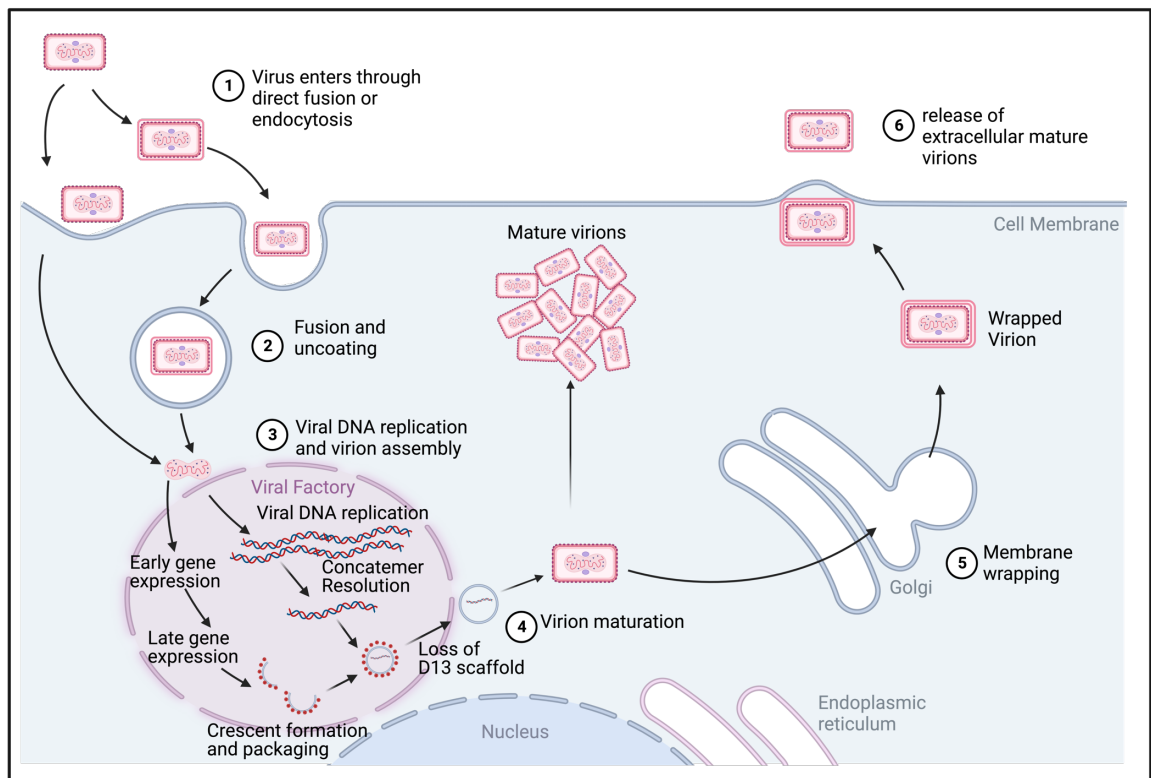


Figure 1.2: Vaccinia virus replication cycle.

The schematic shows steps in VACV replication cycle. (1) and (2) VACV enters the cells through either direct fusion with the cell membrane releasing the core into the cytoplasm or through macropinocytosis which activates viral fusion through the increased acidity within the endosome. (3) Viral DNA replication and virion assembly occurs within the viral factory. Gene expression occurs in consecutive stages, with early gene expression occurs immediately following internalization resulting in genome replication. This is followed by intermediate gene expression occurring during genome replication which is then followed by late gene expression. Late genes encode many of the structural proteins that are involved in virion assembly. The viral genome replicates into long concatemers that then get resolved into monomeric genomes before getting packaged into immature virions. Virion assembly occurs through first crescent formation that is surrounded by D13 protein scaffold. After genome packaging, the D13 scaffold is lost and virion maturation follows. (4) Maturation is characterized by proteolytic processes causing the transformation of the round immature virion (IV) to adopt the classic brick-shaped form known as a mature virion (MV). The MV accumulates within the cytoplasm of the cell and gets released during cell lysis. (5) However, a small percentage can acquire two additional membranes from the trans-Golgi network forming the wrapped virion (WV). Unlike the MV, WV can migrate to cell surface and fuse with the cell membrane to release a two membraned enveloped extracellular virus (EV). This image was adapted from “ZIKA infection cycle” template and created with BioRender.com.

1.3.2. Factory formation

The virion contains all the viral proteins needed for early gene transcription. As soon as the virus core is released into the cell, virus early gene expression starts which is a prerequisite to genome replication (83, 84). VACV replicates within viral factories in the cytoplasm of infected cells. The factories appear to be partially wrapped in endoplasmic reticulum (ER) membranes that are thought to facilitate viral protein synthesis and DNA replication (85). Each infecting virus particle gives rise to one viral factory that can be detected within an infected cell approximately two hours post infection (86). These viral factories expand in size as the DNA replicates and with that expansion, and later during development, the integrity of the surrounding membranes is compromised (87, 88). Later during the infection, factories can merge which is required for production of recombinant viruses (89, 90). As viral factories grow, they serve as sites of genome replication, genome expression and viral assembly (91).

1.3.3. Genome replication

Viral genomes replicate into long head-to-head, head-to-tail, and tail-to-tail concatemers that are processed into unit-length genomes by the A22 viral resolvase (92–95) (Figure 1.3). Viral DNA replication is catalyzed by a DNA polymerase encoded by the E9L gene (96–98). The E9 DNA polymerase can also catalyze repair of double-stranded breaks through a recombination reaction dependent on the 3'-to-5' exonuclease activity (96, 99–101). Other viral proteins involved in replication include the D5 helicase-primase protein (102–105), D4 uracil DNA glycosylase (106, 107), A50 viral DNA ligase (108–110) and G5 endonuclease (111). A few other essential viral proteins are the A20 processivity factor (112, 113), which forms a replication-repair holoenzyme complex with D4 and E9 (114, 115), and the scaffolding protein H5, which also associates with the holoenzyme complex (116, 117). The I3 single-stranded binding protein also plays an essential role in DNA replication, as well as recombination (118–122).

A specific origin of replication for poxviruses has not been identified. A self-priming model of replication has been previously proposed in which a nick introduced near the end of the genome provides the DNA polymerase with a free 3'OH end to prime DNA (83). However, earlier studies have shown that any plasmid transfected into a virus-infected cell is able to replicate and form high molecular weight DNA concatemers, even if these plasmids

do not encode any virus DNA sequences (68, 123). This suggests that the viral replication machinery does not require a specific DNA sequence encoding an origin of replication. Nonetheless, transfection assays using minichromosomes bearing ~200 bp of VACV DNA encompassing the hairpins, mismatched bases, and CRS, exhibit a replicative advantage compared with molecules composed of unrelated DNA (124). Moreover, using deep sequencing to detect RNA primed strands revealed an abundance of reads derived from the hairpin and CRS junction (125).

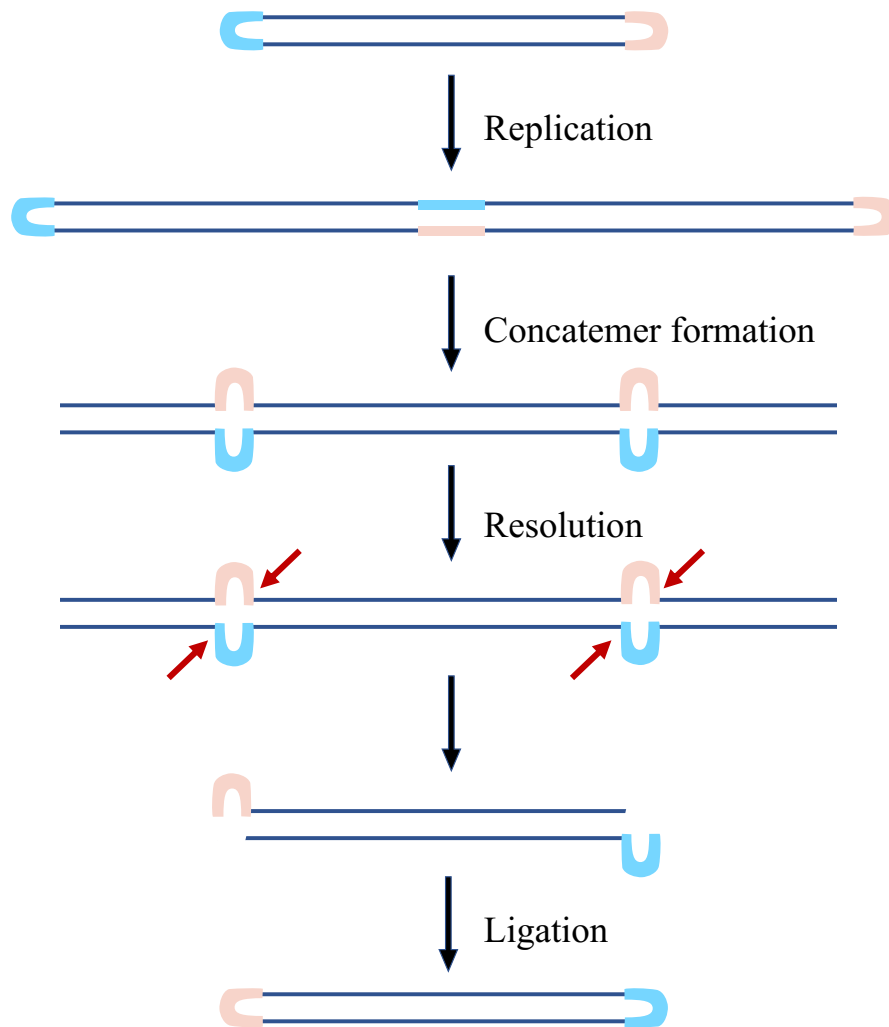


Figure 1.3: Genome replication and concatemer resolution.

Poxvirus genomes are double stranded molecules enclosed in hairpin ends. The genome replicates through long concatemers which are believed to subsequently fold into cruciform junctions at sites encoding the hairpin ends. That forms a series of Holliday junctions that can then get resolved through cleavage by the A22 viral resolvase. The nicked junctions are then ligated to form the mature monomeric genome units. The schematic of viral replication and resolution was adapted from Li et al., 2016 (126).

1.3.3.1. Genetic recombination

DNA molecular recombination is a process by which genetic material is exchanged between two related DNA molecules or even within the same DNA molecule. Usually, a recombination reaction requires similar sequences encoded on the two duplex DNA strands and is called homologous recombination (127, 128). However, recombination between non-homologous sequences can also occur and is sometimes described as “illegitimate” recombination. Even though most of the recombination catalyzed by poxviruses is homologous recombination, non-homologous recombination can also be detected but at a much lower frequency (128–131). Homologous recombination is critically important for DNA damage repair and is intrinsically linked to genome replication. Consequently, many viral proteins are shared between the two processes. These proteins include (128) the E9 viral DNA polymerase (100), the I3 single-stranded binding protein (122), the A22 viral resolvase (132), the G5 endonuclease (133) and the A50 DNA ligase (88). The links between replication and recombination are not unique to poxviruses, it’s also seen in cells infected by other viruses and by bacteriophages (128, 134). Studying and separating the processes that catalyze replication from recombination has been difficult due to the inability to recover mutant viruses that are deficient only in recombination (135). Anything that blocks DNA replication (e.g., drugs) also inhibits recombination. The challenge is best illustrated by the different ways in which the E9 polymerase catalyzes reactions required for both genetic recombination and DNA replication (100, 101, 136, 137). The E9 5’-3’ exonuclease activity catalyzes both the single-stranded annealing reactions that are essential for recombination repair of double-stranded breaks (137, 138).

1.3.3.2. Poxvirus reactivation

Poxvirus DNA is not infectious, meaning that transfecting virus DNA into a cell does not yield a productive infection. Studies as early as the 1930s showed that a heat-inactivated poxvirus could be reactivated using an infectious helper virus (128, 139–143). Later, in the early 1980s Sam and Dumbell show they could reactivate rabbitpox, an Orthopoxvirus, by transfecting rabbitpox virus DNA into cells infected with ectromelia or VACV, other Orthopoxviruses (144). This study demonstrated homologous reactivation, which can also

promote recombination between genetically similar viruses. Another study by Scheifflinger *et al.*, was the first to demonstrate reactivation of VACV DNA using a heterologous Avipoxvirus, in this case fowlpox virus (145). They screened for reactivated viruses using a mammalian cell line where fowlpox virus does not grow. This technique permits insertion of foreign DNA into the reactivated virus through homologous recombination. Subsequently, this led Yao and Evans to show that a Leporipoxvirus, SFV, could also be used to reactivate and recombine VACV DNA (146, 147). In this method, the reactivation step was performed in BGMK cells, which support the growth of both SFV and VACV, and then the reactivated VACV were isolated using BSC-40 cells that permit only VACV growth. In this study the reactivation step was coupled with the formation of recombinants composed of overlapping and co-transfected VACV DNA restriction fragments. This provided a method by which one can efficiently manipulate large segments of the VACV genome (146, 147). This approach was later used by Noyce *et al.*, to reactivate horsepox virus (HPXV) using ten chemically synthesized and overlapping DNA fragments plus pairs of oligonucleotides encoding the mismatched hairpin ends (148). The development of this technology provided the opportunity to elucidate the function of different poxvirus genomic elements that are inherently hard to manipulate using traditional molecular techniques.

1.3.4. Genome resolution

Many early studies have looked at the process of concatemer resolution. After the formation of genome concatemers during replication, the complementary and semi-self-complementary sequences of hairpin ends permit the formation of the cruciform junction (68, 95, 149) (Figure 1.3). These junctions are Holliday junctions, and such structures can be cleaved by a dimeric viral resolvase encoded by the A22R (150). These studies have shown that the main requirement for concatemer resolution is the presence of a “concatemer resolution site” or CRS (63, 65–67, 69, 95). The CRS sequence is highly conserved among poxviruses and is found close to the AT-rich hairpin ends. This motif has also been shown to encode late promoter activity and concatemer resolution depends on late gene transcription (66, 151). The presence of a self-complementary sequence lying between the two CRS sites in a concatemer is required for resolution, however, the intermediary sequence does not seem to matter (69, 95). Another interesting observation is the fact that a cell infected with a leporipoxvirus, Shope fibroma virus (SFV), contains machinery able to resolve transfected

plasmids encoding either SFV or VACV concatemer junctions and CRS elements into linear units sometimes called minichromosomes. The same reaction is observed in VACV infected cells, however, in both cases the homologous resolution appears to be slightly more efficient than heterologous resolution (68). What role the hairpins or mismatches within the hairpin ends play in this process is not yet understood. However, we know that resolution requires the presence of a palindromic sequence, even though it can be completely base paired with no mismatched bases, between two CRS sites (69, 95).

1.3.5. DNA packaging and morphogenesis

1.3.5.1. Crescent formation

The first sign of viral assembly is the appearance of membrane crescents within the viral factories (152) (Figure 1.2). These crescents are formed from ER membranes that are associated with trimers of the scaffold protein D13 (153–156). D13 is essential for the formation of the honeycomb lattice that surrounds an immature virion (IV). By interacting with another membrane binding protein, A17, D13 acts as a scaffold to promote the remodeling of the membranes into the typical round IV structures (157–159). Crescent formation and morphogenesis depend on many other proteins, including A14 (157, 158), L2 (160, 161), A30.5 (155), A11 (162, 163), H7 (164), and A6 (165). As each crescent is forming and growing the DNA is packaged along with core proteins to create a closed and spherical IV. The specific processes by which the DNA is packaged and condensed into a mature nucleoid are not yet completely understood. However, the literature suggests that VACV A32, A13, and the I6 telomere binding protein are all involved in that process (166–168).

1.3.5.2. Virus morphogenesis

During virion assembly and maturation, VACV goes through different forms that exhibit different characteristics (152). The first is the immature virus, or virion, (IV) form that is spherical and packaged with DNA plus associated core proteins. As previously noted, the IV membrane is acquired with the help of the scaffolding protein D13 (153–156). The D13 trimer interacts with the N-terminus of the A17 membrane protein (159). During the maturation process, the A17 protein is cleaved by 17 protease, which in turn causes the dissociation of the D13 protein scaffold (159). Virus maturation involves DNA condensation

onto core proteins (169) and also leads to the formation of two additional lateral bodies that are located between the viral membrane and the core (152). This transformation causes the virus to adopt the classic brick-shaped form known as a mature virion (MV). The MV form is found in the cytoplasm (170), but it can also acquire another two membranes assembling what's called wrapped virions (WV) (171) (Figure 1.2). The wrapped form can exit the cell via fusion with the cytoplasmic membrane bilayer and produce what's called the extracellular virion form (EV) (Figure 1.2). Even though both the EV and MV forms are infectious, viral dissemination within a host is thought to be primarily driven by the EV form (172). This is because the EV form is more resistant to neutralizing antibodies as well as complement (173, 174). A recent paper from our laboratory used super-resolution fluorescence microscopy and different proteins as markers for the different forms, to measure the proportions and timing of formation of each viral form over the course of infection (87). The study showed that during the early stages of infection, the IV with D13 scaffold are most prevalent and found only in viral factories. By seven hours post infection, the proportion of MV increases to reach a ratio of almost 1:1 relative to IV and are mostly found in clusters outside of the viral factories (87). The WV forms appear five to six hours post infection and are mostly found at the cell periphery. These are less common and make up less than 10% of all virion forms. As the infection continues the proportion of MV gradually increases and by 24 hours post infection, the MV form accounts for more than 98% of the virus particles and there can be more than 3500 virions in single infected cell (87).

1.3.5.3. Telomere binding proteins

The hairpin ends of poxviruses appear to be involved in DNA packaging and virion maturation. Experiments have identified at least two DNA binding proteins, I1 and I6, that both bind to the telomere ends of the viral DNA (83, 168, 175, 176).

I1 is a DNA binding protein that binds both single-stranded and double-stranded DNA, with no sequence preference. However, it binds with higher affinity to the telomeric ends of vaccinia virus if these ends bear extrahelical bases compared to a double stranded DNA that is completely base paired (176). Studies using a recombinant virus with inducible I1L gene expression showed that virion maturation ceased under non-permissive conditions. That arrest in maturation is not due to a defect in replication, protein expression, nor genome resolution

or packaging. Consequently, under non-permissive conditions there is an accumulation of non-infectious particles at the immature virion stage of development.

On the other hand, the I6 protein only binds to hairpin ended molecules bearing extrahelical bases. At least two extrahelical bases, spaced five bases apart, are required to efficiently bind I6 to the hairpin. Like I1 protein, I6 does not require a specific sequence to bind to DNA, however, it does preferentially bind to molecules terminating in viral hairpin ends compared to non-viral sequences (176). It is not yet understood if that difference in binding efficiency is due to the number of extrahelical bases, a requirement for specific viral sequences, or has something to do with the AT-rich sequences characteristic of viral hairpin ends. A temperature sensitive I6 mutant showed no defect in replication, gene expression, nor resolution under non-permissive temperature conditions. However, under non-permissive growth conditions, there was an arrest in the maturation process that caused the accumulation of spherical viral particles (168). These aberrant viral particles lack DNA and cannot be rescued by a return to permissive temperatures. This suggests that these empty particles are “dead-end” products, that is they are not functional assembly intermediates (168).

1.3.5.4. Proteins involved in DNA encapsidation

I6 is not the only protein known to play a role in virus DNA packaging. A32 and A13 are two other proteins that also serve some role in this process (166, 167). Mutations or deletion of any of these three proteins produces aberrant virions lacking DNA. I6 protein is known to interact with A32 (83) and this is thought to form a complex that catalyzes the ATP-dependent translocation of I6-bound DNA into the virion (177, 178). In this model the mismatch and hairpin binding properties of I6 could be envisioned to serve as a “flag” that marks A22 resolution products as being ready for packaging. Finally, it has also been proposed that the membrane bound protein, A13, can act as an anchor on the virion membrane to promote DNA encapsidation (179).

1.4. Project rationale

The main objective of my thesis research was to investigate the role the mismatched nucleotides encoded in poxvirus hairpin telomeres play in the viral life cycle. Earlier studies have investigated their role in viral replication and concatemer resolution, mostly using transfection methods. The conclusions that can be drawn from these studies is that

DNA replication does not depend on any particular virus DNA sequence and that concatemer resolution requires only the presence of two CRS sites and a complementary sequence between two sites. It does not require the presence of mismatches (63, 65–67, 69, 95). Thus, it is not yet fully understood if the hairpin ends or the associated mismatches play a role, if any, in DNA replication or concatemer resolution.

Although the sequence of the hairpin ends is not conserved among poxviruses, all known complete poxvirus genomes encode mismatched bases near the hairpin ends of the genome. These mismatches serve as a binding site for two poxvirus telomeric binding proteins, I1 and I6 (83, 168, 175, 176). These two proteins bind preferentially to hairpin DNA bearing mismatched nucleotides and play a role in genome packaging. Biochemical studies have shown they do not seem to require mismatches formed from specific sequences (176), although the number of mismatched sites is important as the I6 protein requires at least two base mismatches to bind to hairpin ended oligonucleotides (176). Interestingly, I6L mutants exhibit an arrest in virion maturation, producing non-infectious immature virus particles that lack DNA (168). These studies show that the hairpin ends play an important role in genome packaging and virion maturation.

A major limitation in the studies cited above has been our inability to test some of the hypotheses arising from these observations by directly manipulating the sequences encoded at the ends of the genome. All these many earlier studies used transfected plasmids encoding cloned telomeres to study these structures. However, it is unclear if that is a true representation of their function or how any alterations might affect virus growth or fitness. In 2018 our laboratory described a method for reactivating synthetic Orthopoxviruses (148). This technique permits the study of genomic elements that have been hard or impossible to manipulate using conventional methods, including the hairpin ends. I used the technique to change the sequence of the VACV telomeres and study the effects these changes had on the virus life cycle and fitness.

This was accomplished by first designing a series of different hairpin oligonucleotides and then using them to try and reactivate VACV virus. This produced a collection of viruses encoding different mutant hairpin ends although it proved impossible to make a virus lacking all the hairpin mismatches. I then used the viruses that I was able to recover to study what effects these hairpin mutations had on virus fitness and growth. I used one

of the hairpin mutants, with the greatest defect in growth, to investigate the reasons for the defect.

In the main my studies show that the normal structure of the hairpin ends, with its six mismatched elements, does not play an essential role in virus genome replication or concatemer resolution. Nor are all the mismatches needed to promote genome packaging. However, deleting most of the mismatches does affect virion maturation, thus producing an abundance of immature and non-infectious particles. This leads to the conclusion that at least a few mismatches are an essential feature of poxvirus telomeres and, moreover, the full complement of mismatched nucleotides are required to ensure proper virion maturation

Chapter 2: ***Materials and Methods***

Parts of this chapter of the thesis have been published as “Mira M. Shenouda, Ryan S. Noyce, Stephen Z. Lee, Jun L. Wang, Yi-Chan Lin, Nicole A. Favis, Megan A. Desaulniers, David H. Evans, The mismatched nucleotides encoded in vaccinia virus flip-and-flop hairpin telomeres serve an essential role in virion maturation. *PLoS Pathog.* 18 (2022), doi:10.1371/JOURNAL.PPAT.1010392.”

2. Chapter 2: Materials and Methods

2.1. Cells and viruses

BSC-40 cells (African green monkey kidney cells) and BGMK cells (Buffalo green monkey kidney cells) were purchased from American Type Culture Collection (ATCC). BSC-40 cells were cultured and used between passages 30 and 50. Cells were cultured in Minimum Essential Media (MEM) supplemented with 1% L-glutamine, non-essential amino acids, sodium pyruvate and antibiotic-antimycotic. The cell media was supplemented with 5% fetal bovine serum (FBS) or an FBS substitute Fetalgro (RMBIO) and cells were incubated at 37°C and 5% CO₂ atmosphere. The MEM media containing all the supplements along with 5% serum is referred to for the rest of the report as complete media, while media containing all supplements, but no serum, is referred to as serum-free media. Both are adherent cell lines that were propagated on cell culture plates and passaged every two to three days. Propagating the cells involved washing the plates with phosphate buffered saline (PBS) and then incubating the cells with 0.25% Trypsin-EDTA (Gibco) for 5-10 min at 37°C until they were fully detached. Complete media was then added to the cells and the cells were then reseeded onto new plates to be further passaged or used.

VACV strain WR, and SFV were purchased from ATCC. VACV strain A2K was a gift from the late Dr. M. Buller (St. Louis MO). A plaque purified clone of A2K was purified and sequenced by our laboratory (GenBank MN974380). VACV-A5-YFP WR strain was generously provided from Dr. B. Moss (180).

2.2. Infecting cells with virus and calculating viral titres

The cells were seeded onto cell culture plates and after 24 - 48 hr, and once the cells reached >90% confluency, the media was aspirated off. The virus stocks were diluted in serum free media and then the cells were infected with the viral inoculum. The volume of serum free media used to infect the cells was 25% of the volume normally used in the plate. For example, if I was infecting a 6-well plate that normally used 2mL media per well, the inoculum was 0.5mL per well. The cells were infected at 37°C in a 5% CO₂ incubator for 1hr, then the inoculum was aspirated off, and warmed complete media was added to the cells. In experiments requiring synchronized infections, the cells were infected on ice for 1hr, and 1% (10 mM) HEPES buffer was added to the inoculum in serum free media.

To determine viral titres, BSC-40 cells were infected with media containing different dilutions of virus, typically ranging from 10^{-3} to 10^{-7} . After one hour of infection, the viral inoculum was aspirated, and the cells were overlaid with complete media containing 1% carboxymethyl cellulose (CMC). Two-to-three days later the infected cells were fixed and stained with a crystal violet solution (0.13% crystal violet, 5% ethanol, and 30% formaldehyde). The cells were fixed for at least an hour, the media was discarded, and the plates were washed with water. The now visible viral plaques were counted to calculate the viral titre using the following equation:

$$\text{Viral titre} = \frac{\text{Average count of plaques per well}}{(\text{Volume of inoculum}) \times (\text{dilution factor})}$$

2.3. Preparation of virus stocks

To prepare viral stocks, the cells were seeded onto 150mm plates to 90% confluency. Between 10-to-35 plates were infected with virus at an MOI of 0.03 PFU/cell in complete media supplemented with 5% Fetalgro. Two-to-three days later, 90% of the cells appeared to be infected as indicated by the way they were rounding up. The infected cells were harvested using a cell scraper and recovered by centrifugation at $2000\times g$ for 10 min. The media was discarded, and the cell pellet was either used immediately or frozen at -80°C to be purified later. The pellet was resuspended (or thawed and resuspended) in cold 10mM Tris pH 9.0 with 2mM MgCl_2 , at $150\mu\text{L}/\text{plate}$ to a maximum of 5.5mL and broken with 20-25 strokes of a tight pestle of a Dounce homogenizer. The homogenate was centrifuged at $2000\times g$ for 10 min, the supernatant was transferred to a clean tube and the pellet was re-extracted with another 5.5mL of 10mM Tris and centrifuged. The two supernatants were pooled and 50U/mL of Benzonase (Millipore) was added and then incubated at 37°C for 30 min to digest any contaminating DNA. The supernatant was centrifuged a third time to remove any residual particulates and then the volume was increased to 19mL using 10mM Tris pH 9.0 with 2mM MgCl_2 . The virus stock was then sucrose purified by carefully overlaying the supernatant onto 19mL of ice cold 36% sucrose in 10mM Tris pH 9.0 buffer. The tube was centrifuged at $26,500\times g$ for 90 min, the supernatant discarded, and the pellet resuspended in 10mM Tris pH 8.0, typically at $100\mu\text{L}$ per plate to achieve an average of 2×10^8 PFU/mL. The virus stock was then sonicated for 1.5 min using a 30s-on-30s of pulse cycle, filtered through a $70\mu\text{m}$ pre-wet strainer, aliquoted, and frozen by snap freezing in a dry ice/ethanol bath or in liquid nitrogen. To determine the titre of the stock, an aliquot was thawed in a warm water bath and

sonicated for 1.5 min using a 30s-on-30s off cycle. The sample was vortexed, 10^{-3} to 10^{-7} dilutions prepared, and titered on BSC-40 cells. This step was repeated two more times and an average titre was calculated. This protocol was adapted and modified from S. E. Smallwood *et al.* (181).

2.4. Virus growth

To measure viral growth curves, BSC-40 cells were seeded onto 6-well plates 24hr prior to infection. One well was used to count the cells and determine cell number. The cells were infected with an MOI of 0.01 PFU/cell in 0.5mL of serum free media per well for 1hr, then 1mL of complete media (with 5% FBS) was added to each well. At each timepoint, except zero-hour, the cells were scraped from the wells, transferred to screw-cap tubes, and frozen at -80°C until ready to be titered. For the zero-hour timepoint, the media was removed and 1mL of complete media (with 5% FBS) was added to the well then 0.5mL of viral inoculum. Immediately after adding the inoculum, the cells were recovered, transferred to a screw-cap tube and frozen at -80°C . The samples were titered as described above (Section 2.2).

2.5. DNA isolation

I used two methods to isolate virus DNA. To quickly prepare the DNA needed for PCR, the infected cells were lysed in cell lysis buffer (1.2% SDS, 50mM Tris pH 8, 4mM EDTA, and 4mM CaCl_2) supplemented with $0.5\mu\text{g}/\mu\text{l}$ proteinase K for 4 - 24hr at 37°C . The solution was then mixed with buffer-saturated phenol and centrifuged. The aqueous layer was collected and mixed with $2.5\times$ volume of 95% ethanol and $0.1\times$ volume of 3M sodium acetate pH 5.2 and placed at -80°C for at least 1hr. The sample was centrifuged at $16,000\times g$ for 30min, the DNA pellet was washed once with 70% ice-cold ethanol, and then air dried. The pellet was resuspended in either water or 10mM Tris pH 8.5.

To isolate higher quality DNA from a viral stock for reactivation or sequencing experiments(182), a $200\mu\text{L}$ aliquot of virus was lysed in $100\mu\text{L}$ lysis buffer (50mM Tris-HCl pH 9.5, 0.7M NaCl, 10mM EDTA, and 1%SDS) for 10 min and then proteinase K was added to a final concentration of $0.5\mu\text{g}/\mu\text{l}$. The solution was incubated at 37°C overnight. For isolation of DNA from cells for qPCR or Southern blot analysis, the cell lysis step was followed by the following steps. An ultrapure phenol-chloroform-isoamyl alcohol solution (25:24:1) was added at a 1:1 ratio to the DNA extract mixture and centrifuged at $16,000\times g$

for 10min. The aqueous layer was mixed again with phenol-chloroform-isoamyl alcohol and centrifuged again. Then, the aqueous layer was added to equal volume of chloroform: isoamyl alcohol (24:1), mixed and centrifuged. The DNA was ethanol precipitated, recovered, and resuspended in 10mM Tris pH 8.5 as described above. The solution was incubated at 37 - 50°C for 1hr to ensure the DNA was fully dissolved and then the concentration of DNA was determined using either a Nanodrop spectrophotometer or a Qubit dsDNA HS assay kit (Invitrogen).

2.6. Hairpin design and endonuclease digestion

PAGE-purified and 5'-phosphorylated oligonucleotides were purchased from Integrated DNA Technologies (IDT). The sequences of the oligonucleotides are shown in Table 2. The 5'-phosphorylated ACA overhang sequence is shown in lower case letters, the concatemer resolution site is bolded and the terminal hairpin loop is underlined. The lyophilized DNA was dissolved in water, heated at 95°C for 5 min, and snap cooled on ice for 10 min to facilitate hairpin formation. The folded structures that these DNAs are assumed to adopt were calculated using the Mfold web server (183). To validate the predicted secondary structures, I used mung bean endonuclease (Promega). These reactions contained 10U of nuclease, 500ng of hairpin DNA, and “cutsmart” buffer (New England BioLabs). The reactions were incubated for 1hr at 37°C and then the DNAs were size fractionated by electrophoresis through a 4% Ultrapure agarose gel (Invitrogen) alongside a size marker (Ultra Low Range GeneRuler, ThermoFisher Scientific).

Table 2: The sequences of synthesized oligonucleotides.

Table was adapted and modified from Shenouda, M et al., 2022 (184)

| Hairpin Name | Sequence of the synthesized oligonucleotides (5'-3') |
|----------------|---|
| S | aca TTTTTTCTAGACACTAAATAAAATATTTAAATATAATATTAATGTACT AAA CTTATATATTATTAATTTATCTAACTAAAGTTAGTAAAT TATATATATA ATTTTATAATTAATTTAATTTTACTAATTTT ATTTAGTGTCTAGAAAAAAA |
| SΔ6 | aca TTTTTTCTAGACACTAAATAAAATTTAAATATAATATTAATGTACTAAA ACTTATATATTTAATTTATCTAACTAAAGTTAGTAAAT TATATATAAAT TTATAATTAATTTAATTTTAAATTTT ATTTAGTGTCTAGAAAAAAA |
| SΔ5-6 | aca TTTTTTCTAGACACTAAATAAAATTTAAATATTAATGTACTAAA ACTTA TATATTATTAATTTATCTAACTAAAGTTAGTAAAT TATATATAAATTTTATA ATTAATATTTTAAATTTT ATTTAGTGTCTAGAAAAAAA |
| SΔ1-3 | aca TTTTTTCTAGACACTAAATAAAATATTTAAATATAATATTAATGTACT AAAAT TATATATTAATTTACTAACTAAAGTTAGTAAATTAATATAAATTTTA TAATTAATTTAATTTTACTAATTTT ATTTAGTGTCTAGAAAAAAA |
| SΔ3-6 | aca TTTTTTCTAGACACTAAATAAAATTTAAATATTAATTTAAAT TATATAT TATTAATTTATCTAACTAAAGTTAGTAAAT TATATATAAATTTAATTAATA TTTTAATTTT ATTTAGTGTCTAGAAAAAAA |
| SΔ1-5 | aca TTTTTTCTAGACACTAAATAAAATATTTAAATATTAATTTAAAT TATA TATTAATTTACTAACTAAAGTTAGTAAATTAATATATAATTTT AAATTAATATT TTACTAATTTT ATTTAGTGTCTAGAAAAAAA |
| SΔ2-6 | aca TTTTTTCTAGACACTAAATAAAATTTAAATATTAATTTAAAT TATATAT TAATTTATCTAACTAAAGTTAGTAAATTAATATATAATTTT AAATTAATATTTT AATTTT ATTTAGTGTCTAGAAAAAAA |
| SΔ1Δ3-6 | aca TTTTTTCTAGACACTAAATAAAATTTAAATATTAATTTAAAT TATATAT TATTAATTTACTAACTAAAGTTAGTAAAT TATATATAAATTTAATTAATAT TTTTAATTTT ATTTAGTGTCTAGAAAAAAA |
| SΔ1-6 | aca TTTTTTCTAGACACTAAATAAAATATAAAATTTAAATTAAT TATAAAAT ATATATATAATTTACTAACTAAAGTTAGTAAAT TATATATAAATTTTATAAT TAATTTAATTTTATATTTT ATTTAGTGTCTAGAAAAAAA |
| SFV | aca TTTTTTCTAGGGTTATAAAT TACTTACATAATGTAATTGATAAAAAATTA ATAAATGATTATATTTATCC TTAAGGATAAATTAACATTTCTATTTTACATT ACATTATGTAAGTAATTT TATAACCCTAGAAAAAAA |
| S – AT to GC | aca TTTTTTCTAGACACTAAAT GGGGCATTCCGGGCATAATGCCGGCGTACC GGGGTCCGCGCGCTATCGGCCCGTTCCGGTTAA ACCACGGCCGTGCGCGCG GCCCCGTAGCCGGCTTAGCCCCGCTAGCCCC ATTTAGTGTCTAGAAAAAAA |
| Entomopoxvirus | aca TTTTTTTATCATAATAAAT TTTATATTATGGATCAAATGTTTATAAAGCA CAATTGCGAGAGTAACTTAATGGACGAGTGCATTTACGTCAAATTAATGTTGA TCCATACGAATAAAATTT ATTATGATAAAAAAA ’ |

2.7. Viral DNA replication and genome copy numbers

To measure genome replication, a single-step growth curve was established using BSC-40 cells. The cells were infected with virus at an MOI of 3 PFU/cell and samples were harvested at different time points over a 24hr period. The DNA was isolated as described

above, then quantified using a Nanodrop spectrophotometer. The qPCR protocol was adopted from Baker and Ward 2014 (185) and used primers and probes targeting the E9L and C23L genes.

One assay used the E9L polymerase gene to estimate genome copy numbers. The two primers used were E9L Forward: 5' – CTCTGCTCCATTTAGTACCGATTC – 3' and E9L Reverse: 5' –TACTCATACGCTTCGGCTAAGA–3'. The internal probe was labeled with a 5' 6-FAM (6-carboxyfluorescein), an internal ZEN and 3' quencher Iowa Black® FQ (5' /56–FAM/AGATCATTC/ZEN/TACGTCCTATGGATGTGCAAC/3IABkFQ/ 3') and was purchased from IDT. To establish a standard curve containing known amounts of PCR template, a gene block of the following sequence was used:

5' GGATTGGCAAACCGTAACATACCGTTAGATAACTCTGCTCCATTTAGTACCGATTCTAG
ATACAAGATCATTCTACGTCCTATGGATGTGCAACTCTTAGCCGAAGCGTATGAGTATAGA
GCACTATTTCTAAATCCCATCAGACCATAT–3'.

For genome copy numbers based on C23L gene, the primers, probe, and gene block were:

- 5' –AGACACACGCTTTGAGTTTTG–3'
- 5' –TCAAGTATGTGCGACGGATCG–3'.
- 5' /56–FAM/AGTGAAGTA/ZEN/TCATCGGTTGCACCTTCA/3IABkFQ/3'
- 5' TCCAATTTTCAGATGAATAGAGTTATCGATTCAGACACACGCTTTGAGTTTTGTTG
AATCGATGAGTGAAGTATCATCGGTTGCACCTTCAGATGCCGATCCGTCGACATACT
TGAATCCATCCTTGACCTCAAGTTCAGATGATTCCTTG–3'.

The qPCR master mix was prepared at 4× concentration, containing 2 μM each primer and 1 μM probe. The master mix was aliquoted in black tubes to protect the light-sensitive fluorophore and stored at -20°C. To prepare the standard curve, the gene block was resuspended in 10mM Tris pH 8.0 to a concentration of 10ng/μL, this provided a gene block at a 6.49×10^{10} gene copies per μL. Three-fold dilutions of the gene block were made starting with highest concentration of 2×10^9 copies/μL. To prepare the samples, 2-5μL of DNA was added to 5μL of the 4× primer-probe mix and 10μL of 2× TaqMan qPCR master mix (Quantabio – PerfeCTa Fastmix II) and volume adjusted to 40μL using water. That gave a final concentration of 500nM for the primers and 250nM for the probe. The assay was programmed to run at 95°C for 2min, and then 40 cycles of 15s at 95°C, and 30s at 60°C with

the fluorescence read at the end of each cycle. The standard curve was generated using cycle quantification (C_q) values from the standard samples and the gene copy number. The standard curve was then used to calculate the copy numbers of each unknown sample. These calculations were obtained using Real-Time PCR Analysis software from Bio-Rad.

2.8. Concatemer resolution and Southern blot assays

The DNA prepared for the qPCR analysis was also used to study the kinetics of concatemer resolution. The DNA was quantified by spectrophotometry and also fractionated on an agarose gel and stained with SYBR dye to further confirm the amounts. The DNA was digested with *Aflw44I* (ThermoFisher Scientific) in FastDigest buffer at 37°C overnight and then the enzyme was heat inactivated at 80°C for 5 min. Loading dye was added to 20µg of digested DNA which was then size fractionated on a 0.8% agarose gel with SYBR Safe dye (ThermoFisher Scientific) added to the gel, imaged on Bio-Rad Molecular Imager Gel Doc™ XR⁺ and analyzed using Bio-Rad Image Lab software. The gel was washed in deionized water and then the DNA was depurinated in 0.25M HCl for 30 min at room temperature. The gel was rinsed and incubated in a denaturing solution (1.5M NaCl, 0.5M of NaOH, pH 13) for 30 min at room temperature, then washed in water and neutralized in 1.5M NaCl, 1.3M Tris-HCl, pH 7.5 for 15 min at room temperature. This step was repeated twice. The DNA was blotted onto a Biorad B Nylon membrane (ThermoFisher Scientific) through capillary transfer overnight in 10× SSC (1.5M NaCl, 0.15M sodium citrate pH 7). After transfer, the membrane was washed in 2× SSC and then the DNA was crosslinked onto the membrane using a UV Stratolinker. Alternatively, 3µg of DNA was denatured in 0.4M NaOH, 10mM EDTA for 10 min at 100°C and then applied to a membrane using Bio-Dot SF microfiltration apparatus (Bio-Rad). To detect the DNA, I used the North2South chemiluminescent hybridization and detection kit (ThermoFisher scientific) and followed the manufacturer's protocol.

I used three different probes to detect the DNA. In the one, I used Biotin-16-dUTP (added at a 40:60% ratio with dTTP) in a PCR reaction to generate the labelled probe. The sequence of the primers used were 5' – GATTCTTCCTCCAAACAGTTAACG and 5' – AGACACACGCTTTGAGTTTTG. I used the ITR plasmid as a template for the PCR reaction. The next method involved using Bio-Nick Labeling System (Invitrogen) to nick translate

a PCR product or plasmid as probes. To generate the plasmid, I cloned an ITR fragment into pcDNA3.0 vector. The primers I used to generate the ITR fragment were

5' -AAAGGATCCAGACACACGCTTTGAGT and

5' -AAACTCGAGGATTCTTCCTCCAAACAGTTAAC .

2.9. Flow virometry

All solutions and buffers were passed through a 0.1µm Acrodisc syringe filter (Pall Corporation) before use. Serial dilutions of the virus stock were prepared in filtered PBS and then 9 µL of 4% paraformaldehyde (PFA) in PBS was added to 9µL of each diluted virus sample to a final concentration of 2% PFA. The solution was mixed and fixed on ice for 20 min. To stain the virus DNA, 2µL of a 25× solution of SYBR gold (Thermofisher Scientific) in filtered PBS was added to the fixed virus and stained on ice for a further 30 min in the dark. If the staining step was to be omitted, 2µL of PBS was added instead. The solution was then diluted 10-fold by adding 180µL of PBS to the 20µL of virus and immediately applied to a BD Cytoflex flow cytometer. The data was collected and analyzed using FlowJo (version 10.6.0).

2.10. Super-resolution fluorescence microscopy

Cells were seeded onto glass coverslips (previously sterilized using 95% ethanol) and located in 24-well plates. The cells were incubated overnight until they reached 50-70% confluency and then infected with an MOI of 3 PFU/cell on ice to synchronize the infection. After one hour, the cells were washed with PBS and warm media was added. This marked the zero-hour time point. At different time points post infection, the coverslips were transferred to a new 24-well plate containing a PBS wash buffer. The PBS was aspirated, 4% PFA in PBS was added to the well, and the cells were fixed for at least 30 min at 4°C. The fixative was then removed and discarded. A quenching agent (0.1M glycine, 0.1% Triton X-100 in PBS) was added to the cells and further incubated at room temperature for 20 min. The quenching solution was removed, the cells were washed three times in PBS-T (0.1% Tween 20 in PBS), blocking buffer was added (3% BSA in PBS-T), and the cells incubated for at least another 30 min at room temperature or at 4°C overnight.

To detect cell and/or virus antigens, the fixed and infected cells were then incubated with primary antibody in blocking buffer at room temperature for 1.5hr or overnight at 4°C. The

cells were washed three times with PBS-T buffer and then incubated with a secondary antibody at a dilution of 1:2000 and a DNA stain (DAPI or Hoechst) at a dilution of 1:500 to 1:1000 in blocking buffer for at least 45 min at room temperature. The primary and secondary antibodies used are listed in Table 3. The excess antibodies and dyes were removed by washing three times with PBS-T. To mount the coverslips, the coverslips were first dipped into water and tapped onto a Kimwipe to remove excess water. The coverslips were then mounted using SlowFade Gold antifade reagent (Invitrogen) and sealed with clear nail polish. Alternatively, ProLong Glass Antifade mountant (Invitrogen) was used and left to cure at room temperature for 24 hours. The cells were then imaged using a Deltavision OMX super resolution microscope and the data analyzed and processed using SoftWoRx image processing software.

To image viral particles (186), sterile fibronectin coated coverslips (GG-12-Fibronectin – Neuvitro) were inserted into 12-well plates and hydrated by soaking with PBS. The virus was sonicated, diluted in PBS, and 100 μ L of inoculum was spotted onto the center of each coverslip and incubated at room temperature for 1hr. The inoculum was removed with a pipette, 4% PFA fixative was added, and incubated for 30 min on ice. After fixing the sample, the same quenching, blocking and DNA staining and coverslip mounting protocol was followed as described in the paragraph above.

Table 3: List of antibodies used and their dilutions.

| Protein detected | Origin | Source | Dilution |
|-------------------------|---------------|---------------|-----------------|
| VACV D13 | Rabbit | Dr. B. Moss | 1:500 |
| VACV I3 (10D11) | Mouse | ProSci | 1:10000 |
| VACV B5 | Mouse | Dr. S. Isaacs | 1:10000 |
| Anti-mouse | Goat | Invitrogen | 1:2000 |
| Anti-rabbit | Goat | Invitrogen | 1:2000 |

2.11. Electron microscopy

ACLAR sheets (provided from the Cell Imaging core facility) were cut into 1.3 cm squares, sterilized using 95% ethanol, and left to dry completely. BSC-40 cells were seeded onto the ACLAR sheets in 12-well plates and cultured until they reached 90-95% confluency. The cells were infected with virus on ice for 1 hour, the inoculum was aspirated off, and warm media was added. At different timepoints, the ACLAR sheets were moved to a new plate containing PBS in the wells. To fix the cells, the PBS was removed and 500 μ L of fixative (2% paraformaldehyde, 2.5% glutaraldehyde in 0.1M sodium-cacodylate buffer with 2mM CaCl₂, at pH 7.4) was added to each well. The cells were incubated in this fixative for 20 min at room temperature and stored at 4°C overnight.

Alternatively, to evaluate viral binding and entry into cells, BSC-40 cells were seeded in 6-well plates and allowed to grow to 90-95% confluency. The cells were washed in PBS then incubated in 1mL Versine (0.48mM EDTA in PBS) for 15 min at 37°C. A pipette was used to break up the cells and then they were further incubated for another 5-10 min at 37°C. The cells were recovered by centrifugation, the media discarded, and resuspended in 1mL of serum-free media and counted. The cells were infected in suspension in a 15mL Falcon tube with viral inoculum at an MOI of 10 PFU/cell on ice for 1hr. Warm complete media was added to the tubes and then the virus-cell suspension was incubated for another 30 min at 37°C. The cells were recovered by centrifugation at 300 \times g for 5 min and the media discarded. Fixative was added (2% paraformaldehyde, 2.5% glutaraldehyde in 0.1 M sodium-cacodylate buffer with 2mM CaCl₂, at pH 7.4) and the cells were incubated overnight at 4°C. The cells were washed 3 \times with 0.1M sodium cacodylate buffer and resuspended in 7% low gelling agarose in water. The agarose was allowed to set and then processed as described below.

To analyze viral particles, a sucrose-purified virus pellet was fixed in 2.5% glutaraldehyde in cacodylate buffer for 20 min at 37°C and then for 40 min at 20°C without disrupting the virus pellet. The pellet was then gently washed three times in cacodylate buffer and resuspended in 7% low gelling agarose.

The fixed samples were post-fixed and stained in freshly made 1% K₄FeCN₆ and 1% OsO₄ in 0.1M sodium cacodylate buffer for 30 min followed by a wash in 0.1M sodium cacodylate buffer and 0.1M sodium acetate buffer pH 5.2. Then the samples were treated with 2% uranyl acetate in 0.1M sodium acetate buffer for 15 min and again washed in 0.1M sodium acetate buffer followed by deionized water. The cells were dehydrated using progressively

increasing ethanol concentrations from 30-90%, and then twice at the 100% concentration. The samples were infiltrated with mixtures of ethanol plus Spurr's resin (EMS #14300) composed of 2:1, 1:1, and 1:2 ethanol-to-resin followed by three exchanges using 100% resin. Finally, the samples were polymerized in a fourth change of resin at 65°C for 48 hours. The blocks were sectioned to 70nm with a Leica EM UC6 ultramicrotome and post-stained with uranyl acetate and lead citrate. The images were acquired using a JEOL F21000 transmission electron microscope equipped with Gatan Orius digital camera at 200kV acceleration voltage. All work was carried out in the Faculty of Medicine and Dentistry's Cell Imaging core facility with the assistance of Ms. S. Amidian.

2.12. Animal Care

All mice were housed in Biosafety Level 2 containment at the University of Alberta. The experiments were reviewed and approved by the University of Alberta's Research Ethics Office, Animal Care and Use Committee, in accordance with the guidelines and policies of the Canadian Council on Animal Care (<https://www.ccac.ca>).

All viruses used to infect animals were viral stocks that were sucrose cushioned, benzonase treated, filtered, aliquoted and titered as described in section 2.3. To confirm the viral titer after dilution for use in animals, three different aliquots were thawed, sonicated and diluted in PBS. After dilution the virus was titered and an average was used to accurately determine the titre of the virus after dilution.

Immunocompromised female Nu:Nu nude mice and NCI SCID-NCr mice were purchased from Charles River Laboratories at 6-8 weeks of age. The former exhibits a defect in the T lymphocytes population while the latter are defective in B and T lymphocytes. Both strains still express intact innate cell populations, such as normal NK cells, macrophage, and dendritic cells. At day zero the mice were anesthetized using gaseous isoflurane and 5µl of PBS or viral inoculum at a dose ranging from 10^4 to 3×10^7 PFU/mL was applied to a 1cm fresh scarification zone near the base of the tail. The inoculum was left to dry for 5 min and then the mice were placed in a recovery chamber to monitor for signs of distress. Once a week the tail scars were photographed. The mice were subsequently monitored and evaluated daily for body weight, physical appearance, mobility, responsiveness, and the presence of poxvirus lesions. Each category was scored out of three, with three denoting the worst condition in that

category. The mice were euthanized if they reached a total clinical score of seven, or a score of three on any of the individual criteria, or if they lost $\geq 20\%$ of their initial body weight.

The lesions found on the tail at the scarification site were dissected at euthanasia and stored frozen at -80°C . The samples were subsequently thawed, placed in a pre-wetted $70\mu\text{m}$ cell strainer, and mashed through the strainer using the end of a syringe plunger followed by two washes with 0.5mL each of Hank's Balanced Salt Solution (GIBCO). Any cell-associated viruses were released from the cells that had passed-through the strainer by freeze-thaw and recovered by plating on BSC-40 cells.

Immunocompetent female Balb/c mice were purchased from Charles River Laboratories at 6-8 weeks of age and immunized (10^6 PFU) on day zero using tail scarification as described above. On day 28 post-vaccination the mice were anesthetized and challenged intranasally with $10\mu\text{L}$ of a lethal (10^6 PFU) dose of VACV WR strain in PBS. The mice were subsequently weighed and monitored daily for signs of disease and distress as described above.

Chapter 3:
Investigating the effects of deleting extra-helical loops from the VACV hairpin ends

Parts of this chapter of the thesis have been published as “Mira M. Shenouda, Ryan S. Noyce, Stephen Z. Lee, Jun L. Wang, Yi-Chan Lin, Nicole A. Favis, Megan A. Desaulniers, David H. Evans, The mismatched nucleotides encoded in vaccinia virus flip-and-flop hairpin telomeres serve an essential role in virion maturation. *PLoS Pathog.* **18** (2022), doi:10.1371/JOURNAL.PPAT.1010392.”

Contributions to this chapter:

MS - Development of methodology, performed experiments, writing and manuscript preparation

RN - Study supervision, conceptualization, development of methodology, technical and experimental assistance, funding acquisition, editorial revisions, manuscript preparation

MD - Methodology, technical & experimental assistance

NF - Technical & experimental assistance and animal support

DE - Study supervision, conceptualization, project administration, resources, editorial revisions, manuscript preparation

3. Chapter 3: Investigating the effects of deleting extra-helical loops from the VACV hairpin ends

Introduction and Summary:

Our laboratory has developed a method that can be used to reactivate Orthopoxviruses using DNA fragments of synthetic origin. This method was first used to reactivate horsepox virus (146, 148) and provided a tool that can also be used to study the hairpin ends of poxvirus genomes. Dr. Noyce designed nine overlapping fragments of DNA using a sequenced sample of VACV strain ACAM 2K (A2K) as a guide. These synthetic fragments included one that has an insertion of a gene encoding yellow fluorescent protein and guanosine phosphoribosyl transferase (YFP/gpt) inserted into the thymidine kinase (TK) J2R locus. This modification helped with screening plaques for the reactivated viruses. Thus, all the reactivated viruses encoded a J2R gene deletion, although for some experiments recombination was used to repair the J2R gene after isolating and sequencing the fluorescent primary isolates. The left and right inverted terminal repeats fragments (LITR and RITR) lack the 70bp repeats but still included the 125 and 54 bp repeats which comprise 682bp of the fragments. Dr. Noyce's previous studies have shown that deleting the 70bp repeats does not affect viral fitness *in vitro*. Consequently, for all the experiments described below, I omitted the repeats from the LITR and RITR fragments used in the reactivation reactions. I also substituted the hairpin ends encoded by VACV strain WR, even though the WR and A2K hairpin ends differ by 7 nucleotides. The WR hairpins were used since the sequence has been previously reported and studied in the context of minichromosomes (63, 67, 69, 92).

The studies described within this chapter focus on the reactivation of VACV using different hairpin ends and the effects of these modifications on the virus growth and viability.

3.1. Reactivation of a synthetic chimeric Acambis 2000 virus (ScA2K)

The A2K virus sequence was divided into nine fragments ranging from 17 to 29Kbp in size (Figure 3.1A). These fragments were synthesized by GeneArt (Life Technologies – Burlington, Ontario) with an overlap of 1Kbp between the fragments. To help with the assembly and cloning the *BsaI* and *AarI* sites were silently mutated in fragments one to

seven, but not in the ITRs. Each fragment was cloned into a plasmid and flanked by I-*SceI* restriction site to permit cutting the fragments out of the plasmid. Fragment three encodes the J2R locus which was removed and replaced with a YFP/gpt gene sequence to allow for ease of screening of the reactivated viruses. For the ITRs, a *SapI* restriction site was inserted upstream of the I-*SceI* site, at the hairpin ends. This digest formed a 3'-CCA overhang that would ligate to the 5'-TGG overhang of a duplex piece of DNA (WR DUP) (Figure 3.1B). This piece of DNA encodes a stretch of 64bp found in the WR sequence between the hairpin and the ITR sequence. For the purposes of my studies, I did not add the 70bp repeats section of the genome onto my synthesized viruses.

To reactivate the virus, the hairpin ends were ligated to the WR DUP sequence at 1:1 ratio overnight at 16°C then heat inactivated at 65°C for 10 min. I then ran the ligation reaction on a 3% ultrapure agarose gel and isolated the ligated DNA from the gel using a gel purification kit. In the meantime, the ITR plasmids were digested with both I-*SceI* and *SapI* at 37°C for 2 hr then inactivated at 65°C for 20 min. After the digestion, FastAP thermosensitive alkaline phosphatase was added to the reaction for 1hr at 37°C then inactivated at 65°C for 20 min. Then 133ng of hairpin/DUP purified fragment was ligated to 1µg of digested ITR at 16°C overnight. Finally, fragments one through seven were digested for 2hr with I-*SceI* at 37°C then heat inactivated at 65°C for 20 min (Figure 3.2).

To reactivate the virus, Buffalo green monkey kidney (BGMK) cells were infected with SFV at an MOI of 0.05 to 0.08 PFU/cell for 2-3 hours, then the cells were transfected with total of 5µg of the DNA fragments. The cells were harvested at 4-5 days post infection, and after three freeze/thaw cycles the cell lysate was plated on BSC-40 cells. BGMK cells were used for the infection/transfection since they support the growth of both SFV and VACV, whereas SFV grows at much slower rate on BSC-40 cells which is why they were used for screening the reactivated VACV (Figure 3.2).

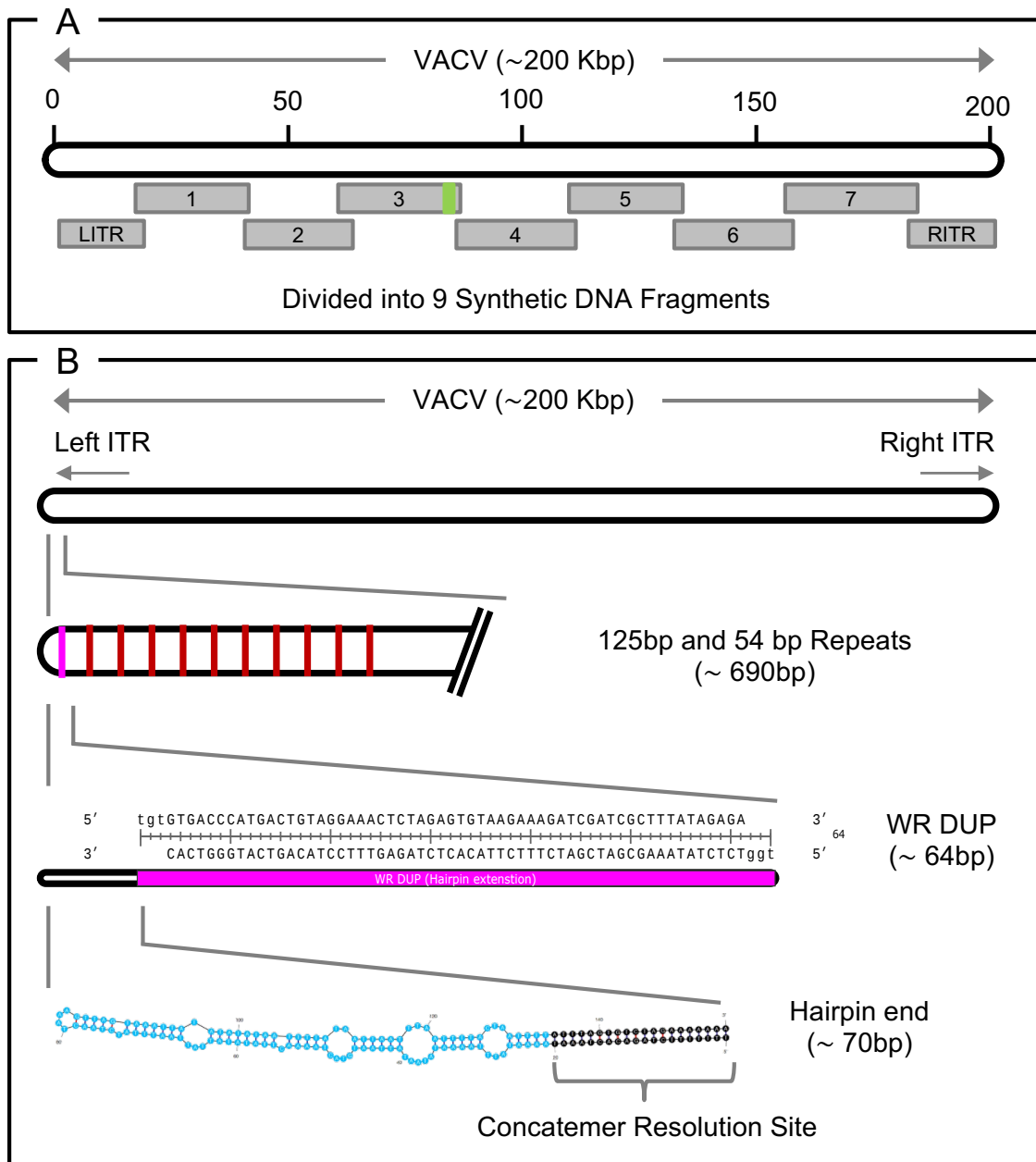


Figure 3.1. The design of the synthetic chimeric VACV (ScA2K).

(A) shows the division of the VACV A2K genome into nine fragments with 1Kbp overlap between the fragments. Fragment three encodes the YFP/gpt gene in the TK (J2R) locus (green). (B) the end of the genome encodes the 125/54 bp repeats (red) within the ITR fragments, which then get ligated to a hairpin duplex of WR strain (WR DUP) (pink) and then is ligated onto the hairpin ends of the virus. The predicted secondary structure of the hairpin with the extra-helical loops is shown at the bottom of the figure and was obtained using Mfold (183). This figure was adapted and modified from Shenouda, M et al., 2022 (184)

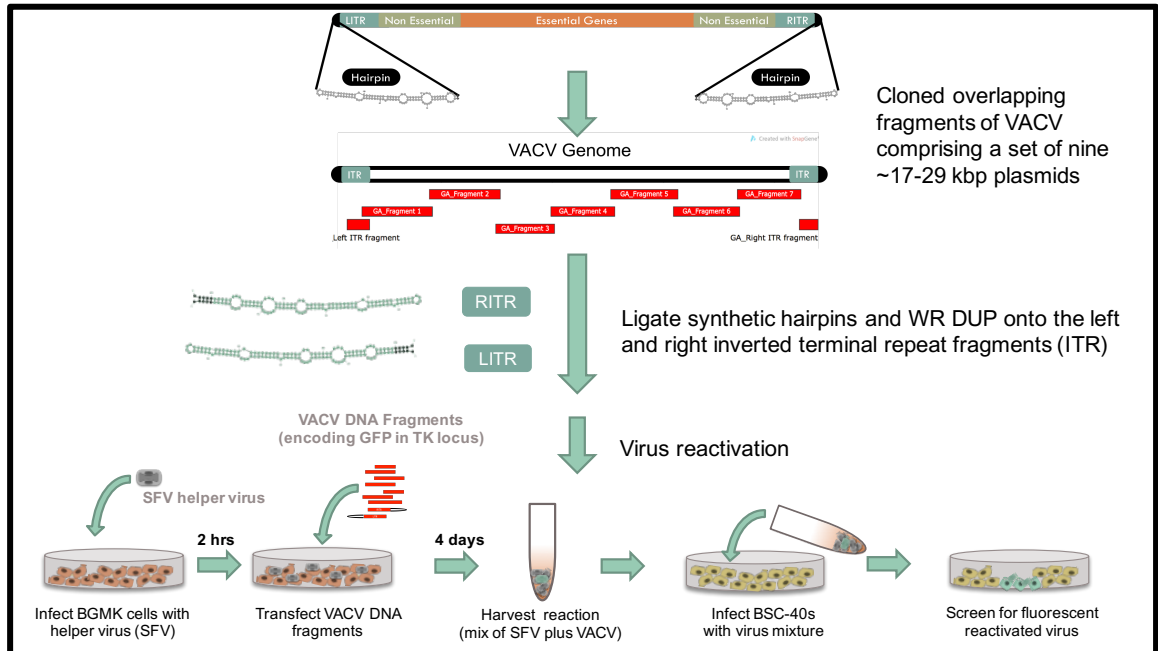


Figure 3.2. Diagram showing the reactivation of a synthetic virus.

The plasmids encoding the synthetic DNA fragments are digested with restriction enzymes and then the ITRs are ligated to the hairpin/DUP sequences. BGMK cells are infected with SFV helper virus and 2hr post infection the digested and ligated DNA is transfected into the cells. After four days, the cells are harvested, and the cell lysate is used to infect BSC-40 cells. The cell monolayer is then screened for fluorescent reactivated viruses, which are then plaque purified.

3.2. Reactivation of Sca2K with either the flip or flop ends (F or S)

As previously described, poxviruses encode two complementary forms of the hairpin ends, flip and flop, which have also been referred to as fast (F) and slow (S) according to their electrophoretic migration properties. It is difficult to determine if the hairpin forms have a certain orientation within the viral genome. It is clear, however, that both forms are present in equimolar amounts. Previously, we have ligated each hairpin end form to both ITRs, essentially producing four different fragments, which were then added to the reactivation. This was done to ensure efficient reactivation and eliminate any variability or bias in the preference of one or the other on the viral end. Because homologous recombination occurs throughout the viral genome and because of the way the terminal Holliday junctions are resolved, we predicted that if we provided only one form of the hairpin end, then the other complementary form would also be recreated after the genomes are replicated (Figure 3.3)

I first tested the ability to reactivate the virus with only one type of hairpin oligonucleotide ligated onto both the left and right ITRs. As anticipated, I was able to reactivate a virus using either the F or S forms ligated onto both the left and right ITRs. When we sequenced the virus that was reactivated using only S hairpins, I could detect both F and S hairpin sequences in equimolar amounts. Therefore, we can assume that within a population of viral DNA molecules, some molecules would have S on both ends, F on both ends, or S and F on either end of the viral DNA molecule (Figure 3.3). For all subsequent studies I used only the S hairpin oligonucleotide (or its derivatives) to reactivate the virus just for ease of experimental design. For the rest of the report, “S” denotes the slow form of the WR strain hairpin end.

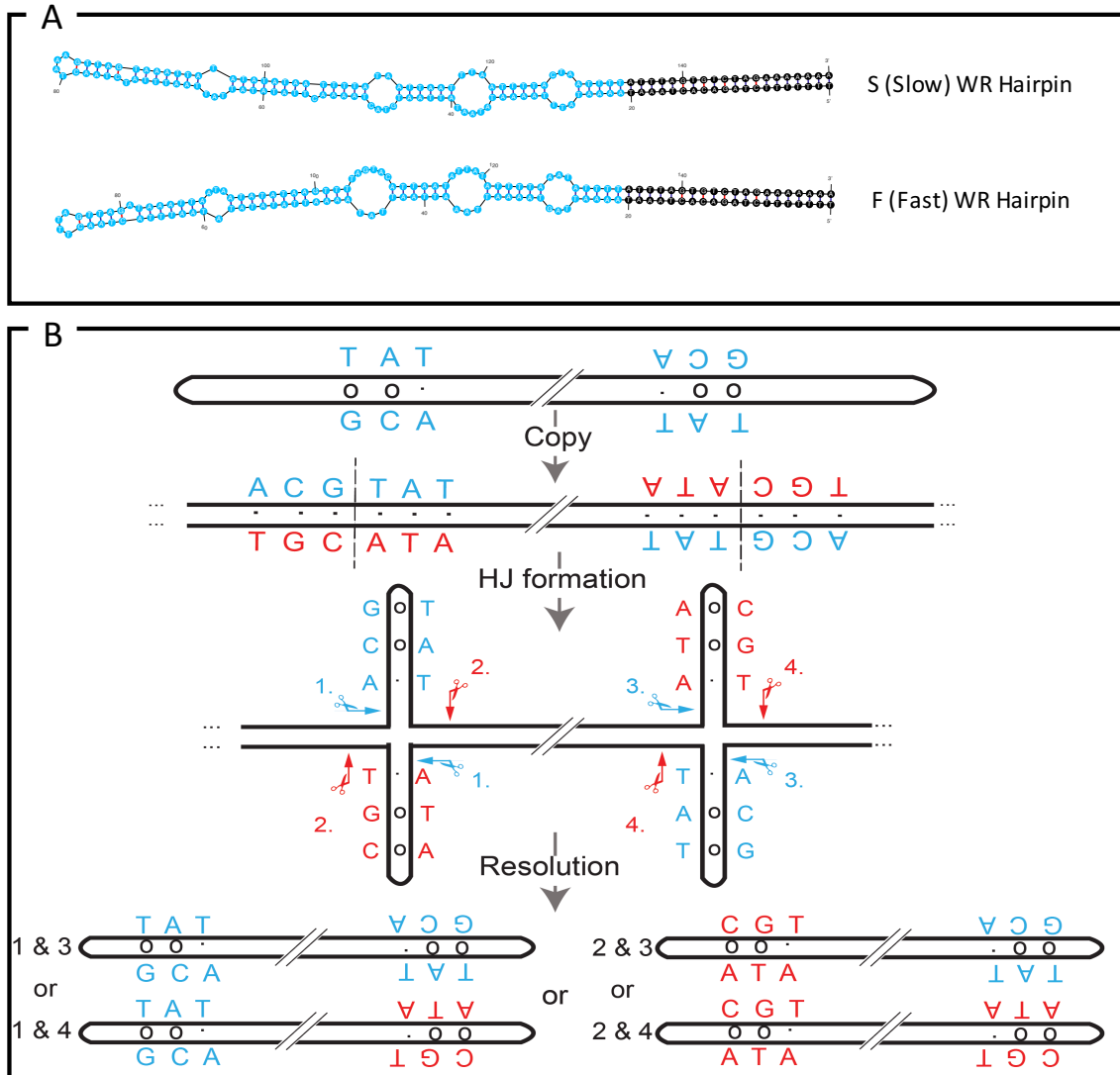


Figure 3.3. Resolution of the viral Holliday junction and hairpin rearrangement.

(A) shows the secondary structure of the S and F hairpin ends of WR VACV strain predicted using Mfold (183). (B) depicts the replication and concatemer resolution reactions that rearrange the hairpin ends. If we assume the S is represented by the blue and F is represented by the red labeling, then this resolution can yield genomes that have both S ends (1&3), both F ends (2&4) or one on each side (1&4 and 2&3). Section (B) of the figure was outlined and drawn by Dr. Evans. This figure was adapted and modified from Shenouda, M et al., 2022 (184)

3.3. Reactivation of Sca2K with Shope fibroma virus hairpin ends

Previous transfection studies have shown that VACV can resolve minichromosomes with both homologous and heterologous hairpin ends, VACV and SFV hairpin ends, but the resolution seemed to be less efficient if the substrate is a heterologous hairpin end plasmid. Because it is very difficult to mutate the hairpin sequence within the viruses, these studies have typically used exogenous plasmid DNA encoding variations of the hairpin and concatemer resolution end sequence. It is not clear whether this system truly represents the function of these hairpins within the viral genome, and the extent of their involvement in viability and fitness of the virus. I took advantage of the methods previously described to reactivate an A2K virus with SFV hairpin and concatemer resolution sequence. Both hairpins encode mismatches, however the S (WR strain) hairpin is longer than SFV hairpin and harbours more predicted extra-helical loops (Figure 3.4.A). I successfully reactivated a chimeric A2K VACV with SFV hairpin ends and that was confirmed by genome sequencing. I next tested how well the virus grows compared to synthetic A2K with WR hairpin. The virus did not exhibit a growth defect in a multi-step growth curve assay on BSC-40 cells (Figure 3.4.B). This suggests that the hairpin ends, though different between the two viruses, truly are interchangeable.

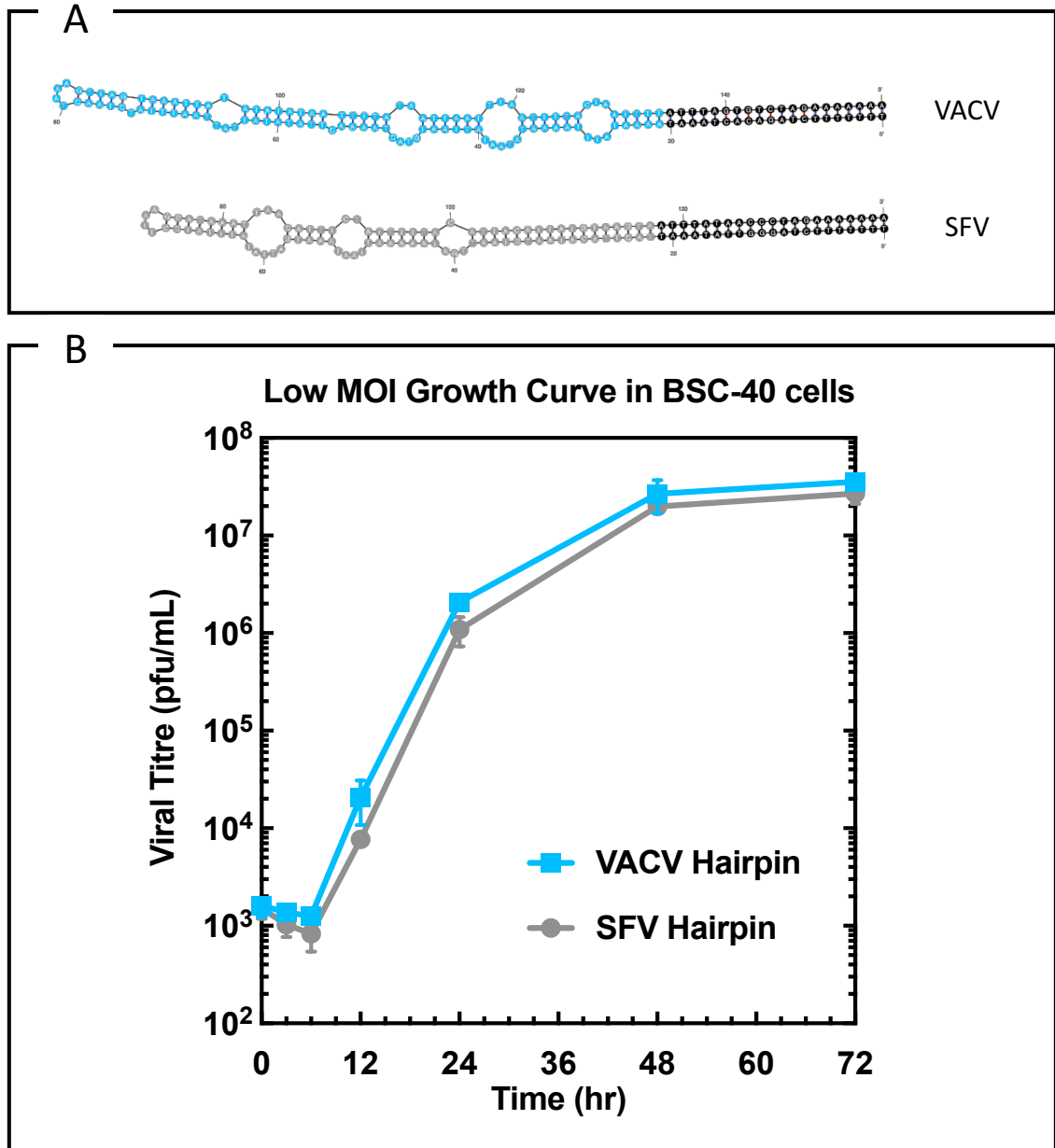


Figure 3.4. Substituting the SFV hairpin for the ScA2K hairpin does not affect viral growth.

(A) shows the difference in the predicted secondary structure of the S (WR) hairpin end of VACV and that of SFV. The computational structures were obtained using Mfold (183) and the black section represents the conserved concatemer resolution sites. (B) BSC-40 cells were infected with either ScA2K- Δ J2^{YFP/gpt}-S or ScA2K- Δ J2^{YFP/gpt}-SFV virus at an MOI of 0.01 PFU/cell. At different time points the cells were harvested and frozen. After three freeze/thaw cycles the samples were titered and plotted as shown. This data represents three independently done experiments. This figure was adapted and modified from Shenouda, M et al., 2022 (184)

3.4. The telomeric repeats of A2K virus are not essential

As previously noted, the synthetic virus that I reactivated lacked the 70bp repeats that were present in the original A2K sequence. However, when designing the left and right ITRs, the synthetic DNA fragments still included the 682bp of 125 and 54bp repeats (Figure 3.1B). Dr. Noyce's studies showed that omitting the 70bp repeats did not affect the ability to recover viruses, nor affect viral growth *in vitro*. However, we did not know what effect deleting the 125 and 54bp repeats would have on these viruses, especially because it would greatly decrease the distance between the first ORF and the hairpin ends. Thus, to delete this fragment from the virus, I used PCR to design and amplify a 1Kbp DNA fragment that would overlap with the first ORF within the ITRs (Figure 3.5A). I then ligated the hairpin ends and the WR DUP to the amplified DNA fragment. This ligated product was then used in the reactivation reaction. The reactivation products were expected to include the ligated fragment, the ITRs, and the seven other DNA fragments. For the reactivation of the virus to occur, the ligated PCR product must recombine with the ITR fragments resulting in the deletion of the 125 and 54bp repeats regions. I was able to reactivate a virus and confirmed its sequence using Illumina sequencing. I then generated a multi-step growth curve which showed that the resulting viruses exhibited no defects in growth (Figure 3.5B).

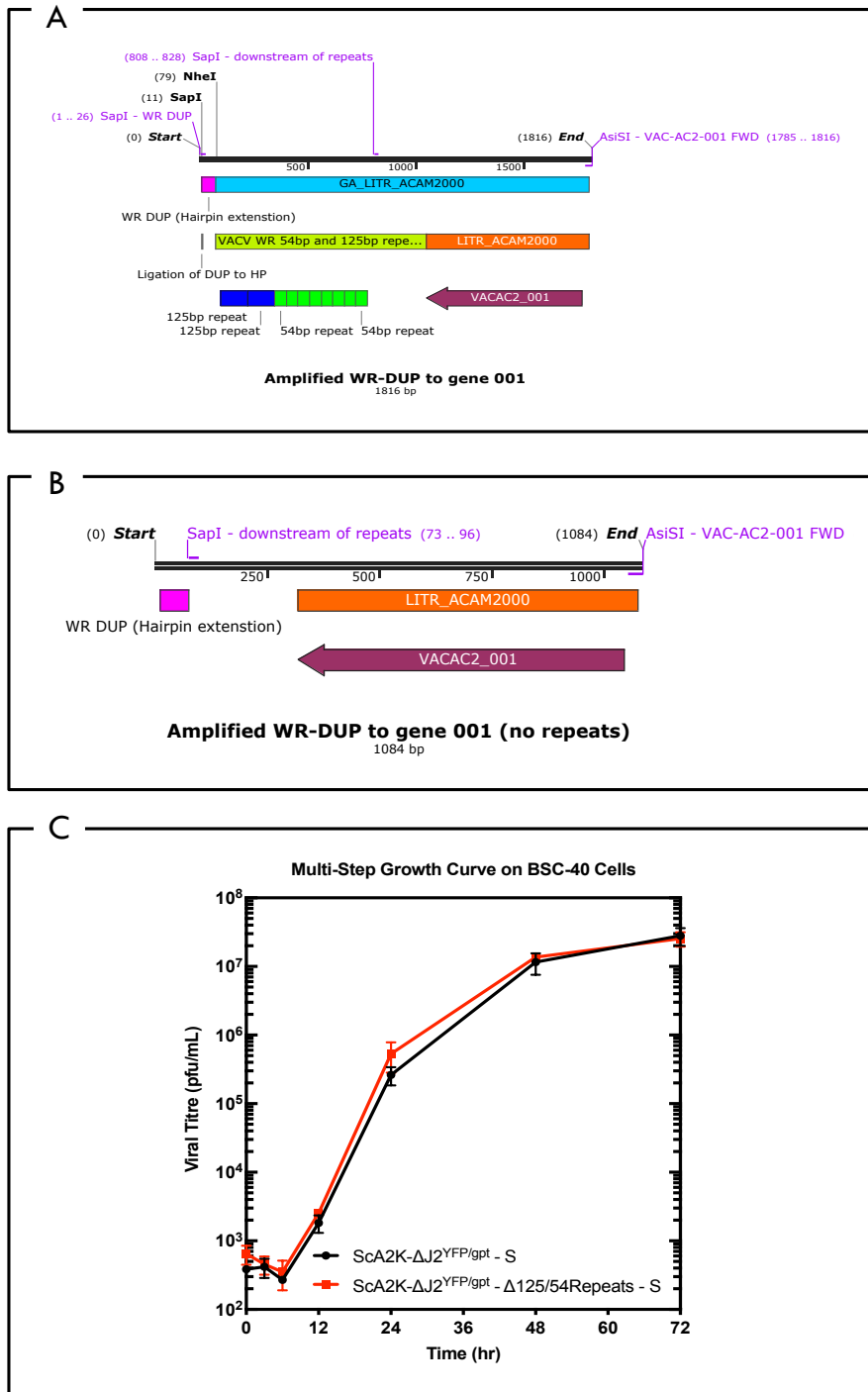


Figure 3.5. Deleting the 125 and 54bp repeats does not affect viral growth.

Panel (A) shows the position of the two primers that were used, flanking the first ORF (VACAC2-001), to amplify the 1Kbp fragment and delete the 125/54 repeats. (B) shows how the PCR product was then ligated to the WR hairpin extension (WR DUP) using the SapI sites. (C) BSC-40 cells were infected with either Sca2K-ΔJ2^{YFP/gpt}- S or Sca2K-ΔJ2^{YFP/gpt}-Δ125/54Repeats - S at an MOI of 0.01 PFU/cell, then the cells were harvested at different time points and frozen. After three freeze/thaw cycles the samples were titered and plotted as shown. These data represents three independent experiments.

3.5. Extra-helical loops are essential for viral viability and reactivation

The presence of extra-helical terminal loops is conserved among all the poxviruses where this has been examined. This points to the importance of their presence within the hairpin end. The mismatches may provide a degree of instability within the hairpin to allow for the formation of the cruciform Holliday junction within the replication cycle (Figure 3.3). They could also provide targets for telomeric binding proteins, such as I6 and I1, to bind to hairpin end (168, 176). To examine these questions, we first tested to see if we can reactivate a virus that did not encode extra-helical loops. To design this hairpin end, I deleted only the nucleotides that would not have a complementary bases on the second strand of the hairpin. This was done to retain as much of the sequence of the hairpin as possible while creating a fully base paired self-complementary form of the hairpin. This hairpin oligonucleotide, named S Δ 1-6, was completely complementary except for the terminal hairpin loop (Figure 3.6). The reactivation experiment was repeated three times and I was not able to recover a virus that lacked all extra-helical bases.

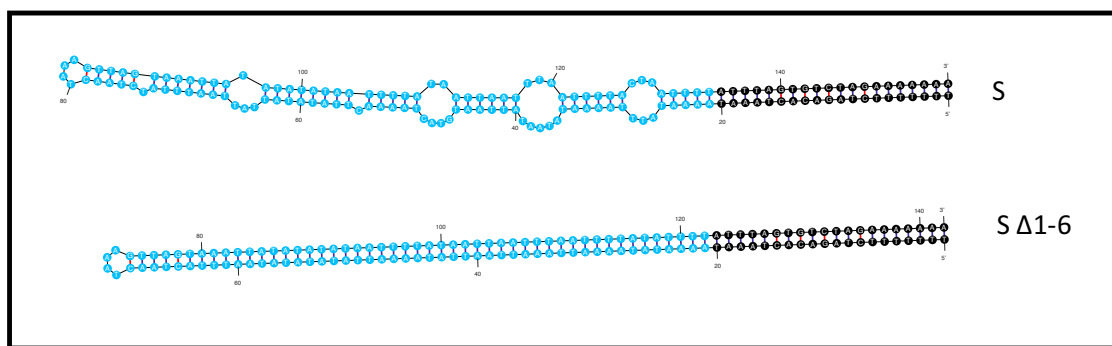


Figure 3.6. Design of a completely base-paired hairpin end.

The secondary structure of the hairpin oligonucleotide after deleting the extra-helical nucleotides of the S Δ 1-6 compared to the WT of hairpin S. The structures were modelled using Mfold (183).

3.6. Designing different hairpin ends by deleting extra-helical loops

My inability to reactivate a virus without any extra-helical loops suggests that they are essential for the reactivation of a virus. I next designed a series of different hairpin ends by deleting complete mismatched-loops (i.e., sequences located on both strands of each mismatched loop) and asking whether the number of extra-helical loops is important for viral viability. The WR S hairpin contained six different extra-helical loops, aside from the terminal loop, based on the computational structure obtained using Mfold (183). These loops were numbered 1 through 6, starting from the hairpin end loop as depicted in Figure 3.7A. I designed different hairpin ends, some with deletions close to the concatemer resolution site and some deletions closer to the terminal loop. The naming of the oligonucleotides was based on which loop has been deleted. For example, oligonucleotide SΔ6 lacks loop number 6 furthest from the terminal hairpin and SΔ4-6 lacks all three loops numbered 4, 5 and 6. Using a single-strand specific endonuclease, mung bean nuclease, to digest the loops, I confirmed that the predicted secondary structure of each hairpin corresponds with the digest produced by the nuclease (Figure 3.7B).

3.7. Reactivating viruses using different hairpin ends

I used these oligonucleotides to reactivate synthetic chimeric A2K virus bearing different hairpin ends. I could reactivate viruses using oligonucleotides that contained two or more loops (Figure 3.7A). However, for the oligonucleotides that only had one loop, only viruses harbouring the SΔ1Δ3-6 ends were recovered from the reactivation. Of the other two hairpin ends, one had only one nucleotide mismatch, and the other had loop number six which was furthest from the hairpin end. This led us to speculate that not only the number of nucleotide mismatches is important but also their position within the hairpin end. Moreover, our inability to recover virus from the SΔ2-6 that has only one nucleotide mismatch, coincides with previous reports showing that the telomere end binding protein I6 requires at least 2 or more nucleotide mismatches to bind to the hairpin (176). All the recovered viruses were sequenced to confirm the addition of their respective hairpin ends and the absence of any other mutations or substitutions.

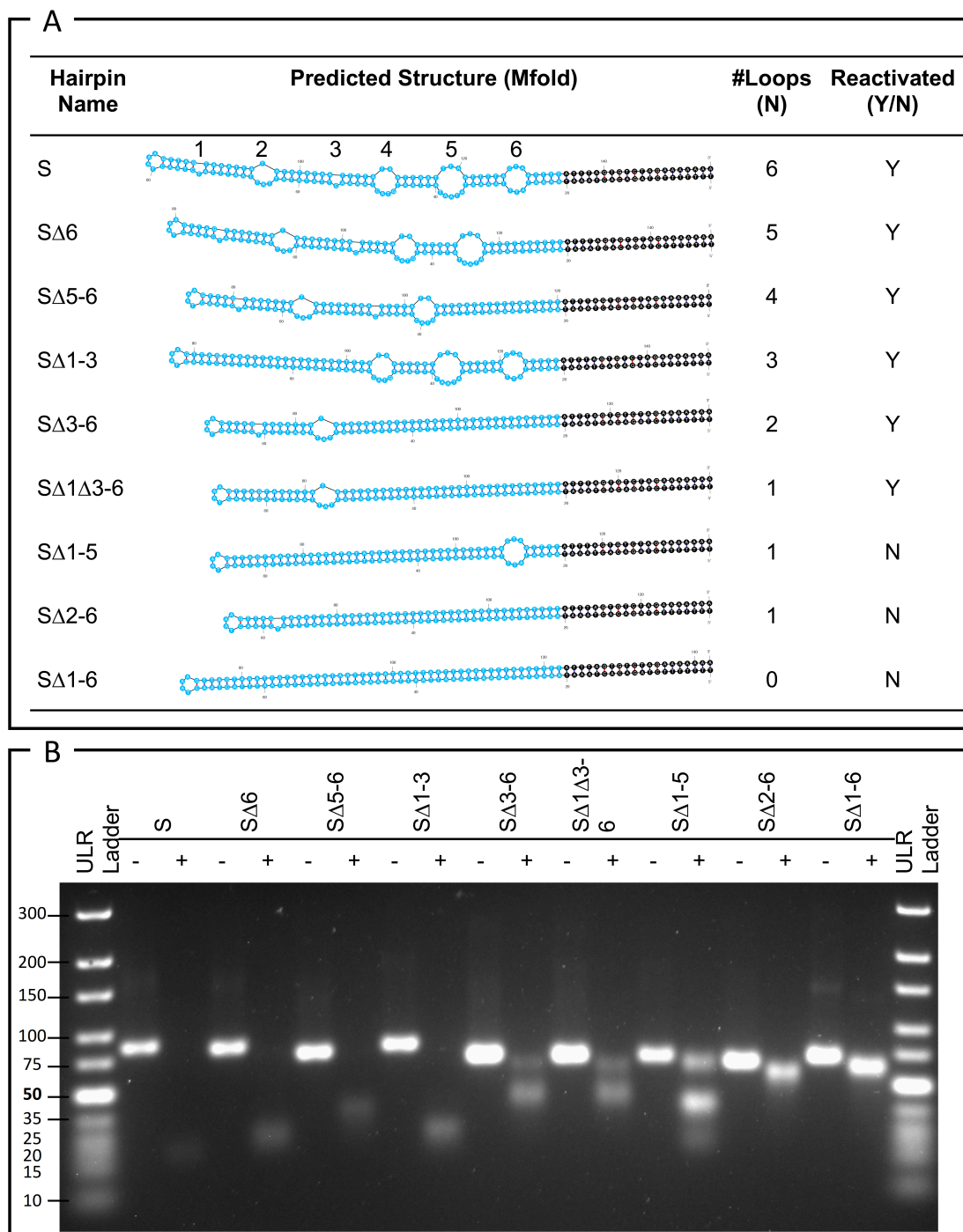


Figure 3.7. Hairpin oligonucleotide secondary structure.

(A) shows the different hairpin secondary structures, the number of extra-helical loops in each, and their reactivation status. (B) shows the products produced by nuclease digestion of the hairpins. The hairpin DNA was prepared by heating at 95°C then cooled on ice. The DNA, 0.5µg, was incubated for 1 hour with or without mung bean nuclease and then fractionated on a 4% agarose gel. The DNA ladder is an Ultra-Low Range marker made by Invitrogen. This figure was adapted and modified from Shenouda, M et al., 2022 (184)

3.8. The number of extra-helical loops affect virus fitness and growth

During the construction process I saw that viruses bearing fewer extra-helical loops seemed to be recovered in lower yields from the reactivation step. Therefore, to investigate the effects of the deletions on viral fitness I measured the ability of these viruses to grow on BSC-40 cells. A low MOI growth curve showed that decreasing the number of extra-helical loops caused a decrease in viral growth (Figure 3.8), suggesting that their number affects viral fitness. The one virus that showed the most significant growth defect, almost 20-fold, was the virus harboring only one loop hairpin, S Δ 1 Δ 3-6. Thus, for all the studies described in the following chapters, this virus, referred to as the mutant virus, was used to further investigate the effects of the loop deletions on the life cycle of the virus.

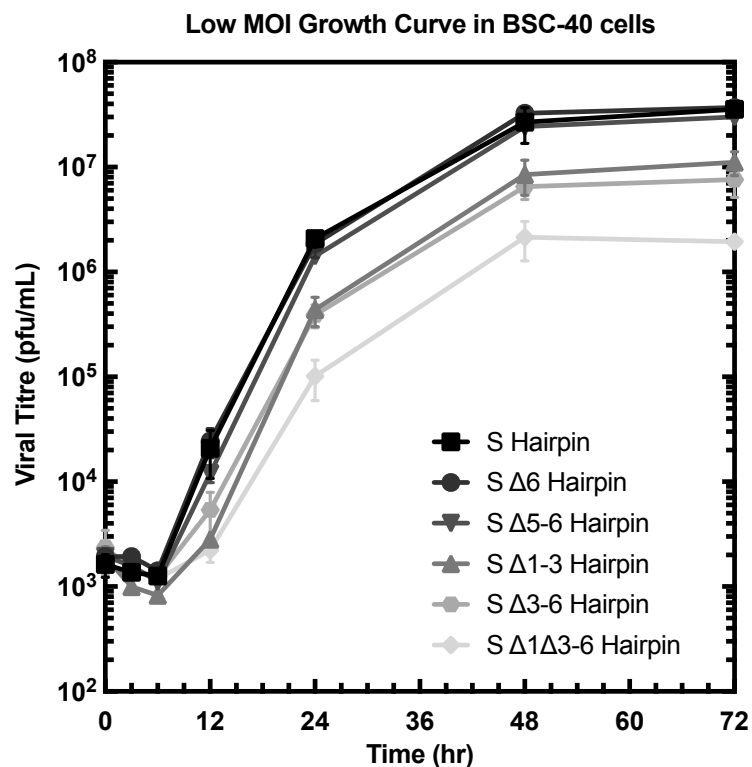


Figure 3.8. *The number of extra-helical loops within the hairpin ends affects ScA2K growth.*

BSC-40 cells were infected with the different viruses at an MOI of 0.01 PFU/cell, then the cells were harvested at different time points and frozen. After three freeze/thaw cycles the samples were titered and the virus yield plotted as shown. These data represent three independent experiments. This figure was adapted and modified from Shenouda, M et al., 2022 (184)

3.9. Increasing the GC content of the hairpin end does not yield a viable virus

The sequence of the hairpin ends of poxviruses are highly AT-rich. Based on this observation, we suspected that the base composition (or melting point) of the hairpin end is an important characteristic. To test that, I designed a GC-rich oligonucleotide hairpin substituting every adenine with a guanine and every thymine with a cytosine. However, I did not change the nucleotides within the extra-helical loops, nor change the sequence of the highly conserved concatemer resolution site. I then used a nuclease digest to confirm the presence of single-stranded loops within the hairpin (Figure 3.9B). My efforts to recover a virus bearing the GC-rich hairpin ends were unsuccessful. (Although I tried this experiment only once, I could still recover reactivated viruses from an experimental control that was performed in parallel and employed WT hairpin ends.) Finally, I tried to rescue a virus using a hairpin oligonucleotide based upon the telomeres of a recently sequenced alphaentomopoxvirus. This was also unsuccessful. The predicted structure of that hairpin end is unusual (Figure 3.9A), which raises the question of whether secondary structures other than just the presence of extra-helical loops and bases also affect viral fitness. It is also possible that the calculated secondary structure of this hairpin oligonucleotide, as drawn in Figure 3.9B, is inaccurate since the mung bean nuclease digest did not yield a 24bp piece of double stranded DNA bearing the concatemer resolution site (shown in black).

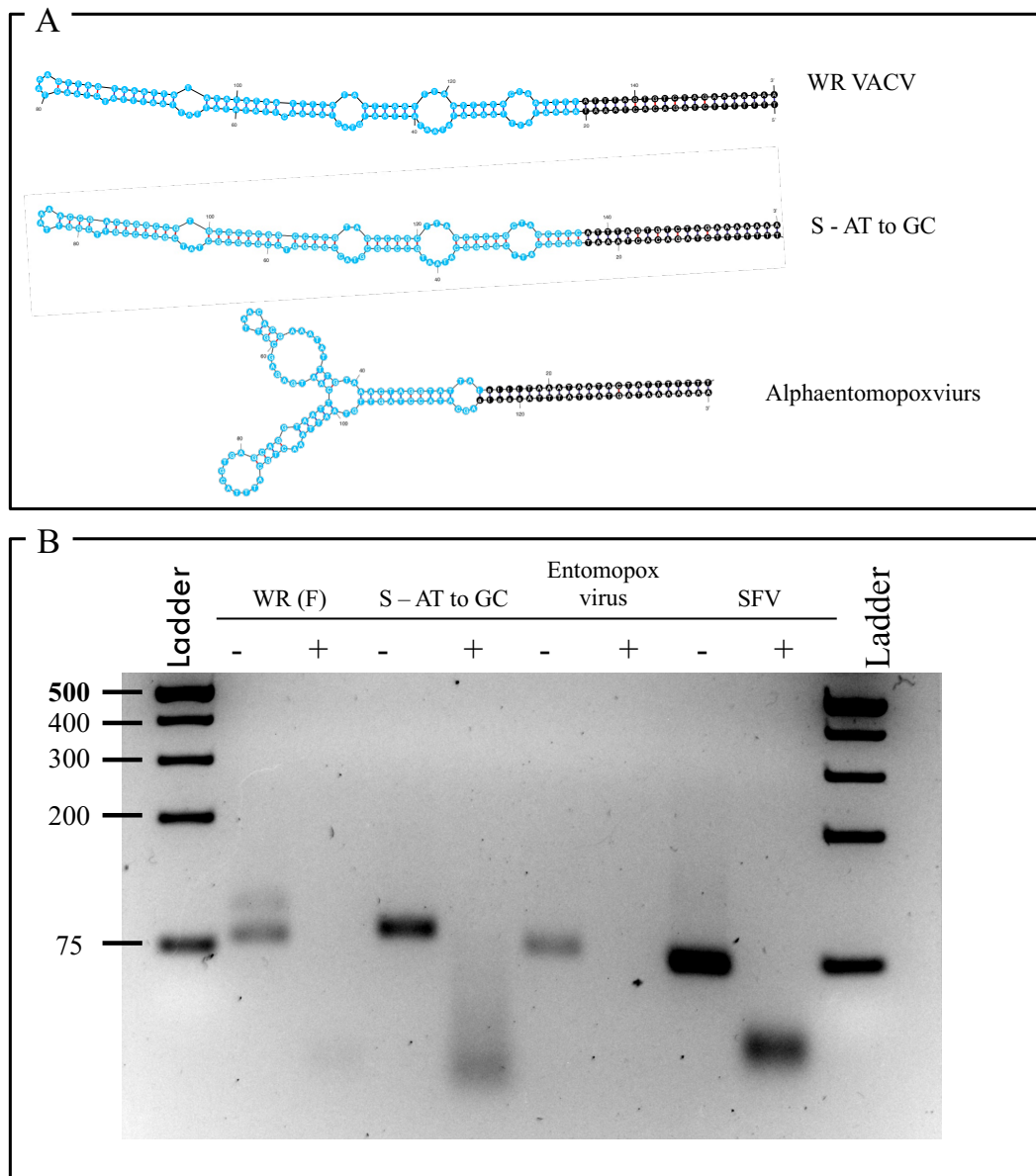


Figure 3.9. The secondary structure of novel hairpins.

Panel (A) shows the predicted secondary structure of the GC rich hairpin end as well as the alphaentomopoxvirus telomere that was sequenced and published in 2014 (183, 187). (B) shows a digest of the different hairpin oligonucleotides. The oligonucleotides were digested with mung bean nuclease for 1 hour with or without the nuclease, and then fractionated on a 4% agarose gel. A GeneRuler 1 Kb Plus DNA ladder from Thermo Scientific was used as a size standard marker.

Conclusions:

In this chapter I have shown that the extra-helical bases encoded in the hairpin ends of vaccinia virus serve an essential role. Progressively decreasing the number of these features creates growth defects that, beyond a certain point, are so severe as to preclude the recovery of mutant viruses. These data, along with data obtained using a chimeric virus encoding SFV hairpin ends, suggests that the presence of the extra-helical loops and their position within the hairpins, is far more important than the sequence, as long as the sequence is A-T rich. This study is the first of its kind in showing the importance of the hairpin loops within a poxvirus genome. In the next chapter, I will focus on the cause of the growth defect seen when too many of the mismatches are eliminated. I will specifically describe data examining the steps in the viral life cycle that could be affected by the deletion of the hairpin extra-helical loops.

Chapter 4:
Exploring the effects of hairpin mutations

Parts of this chapter of the thesis have been published as “Mira M. Shenouda, Ryan S. Noyce, Stephen Z. Lee, Jun L. Wang, Yi-Chan Lin, Nicole A. Favis, Megan A. Desaulniers, David H. Evans, The mismatched nucleotides encoded in vaccinia virus flip-and-flop hairpin telomeres serve an essential role in virion maturation. *PLoS Pathog.* **18** (2022), doi:10.1371/JOURNAL.PPAT.1010392.”

Contributions to this chapter:

MS - Development of methodology, performed experiments, writing and manuscript preparation

RN - Study supervision, conceptualization, development of methodology, technical and experimental assistance, funding acquisition, editorial revisions, manuscript preparation

SL, JW and YL - Methodology, technical & experimental assistance

DE - Study supervision, conceptualization, project administration, resources, editorial revisions, manuscript preparation

Special thanks to Mr. Quinten Kieser with his help during microscopy experiments, Dr. Brittany Umer for assisting with flow virometry protocol and Ms. S. Amidian for her assistance with the electron microscopy.

4. Chapter 4: Exploring the effects of hairpin mutations

Introduction and Summary:

In the previous chapter I described the effects of different hairpin mutations on the viability and fitness of VACV. I concluded that beyond a certain point, a decrease in the number of extra-helical loops greatly affects viral growth. Among the viruses that were significantly attenuated was the virus bearing SΔ1Δ3-6 hairpin ends. This virus showed the greatest decrease in yield over a multistep growth curve. Therefore, for this next chapter I focus on the effects of the SΔ1Δ3-6 mutant hairpins, on other aspects of the life cycle of the virus. I first investigated the effects on viral plaque size, replication, and concatemer resolution, and then examined viral maturation and the formation of infectious viral particles.

4.1. Tagging the virus with a fluorescent marker protein

To help visualize and study the effects of hairpin mutations throughout the viral life cycle, I needed to tag the viruses with an encapsidated fluorescent protein. The most efficient way to do this was to tag the A5 core protein with yellow fluorescent protein (YFP), since our laboratory already had a stock of VACV strain WR encoding YFP fused to the A5 N-terminus (*180*). The A5 core protein is found in all forms of viral particles, including immature, mature and enveloped particles, which allowed us to track the virus through all stages of infection. To be able to use the YFP tag I first had to delete the diffusible fluorescent marker from the TK locus. This was done by reinserting an intact copy of the J2R gene into the reactivated ScA2K-S and ScA2K-SΔ1Δ3-6 genomes using homologous recombination and selecting for non-fluorescent plaques. Homologous recombination was also used to insert the A5-YFP gene into these viruses. Briefly, I used PCR to amplify a fragment of DNA encoding A5-YFP from the recombinant WR strain and flanked with 500bp of homologous sequences. This DNA was then transfected into cells infected with ScA2K-S or ScA2K-SΔ1Δ3-6 viruses. After plaque purification, DNA sequencing was used to confirm that the A5-YFP gene was inserted into the A5L gene locus.

4.2. The S Δ 1 Δ 3-6 mutant virus has a decreased plaque size

When I reactivated the viruses with different hairpin ends, as described in section 3.7, I noticed a difference in plaque sizes. To quantify that difference, I infected BSC-40 cells with either S (WT) or S Δ 1 Δ 3-6 (mutant) viruses on ice for one hour to synchronize the infection and allow for binding of the viruses at 4°C. For this experiment, I used the A5-YFP tagged viruses to visualize the plaques during the infection. After an hour on ice, I overlaid the cells with semi-solid media containing carboxymethyl cellulose (CMC), returned the plates to the incubator and two day later the cells were fixed and stained with crystal violet. I then scanned the plates and used ImageJ (Fiji Version 2.0.0-rc-69/1.52p) (188) to measure the relative areas of 30 randomly selected plaques. The data show a visible and quantitative difference in plaque size between the mutant and WT viruses (Figure 4.1).

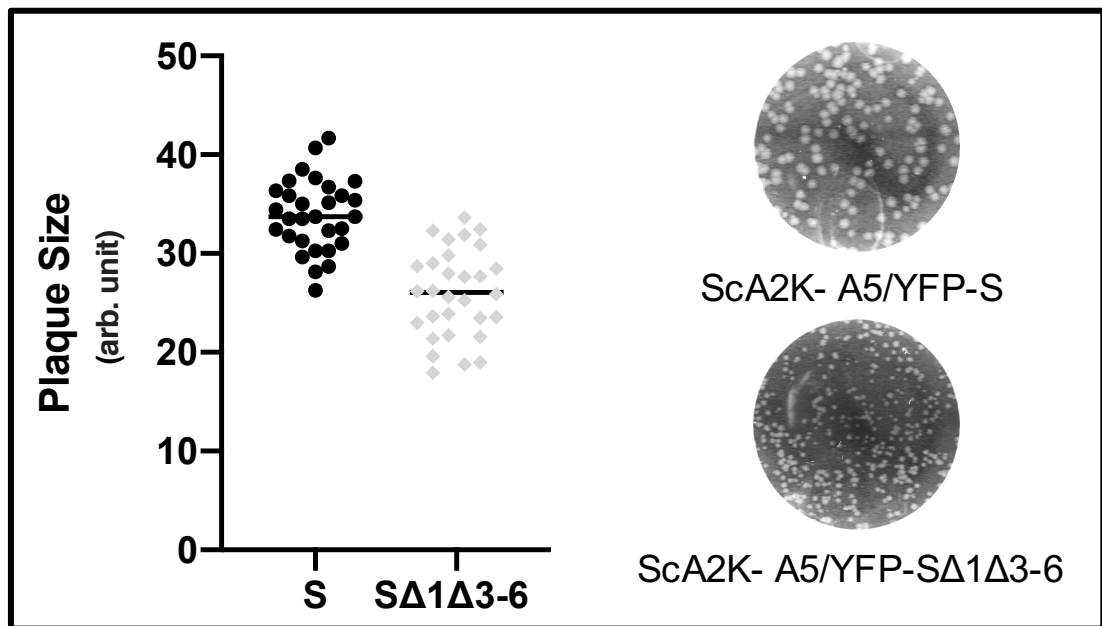


Figure 4.1: Mutant viruses exhibit a smaller plaque size phenotype.

BSC-40 cells were infected with either ScA2K-A5/YFP-S or ScA2K-A5/YFP- S Δ 1 Δ 3-6 viruses at 4°C for one hour. Warm media was added, and the cells incubated for 48 hours. After the cells were fixed and stained, the plates were scanned, and plaque areas were measured using ImageJ. The data were graphed using GraphPad Prism. A P value < 0.0001 was calculated using an unpaired t-test.

4.3. The hairpin mutations cause no defect in DNA synthesis

4.3.1. Genome copy number determined using the E9L gene

I first examined whether the growth defect was due to defective genome replication. I infected cells with either the ScA2K- Δ J2^{YFP/gpt}-S virus or the mutant ScA2K- Δ J2^{YFP/gpt}-S Δ 1 Δ 3-6 virus at a MOI of 3 PFU/cell. The cells were harvested at different times and a mix of cell and virus DNA isolated from whole cell lysates. Using qPCR, I quantified genome copy numbers using primers targeting the DNA polymerase gene (E9L). The E9L gene was used since it is commonly used to measure copy number (185). The data show no significant difference between the numbers of genomes formed over the course of a single-step growth curve in cells infected with mutant and control viruses (Figure 4.2). Thus, the defect is not explained by a difference in genome replication.

4.3.2. Genome copy number based on the C23L gene

To confirm the data obtained above, I also designed primers that amplify sequences encoding the C23L gene. The C23L gene is the first/last ORF encoded within the viral ITRs, the closest gene to the hairpin ends. It has been suggested that the hairpin ends might encode origins of replication (125) and we were concerned that these mutations might more greatly affect the replication of DNA located near telomere ends compared to the replication of genes like E9L which are closer to the centre of the genome. I then used the same DNA isolated in the previous experiment and qPCR to calculate the C23L-based genome copy numbers. Again, there was no significant difference between the genome copy numbers measured within cells infected with virus harboring the S hairpin versus the mutant S Δ 1 Δ 3-6 hairpin (Figure 4.2).

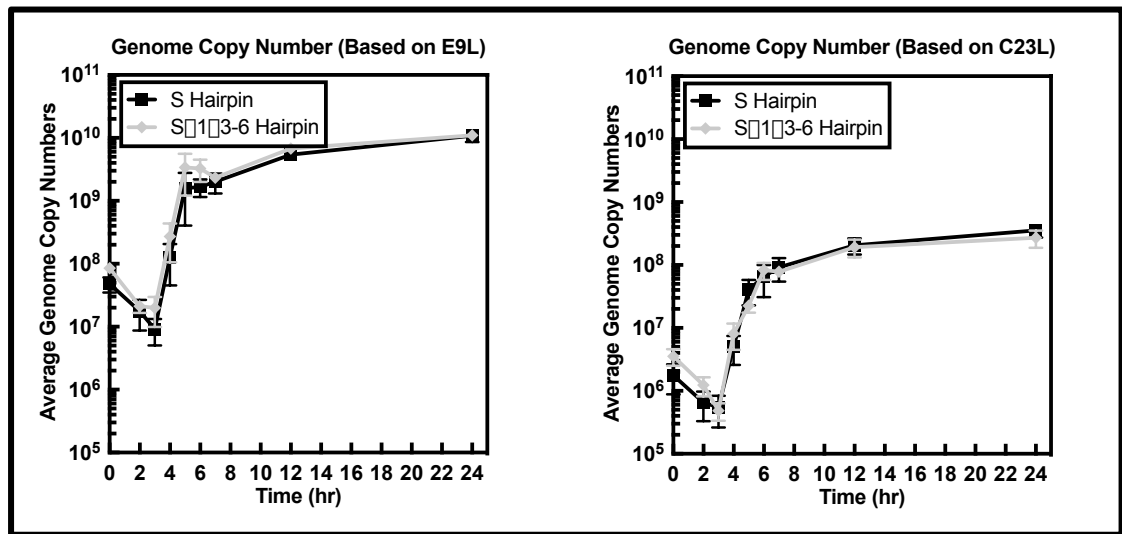


Figure 4.2: Mutant and WT viruses replicate DNA equally well.

BSC-40 cells were infected with the indicated viruses at MOI of 3 PFU/cell, and samples of whole cell DNA were retrieved and purified at different time points. The genome copy number was calculated using qPCR and primers designed to amplify 150bp of either the E9L or C23L genes. The genome copy numbers were calculated based on standard curves obtained using known concentrations of the E9L and C23L 150bp gene blocks. Part of this figure was adapted and modified from Shenouda, M et al., 2022 (184)

Interestingly, the absolute copy number of both samples differed depending upon whether the qPCR targeted the E9L *versus* C23L gene (Figure 4.2). I tested whether this phenomenon is due to C23L being so close to the hairpin end, that the “snapback” DNA is interfering with the denaturation/annealing PCR step. To do so, I digested the 24-hour samples with *EcoRI* or *EcoRI* + *NheI*. The first (*EcoRI* alone) would digest the DNA at 58 sites but keep C23L linked to the hairpin while the latter deletes the hairpin from DNA encoding C23L (along with another 10 sites). The DNA was purified using QIAEXII beads (QIAGEN) and qPCR was performed using either E9L or C23L primer sets. Undigested samples (without the post-digestion purification step) were used as a control. The difference between samples cut with *EcoRI* and *EcoRI* + *NheI* was not substantial and did not explain the difference seen between the undigested samples, using E9L or C23L (Figure 4.3). Any treatment with *EcoRI* +/- *NheI* eliminated the differences in copy number measured with the two different primer sets (Figure 4.3). This suggests that the difference between E9L and C23L qPCR data is due to some differences relating to sample preparation, purity, and/or qPCR efficiency rather than an absolute difference in

the genome copy number. Regardless of the reason(s), the data showed that there is no significant difference in the amounts of replication, between the WT virus with S hairpins and mutant virus with SΔ1Δ3-6 hairpins.

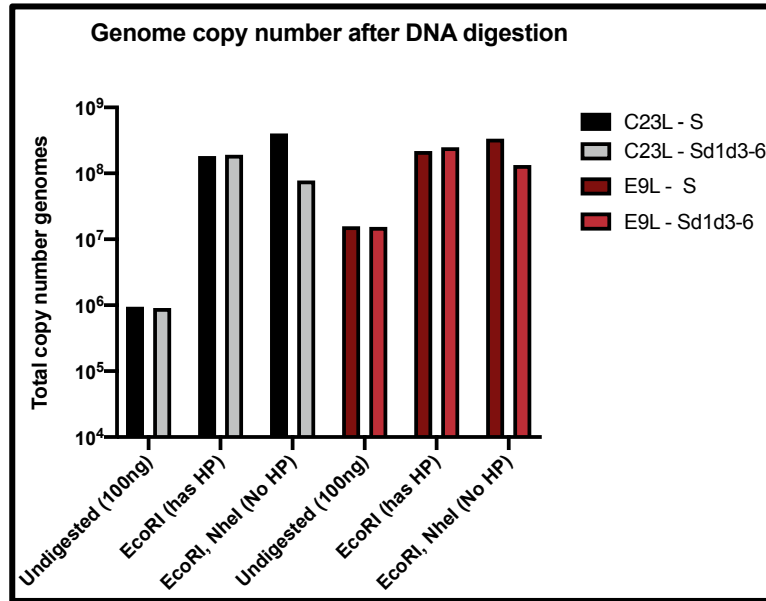


Figure 4.3. Sample preparation affects the measurement of genome copy number.

The samples prepared for Figure 4.2 were either undigested, digested with EcoRI or digested with EcoRI + NheI. The digested samples were further purified using a QIAEXII PCR purification kit by QIAGEN. Genome copy numbers were determined using qPCR and primers targeting the C23L (black/grey) or E9L (maroon/red) genes.

4.4. Telomere resolution is not affected by the mutant SΔ1Δ3-6 hairpin

I next tested if the hairpin mutant virus exhibits a defect in concatemer resolution. The DNA isolated for the DNA replication studies, in section 4.3, was digested with Alw44I restriction enzyme. This enzyme cuts the genome at 11 sites and yields a 2.25Kbp piece encoding the telomeres. If the junctions between the ends of the newly replicated concatemeric genomes are not resolved into mature hairpins, the size of the unresolved fragment is 4.5Kbp (as depicted in Figure 4.4A). Mature hairpins produce fragments half that size (2.2Kbp). After digestion, I sized the DNAs on an agarose gel, transferred the DNA to a membrane, and blotted with a probe targeting sequences encoding the terminal end region. These experiments followed a protocol supplied with a North2South

Chemiluminescent kit (Thermofisher). I tried three different ways to generate the labeled probe. In one I used Biotin-16-dUTP (added at a 40:60% ratio with dTTP) in a PCR reaction to generate the labelled probe. I also used a Bio-Nick Labeling System (Invitrogen) to nick translate a PCR product or plasmid as probes. The PCR method worked best as illustrated by dot blotting against 3 μ g of DNA using a Bio-Dot SF apparatus (Figure 4.4B).

I then used the PCR labeled probe and Southern blots to examine the kinetics of telomere resolution. These data showed that both viruses could resolve the concatemer junction and I did not observe any obvious delay in resolution (Figure 4.4C). The data thus far suggested that the growth defect was not due to a defect in replication or concatemer resolution.

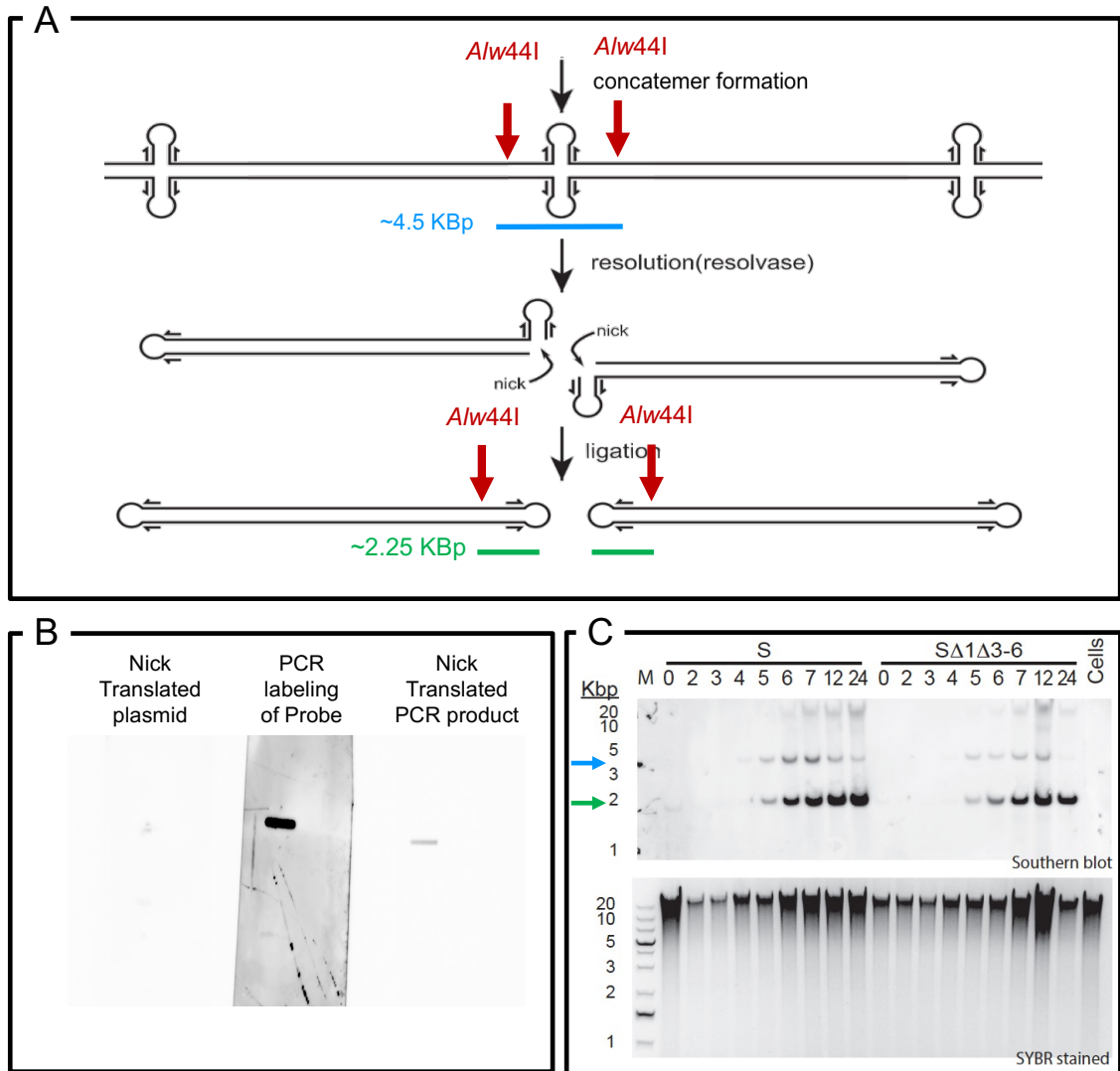


Figure 4.4. Concatemer resolution is unaffected by hairpin mutations.

Panel (A) shows the principle behind the assay for concatemer resolution. The junction is flanked by Alw44I sites and resolution converts a 4.5Kbp fragment to two 2.25Kbp pieces. The figure was adapted and modified from H. Li et al. (126). (B) Different labeling methods yielded different quality probes. All three membranes were imaged simultaneously and using the same exposure time. The PCR labelling method proved best. (C) DNA was extracted from infected BSC-40 cells at the indicated times, digested with Alw44I, fractionated on 0.8% agarose gel, SYBR stained and imaged (lower image), and then transferred to a membrane, Southern blotted and reimaged (upper image). The arrows indicate the fragments encoding the unresolved concatemer junction (4.5Kbp – blue arrow) and the mature telomeres (2.25Kbp – green arrow). Part C of this figure was adapted and modified from Shenouda, M et al., 2022 (184)

4.5. Stocks of SΔ1Δ3-6 hairpin mutant viruses contain increased amounts of defective particles

4.5.1. Using Flow virometry to detect difference in particle count

While preparing viral stocks, I noted that stocks of the mutant viruses were always cloudier than stocks of the WT virus, when adjusted to contain the same concentration of PFU/mL. To investigate whether the cloudiness is due to an increase in particle count, I used flow virometry as a method of counting viral particles.

First, I prepared new stocks for both the mutant and WT viruses simultaneously to eliminate bias from sample preparation. Briefly, I infected BSC-40 cells using an MOI of 0.01 PFU/cell and after 48-72 hours I harvested both samples. Using the protocol described in Chapter 2, I lysed the infected cells using a Dounce homogenizer, and then used a sucrose cushion to separate the virus particles from most of the cellular nuclear debris. The stocks were titered and adjusted to contain equal titers of virus (although these studies were limited by the fact that the highest concentration of the mutant that could be obtained was 4×10^8 PFU/mL.) I then diluted these partially purified stocks of virus and fixed them using 4% PFA. Ten-fold serial dilutions of the samples were prepared and analyzed using a Beckman Coulter CytoFLEX flow cytometer. Using violet side scatter, I was able to detect and resolve particles as small as 100nm. The flow virometry data showed that stocks of the hairpin mutant virus contained a much high number of particles per mL compared to the control virus, when adjusted to contain the same number of PFU/mL. This suggested that the mutant stocks contained higher number of defective particles.

By running different dilutions through the flow cytometer, I noticed that at higher particle concentrations the particle number per mL plateaus, suggesting that an upper limit of detection is reached at higher concentrations. To get an accurate representation of the particle/PFU ratio for the mutant versus the WT virus, I repeated the experiment with multiple different dilutions of virus (Figure 4.5A). This allowed us to get a more accurate representation of the particle/PFU ratio by eliminating a bias caused by underestimating or overestimating particle counts. The lower limit of detection was highly depended on the background particle count within the blank sample and appears to be caused by dust or other cell debris left in the samples (Figure 4.5D). These data showed that the

cloudiness seen in the mutant virus preparations is due to an increase in particle count compared to the WT sample at the same infectious concentration. These experiments were repeated with different viral stocks (Figure 4.5B) and using the viruses expressing A5-YFP as that permitted detecting viral particles using both violet side scatter and virus-borne YFP using the FITC channel (Figure 4.5C). The lower limit of detection was much lower using the A5-YFP viruses because when gating on the FITC-positive viral particles, we eliminated any background impurities if they did not fluoresce in the FITC channel. This was also seen when we stained DNA within viral particles with SYBR Gold, which will be described in the next section. The results obtained showed similar patterns and an average fold difference of 12 between the WT and mutant particle/PFU ratio (Figure 4.5E).

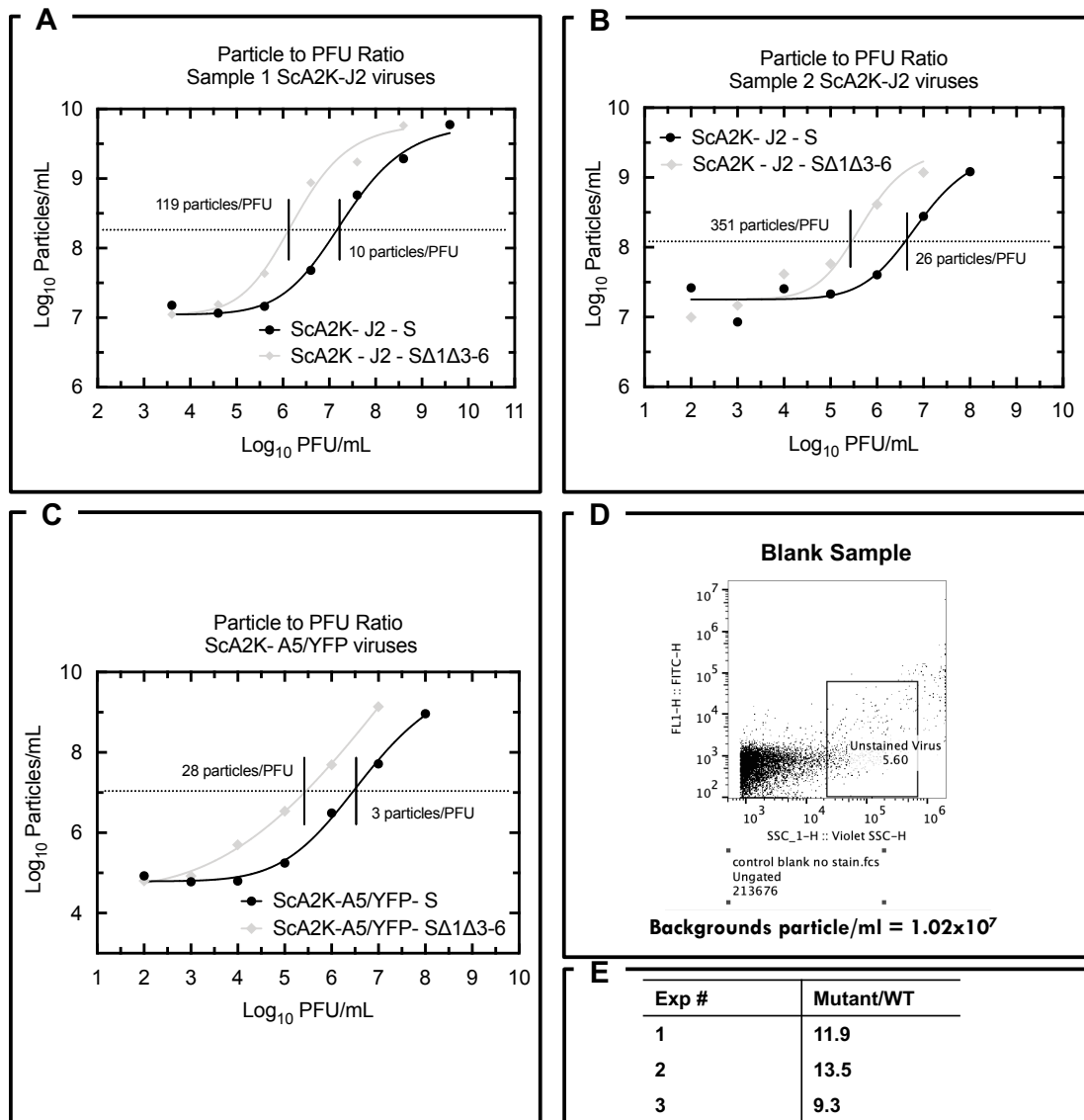


Figure 4.5: The hairpin mutant (*SΔ1Δ3-6*) virus exhibits a 12-fold higher particle/PFU ratio compared to WT virus.

The figures show data acquired using flow virometry experiments. The viral particles were diluted, fixed in 4%PFA then analyzed using a Cytoflex Cytometer (Beckman). The data were analyzed using FlowJo and the tabulated numbers were graphed using GraphPad Prism. (A-C) Three different viral samples were analyzed. The data were graphed, and a non-linear fit of a sigmoidal curve was used to calculate the particle/PFU ratio for each experiment. (D) A flow dot plot of a blank sample showing that back calculation of the background particle count is 10^7 which is the lower limit of the graph in (A). (E) shows the fold difference between the mutant and WT particle/PFU ratio in three different experiments. This was calculated by dividing the particle/PFU ratios calculated in the experiments depicted in A-C of hairpin mutant virus by the WT virus. This figure was adapted and modified from Shenouda, M et al., 2022 (184)

4.5.2. Using fluorescence microscopy to visualize difference in particle count

To obtain visual confirmation of the above data, I used fluorescence microscopy to image the A5-YFP-labeled viral particles. Briefly, I incubated the viruses on fibronectin coated coverslips for one hour at room temperature (166, 186). I then removed the media and fixed the slides in 4% PFA for 30 min, then mounted the coverslips onto a slide and imaged the samples using an OMX super resolution microscopy (Deltavision). The data showed that in samples prepared using viruses diluted to 10^7 PFU/ml, there are more particles in the hairpin mutant virus compared to the WT virus. In fact, visually, the numbers of particles in the mutant sample more closely resembled the numbers seen in the WT sample at 10^8 PFU/ml dilution (Figure 4.6).

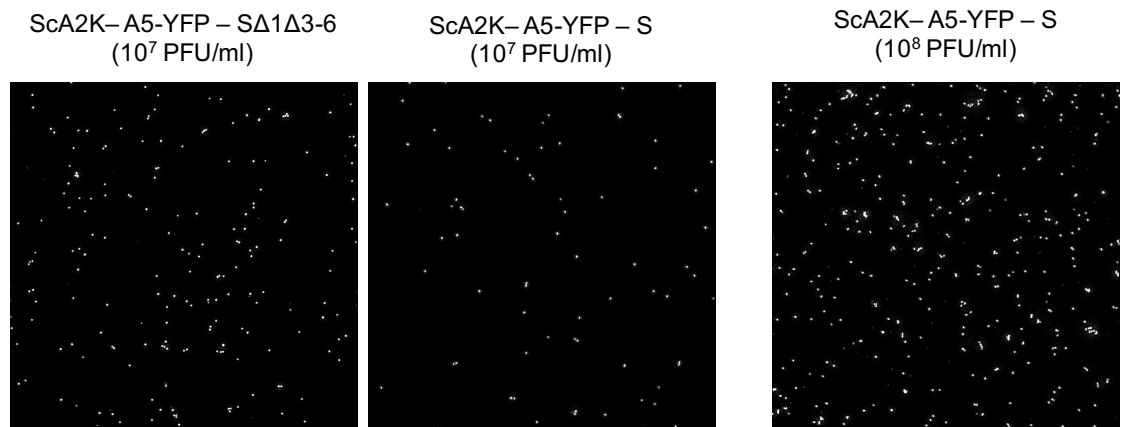


Figure 4.6. Microscopy images showing the increased particle concentration in the mutant viral stocks compared to WT.

The figure shows a visual representation of the difference in particle number between the mutant virus, ScA2K-A5/YFP-SΔ1Δ3-6, and the WT virus ScA2K-A5/YFP-S. Each viral inoculum at the same PFU/mL were bound to fibronectin coated cover slips, fixed, and imaged using an OMX super resolution microscopy (Deltavision). The image on the right shows the WT virus at 10× higher PFU concentration. The signal detected was the A5-YFP signal on the FITC channel.

4.6. The defective particles in the hairpin mutant virus contain DNA

4.6.1. Using flow virometry to detect DNA packaging

I also used flow virometry to look at the DNA packaging efficiency of the hairpin mutant virus compared to the WT virus. Virus samples were diluted, fixed, and then treated with SYBR Gold for 30 min on ice to stain any DNA within the viral particle. The results showed that less than 2% of virus-sized particles remained unstained by SYBR Gold (Figure 4.7A). This suggested that DNA packaging into virions was unaffected by the mutant hairpins. Because the stained particles were gated away from the debris, the lower limit of detection in stained particles was 10^6 particles/mL (Figure 4.7B-C) compared to 10^7 particles/mL in the unstained samples (Figure 4.5A-B). Nonetheless, whether the samples were stained for DNA or not the fold difference of particle/PFU ratio between the mutant and control viruses remained the same at an average of 12-fold difference.

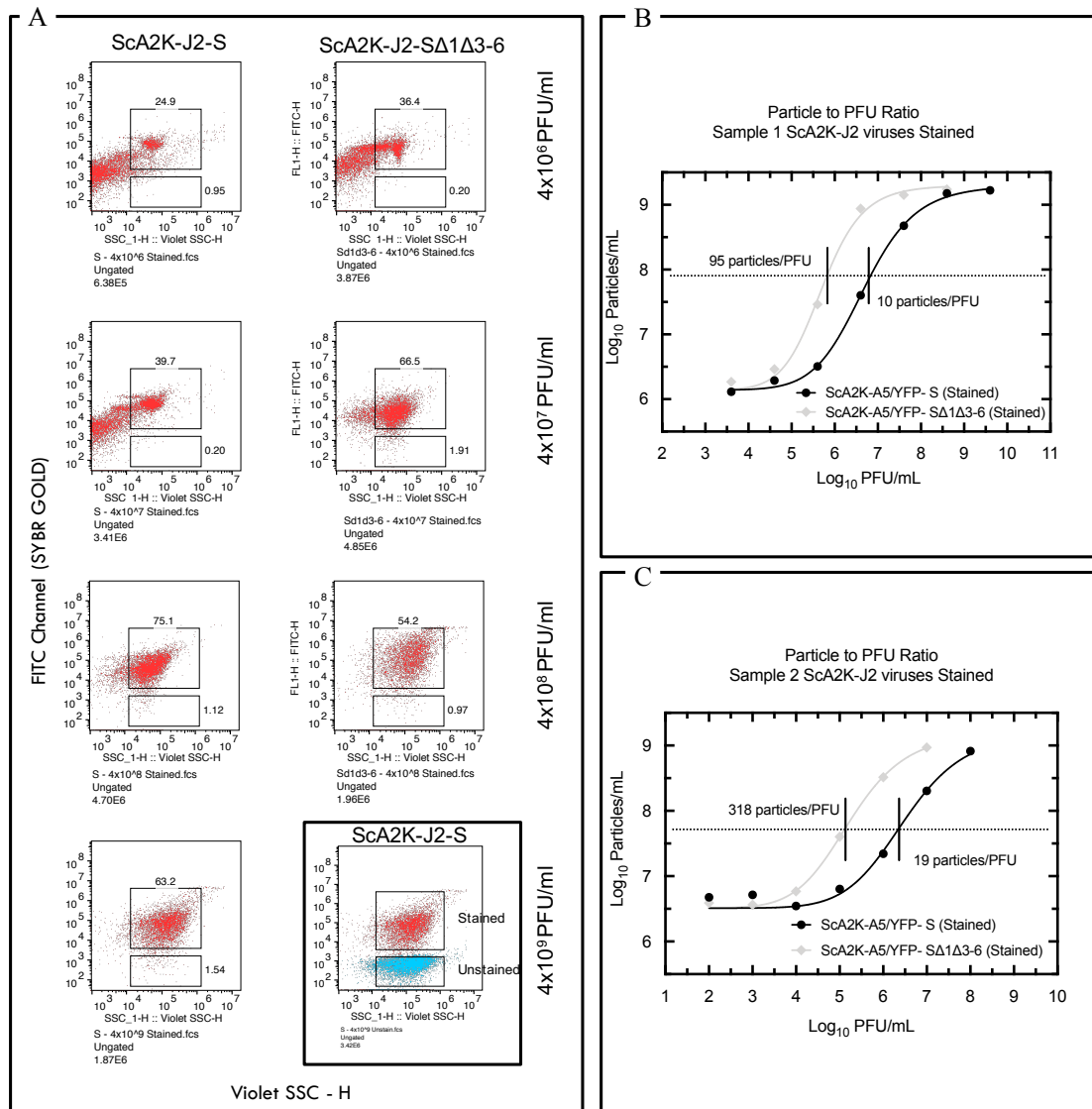


Figure 4.7. Greater than 98% of viral particles are stained with SYBR Gold.

Panel (A) The figure shows flow dot plots of viral particles stained with SYBR Gold. The unstained gate (bottom axis in each plot) was determined using the unstained samples analyzed alongside the stained samples and the vertical boundaries of the gates captured poxvirus-sized particles of >180 nm. The figure shows different dilutions (in PFU/mL) of the samples from each virus. The highest PFU obtained for the mutant virus was 4×10^8 PFU/mL, thus there was no sample analyzed that concentration. The bottom right figure in Panel (A) shows the 4×10^9 Pfu/mL WT sample overlaid with the unstained sample (blue). (B-C) Two different viral samples were analyzed using SYBR Gold staining and flow cytometry. The data were graphed, and a non-linear fit sigmoidal curve was estimated to calculate the particle/PFU ratio. This figure was adapted and modified from Shenouda, M et al., 2022 (184)

4.6.2. Using qPCR to detect DNA packaged in viral particles

To further address the DNA packaging question, I used qPCR to measure the number of genome copies within known numbers of infectious plaque forming units. I titered the viruses and then isolated DNA from different dilutions of these viruses. Quantitative PCR and E9L primers were then used to measure genome copy number in each sample. Because the extraction step can cause the loss of unknown quantities of DNA, I also performed the qPCR adding 2 μ l of diluted but intact viruses to each PCR reaction. The data acquired in both experiments were very similar and showed that all of the viruses contained packaged DNA but there was a 4-7-fold difference between the WT and mutant when one considers the relative ratio of PFU to E9L copy number (Figure 4.8). There are some data points at the higher and lower concentrations that do not fit the curves, probably because these fall outside the range where PCR can provide an accurate measure of DNA levels or is affected by inhibitors in the samples. Nonetheless, the data still show that the mutant viral stocks contain relatively higher quantities of DNA-containing defective particles.

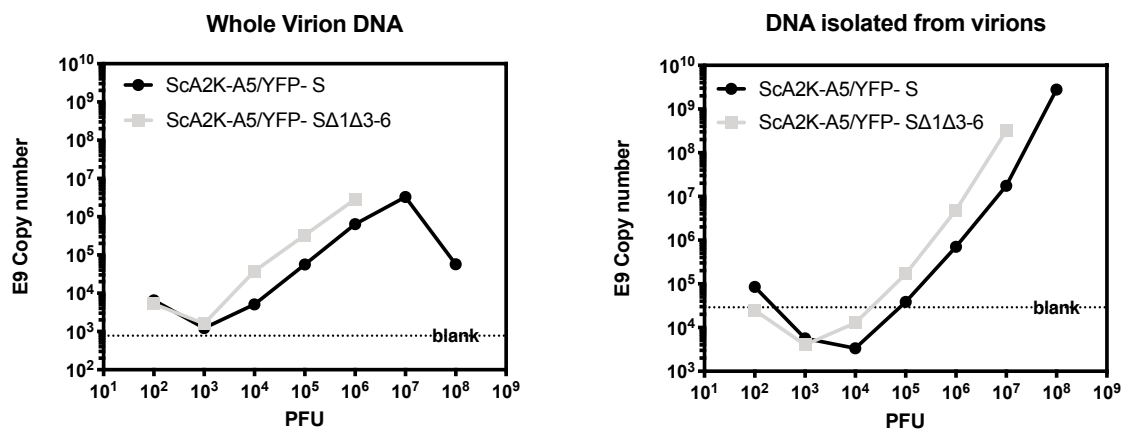


Figure 4.8. *The mutant viral particles contain relatively more DNA when normalized to PFU.*

Either whole virions or DNA isolated from virions were used for qPCR to calculate the genome copy number. The data shows the mutant virus stock contained a greater quantity of DNA at the same PFU. The lower limit of detection was estimated from the blank sample. This figure was adapted and modified from Shenouda, M et al., 2022 (184)

4.7. The formation and assembly of a D13 lattice is not affected by the hairpin mutations

During poxvirus assembly a protein lattice is formed around membranes that are destined to become the mature virus envelope. These first appear as crescent-shaped structures, and then the growing lattice promotes formation of empty immature virions. DNA is then packaged into a spherical virion particle. The lattice consists of D13 trimers which further assemble into hexamers and then into a honeycombed spherical structure. After the formation of the immature virion, the D13 scaffold is lost, and the maturation process begins, leading to the formation of the mature, infectious, and classic brick shaped particles. To study whether there is a defect in the assembly or turnover of that D13 lattice, I infected cells with either WT or hairpin mutant virus, fixed the cells at different time points, and then stained for D13 using rabbit polyclonal antibodies (generously provided from Dr. Bernard Moss). Our results showed that there is no defect in D13 expression, formation of the D13 rings, nor the turnover of D13 during the maturation process. This suggested that the defect lay in a step downstream of immature virus particle formation (Figure 4.9 – blue arrows). Moreover, like the WT virus, the mutant virus also forms inclusion bodies of D13 at 24 hours post infection (Figure 4.9 – yellow arrows).

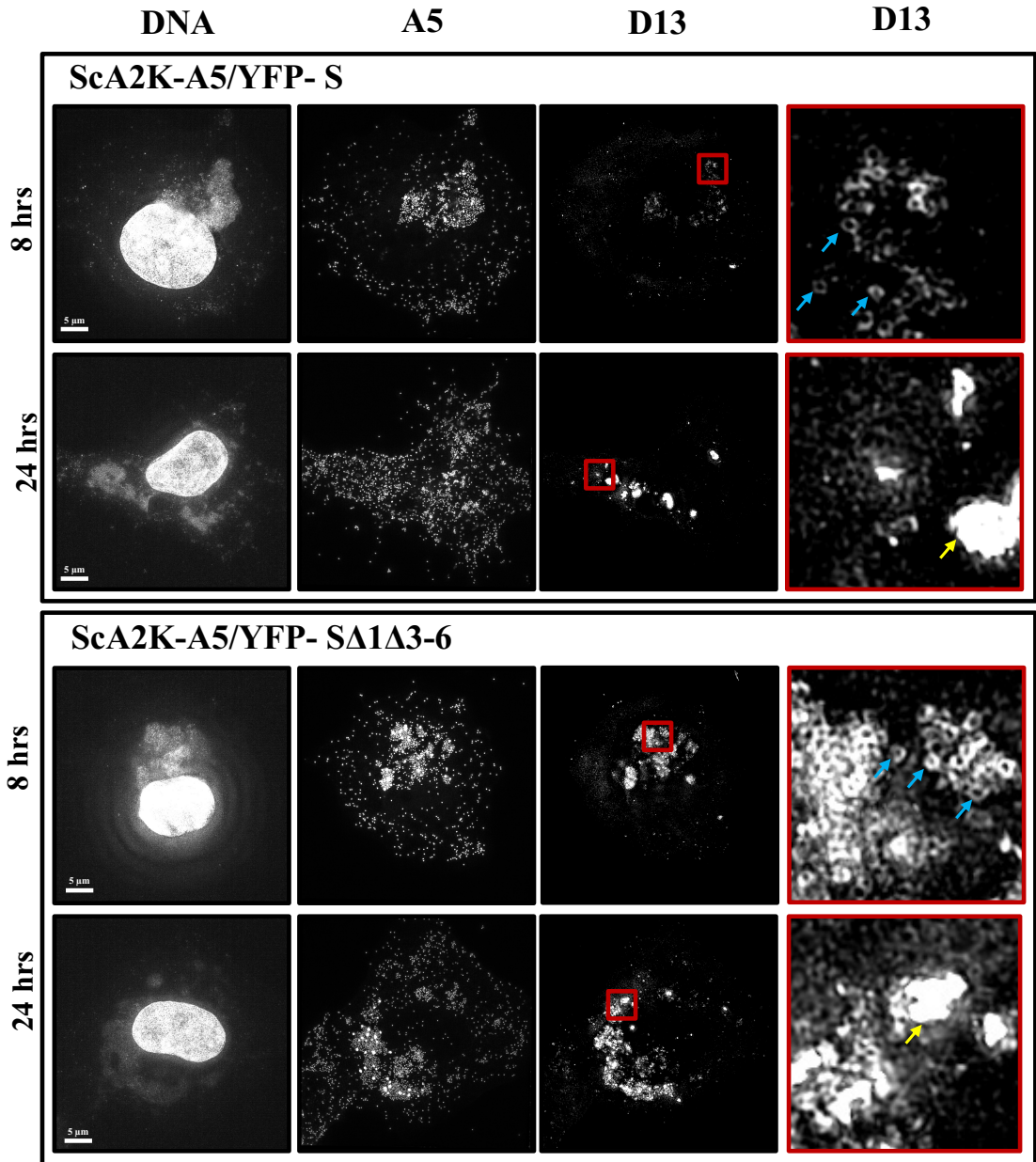


Figure 4.9. There is no alteration in D13 expression or lattice formation.

BSC-40 cells were infected with either ScA2K-A5/YFP-S or ScA2K-A5/YFP-SΔ1Δ3-6 viruses. At different time points the cells were fixed, incubated with a primary polyclonal antibody against D13 followed by secondary antibody directed against the rabbit antibody. Hoechst dye was used to stain DNA and the cells were imaged using an OMX super resolution microscope (Deltavision). The last columns show a magnified field of the D13 channel. This shows the rings formed by D13 within the viral factory (blue arrows) as well as the inclusion bodies that are seen at 24hr (yellow arrows).

4.8. Localization and expression of other viral proteins during an infection

I also stained the infected cells for other proteins to look at the overall effects of the hairpin mutations on the viral life cycle. These included an envelope protein, B5, that can be used as a marker for intracellular enveloped virions and the single-stranded DNA binding protein, I3, that is expressed throughout the infection. The envelope protein B5 formed ring structures as seen in both the WT and mutant virus infections at 24 hours (Figure 4.10). As for the I3 protein, the data shows that there is no delay in the I3 expression between the viruses (Figure 4.11). Thus, there is no apparent difference of expression between the WT and hairpin mutant of either B5 or I3.

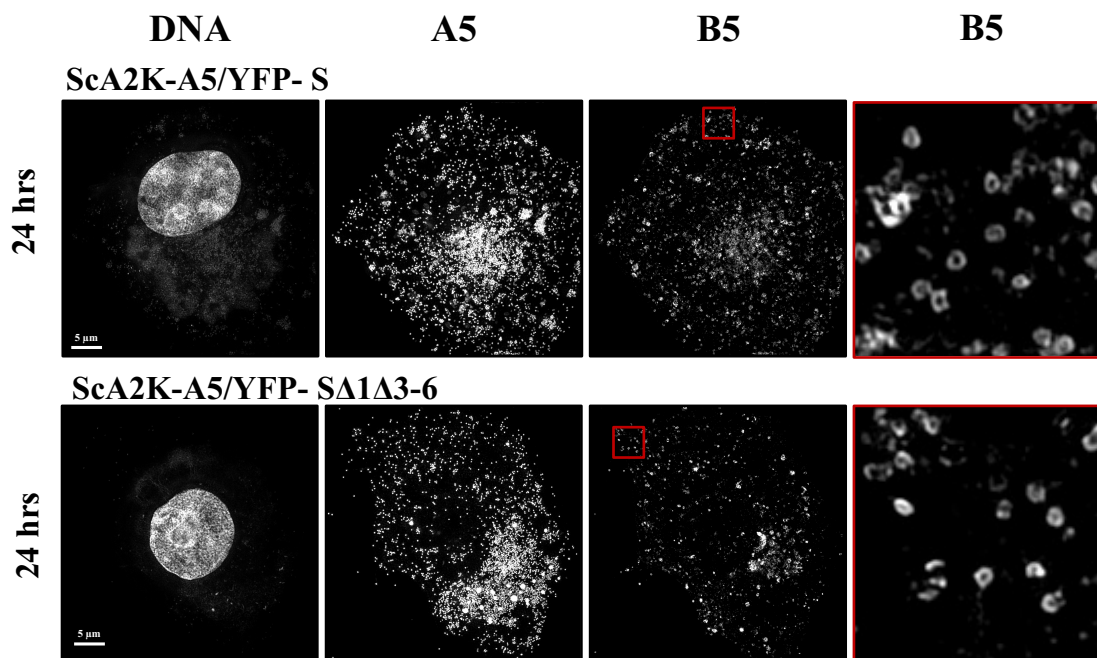


Figure 4.10. *The behavior of the B5 envelope protein is unaffected by hairpin mutations.*

BSC-40 cells were infected with either of the two viruses and cultured for 24 hours. The cells were then fixed and incubated with a monoclonal mouse antibody directed against B5, and then stained with Hoechst and a secondary antibody against mouse mAb. The last column shows a magnified image of the B5 channel showing the B5 rings.

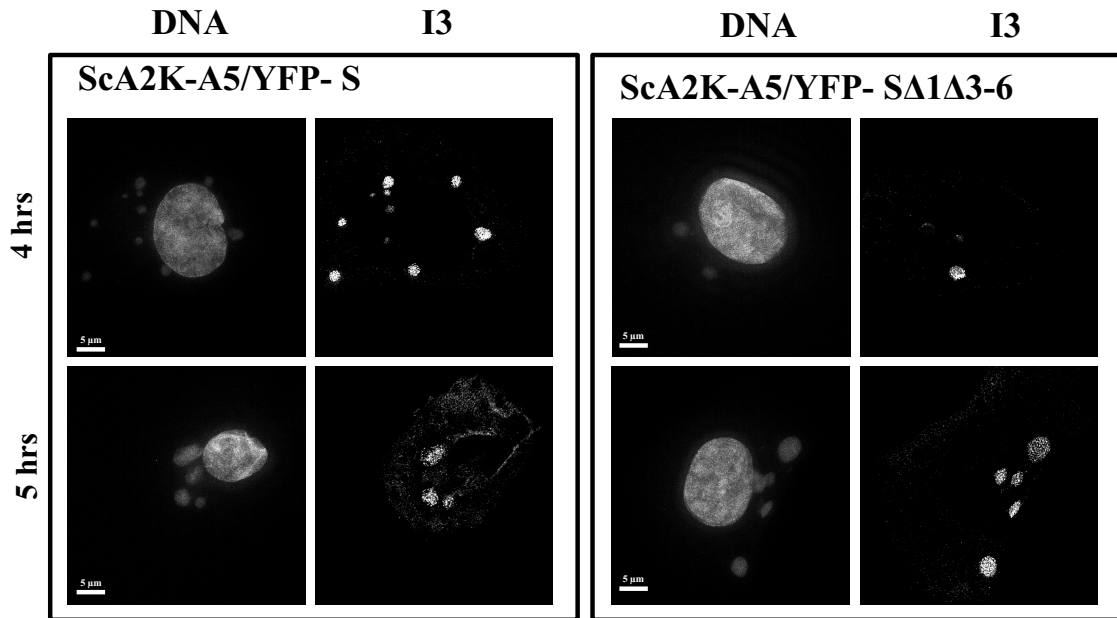


Figure 4.11. The expression of I3 single stranded DNA binding protein is unaffected by the hairpin mutations.

BSC-40 cells were infected with either of the two viruses, then fixed and incubated with a monoclonal mouse antibody directed against I3. The cells were then stained with Hoechst dye plus a secondary anti-mouse mAb antibody. I3 appears to be expressed at comparable levels and shows a similar distribution pattern within the viral factories at four and five hours post infection in cells infected with WT and hairpin mutant virus.

Interestingly, the A5-YFP core protein formed aggregates in cells infected with the mutant virus and imaged 24hr post infection (Figure 4.12 – red arrows). The appearance of these aggregates might indicate a defect in viral core assembly, perhaps causing the accumulation of unbound and unpackaged A5-YFP protein. One can also see that at 2 hr post infection, there were much greater numbers of A5-YFP-labeled particles in cells infected by the mutant virus compared to almost no signal in cells infected with the control virus (Figure 4.12). A5 is a late protein that begins to be expressed five to six hours post infection (87). The cells were infected with equal numbers of infectious particles (MOI = 3 PFU/cell) and so the signal that is seen at two hours post-infection is likely because there are many more YFP-tagged but non-infectious viral particles in the mutant viral stock.

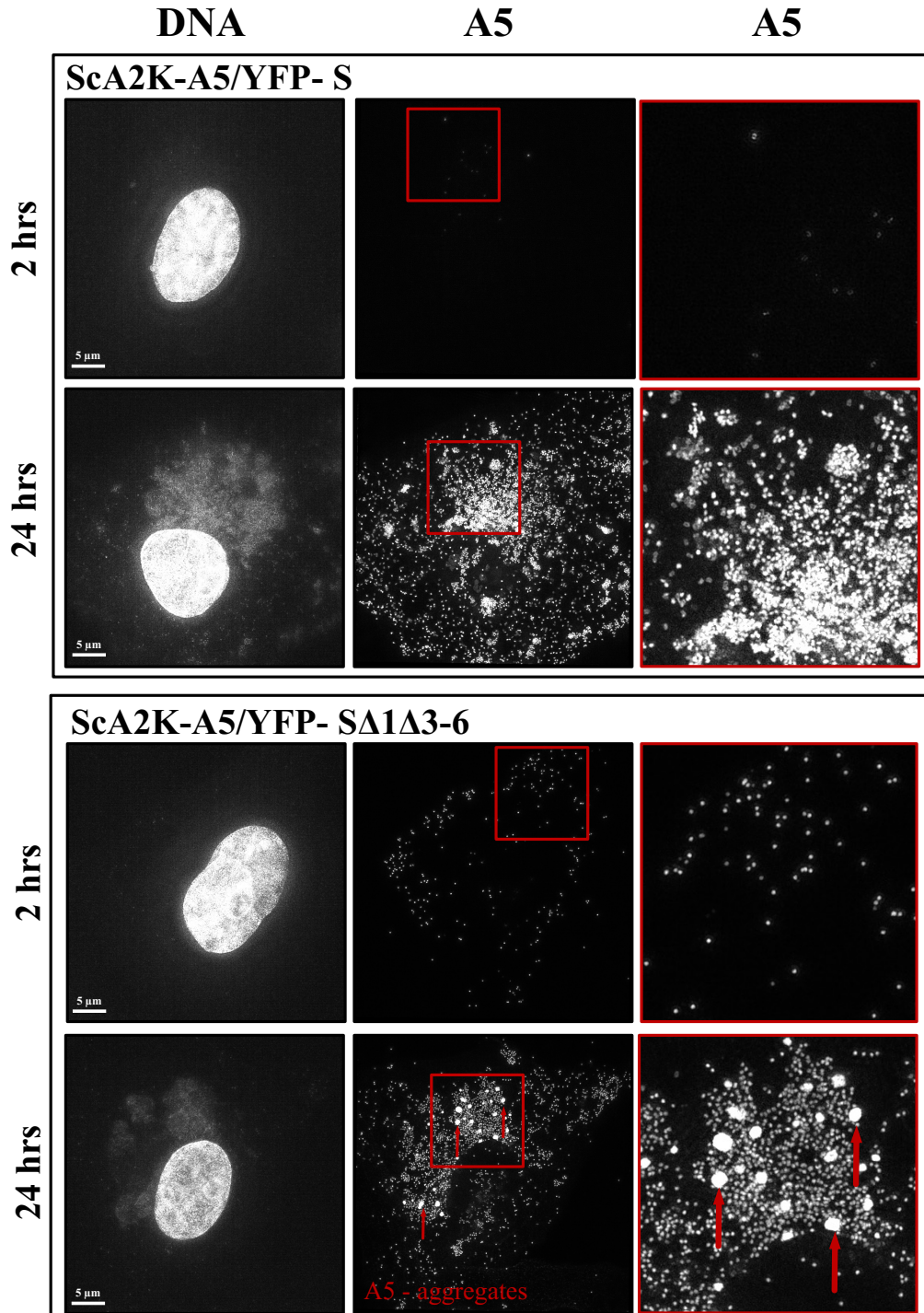


Figure 4.12. The hairpin mutations cause formation of A5-YFP protein aggregates by 24 hours post infection.

BSC-40 cells were infected with the indicated viruses and then fixed and stained for DNA using Hoechst stain. Aggregates of the A5-YFP core protein (red arrows) are seen at 24 hours post infection (bottom panels) and these are much more abundant in cells infected with the mutant virus.

4.9. The SΔ1Δ3-6 mutant virus exhibits a defect in a late maturation step

Lastly, I used electron microscopy (EM) to study viral entry, and the structures of viruses present at 24 hours post infection, and after virus purification.

4.9.1. Presence of immature virions at viral entry

BSC-40 cells were infected with either mutant or control virus for 1hr on ice, to promote virus attachment, and then warm media was added. Thirty minutes later the cells were scraped off the dishes, fixed in a pellet, and processed for EM imaging. These experiments were conducted with the help of Drs. Noyce and Lin, and the EM imaging and processing was performed in the Faculty of Medicine & Dentistry imaging facility at University of Alberta by Ms. Sara Amidian.

These thin sectioned images showed many immature round viral particles attached to the edges of the cells in the hairpin mutant infected samples (Figure 4.13, blue arrows). The same thing was seen in cells infected with WT virus, but the particles exhibited typical mature brick-shaped structures including a darker dumbbell-shaped core (Figure 4.13, red arrows). We also noted that many more particles were seen surrounding the cells infected with mutant viruses, which was not unexpected since although the cells were infected with a MOI of 10 PFU/cell, this was not corrected for the 10-12-fold greater particle numbers in the hairpin mutant sample. This showed that the viral particles in the hairpin mutant samples are of the immature morphological form, which would account for the increase in viral particles and decrease in the infectivity of the virus.

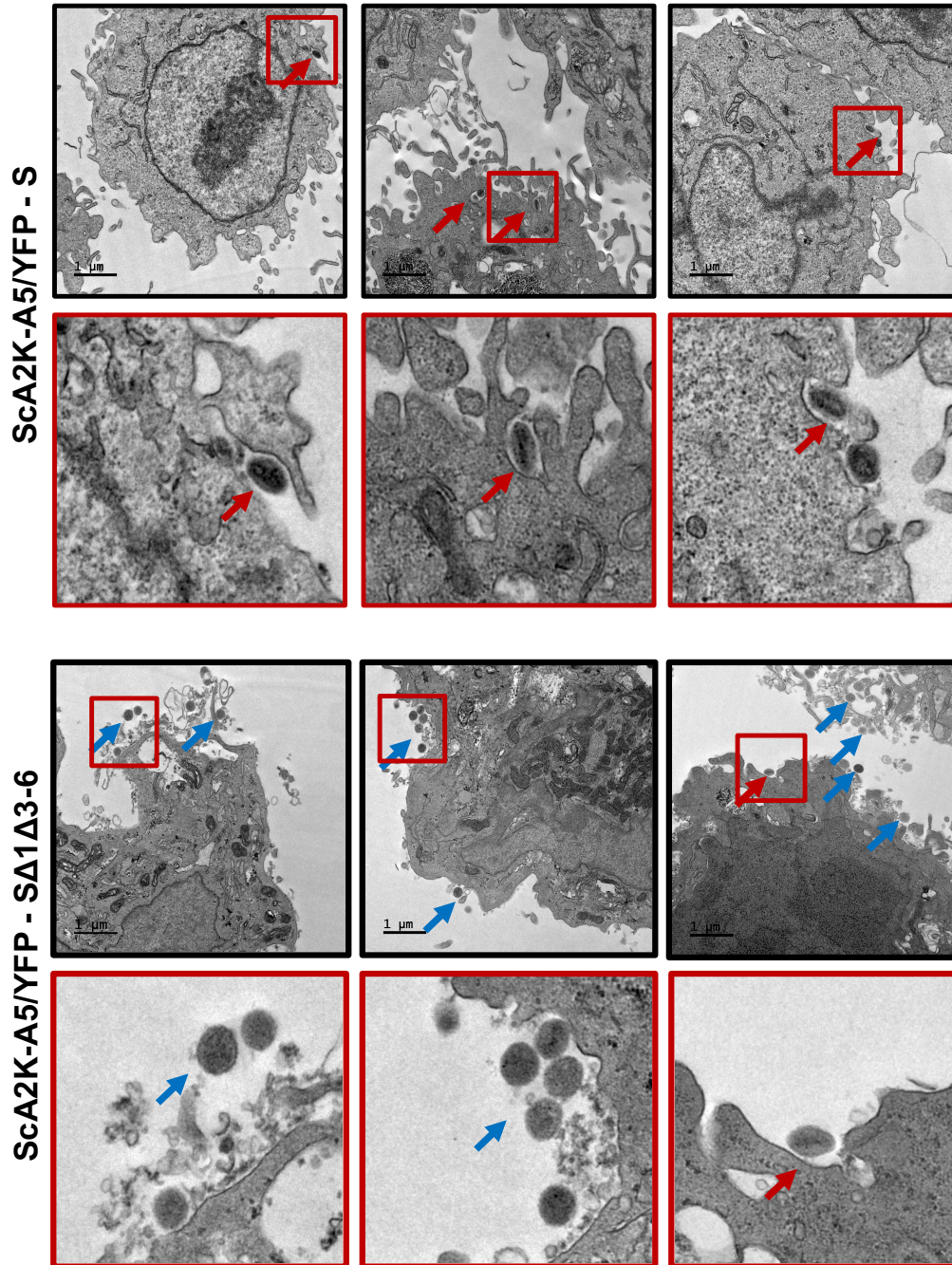


Figure 4.13. Immature virions are seen during the entry stage of infection by hairpin mutant virus.

BSC-40 cells were infected at MOI of 10 PFU/cell with the indicated viruses. After 1hr at 4°, warm media was added to the cells and then they were incubated for another 30 min at 37°. The cells were then scraped into the media, fixed, and processed for EM imaging by embedding in plastic, thin sectioning, and staining. The round immature particles are indicated with the blue arrows and the mature particles are depicted by the red arrows. The red boxes represent a magnified field within the image above it. The samples were prepared with the help of Drs. Noyce and Lin and then processed and imaged by Ms. Amidian.

4.9.2. An abundance of immature viral particles are seen at 24 hours post infection

The cells were cultured on ACLAR sheets for 24 hours and then infected with virus at a MOI of 3 PFU/cell for 24 hours. At that point they were fixed, sectioned, and processed for EM. The EM images showed a greatly increased proportion of round immature viral particles in the cells infected with a hairpin mutant virus compared to the WT virus. We also rarely detected any mature virions in cells infected with the S Δ 1 Δ 3-6 hairpin mutant virus, while these were the predominant form seen in cells infected with WT virus. This suggests that there is a defect in the maturation process that converts immature virions into mature virions (Figure 4.14). This experiment was repeated twice with similar outcomes observed. The defect in viral assembly and maturation would account for the increase in the particle-to-PFU ratio detected in stocks of the S Δ 1 Δ 3-6 hairpin mutant virus.

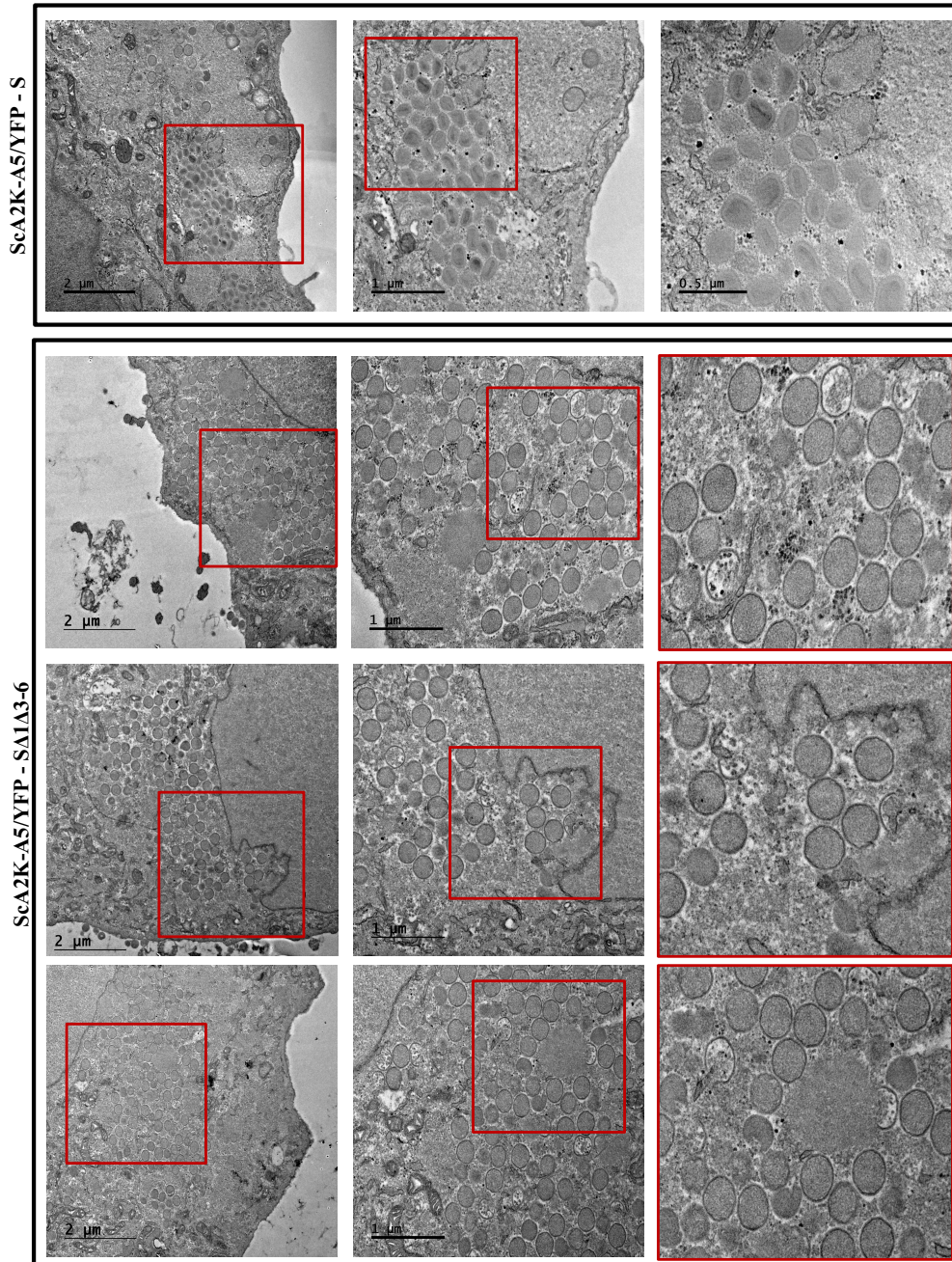


Figure 4.14. Cells infected with mutant viruses contain a greater proportion of IV particles.

BSC-40 cells were infected with a MOI of 3 PFU/cell of either WT or mutant virus. After 24 hours, the cells were fixed and processed for imaging by EM. The top panel shows an example of a cell infected with WT virus. Most of the viral particles exhibit a mature morphology (MV) although a few are round immature virions (IV). The bottom panels show cells infected with the S Δ 1 Δ 3-6 mutant virus containing mostly round immature particles (IV). The images with red outline are digitally magnified. Samples were processed for EM and imaged by Ms. Amidian. This figure was adapted and modified from Shenouda, M et al., 2022 (184)

4.9.3. Mutant viral stocks contain mostly immature virions

Finally, we used EM to look at the virus particles that are found in extracted viral stocks. This confirmed that the abundance of round immature viral particles seen within infected cells creates stocks of viruses containing large numbers of defective particles. Dr. Lin grew the viruses on BSC-40 cells, purified them using sucrose cushions and these stocks were then fixed, embedded in agarose and processed for EM imaging by Ms. Amidian. The data were analyzed and calculated by Drs. Lin and Evans. These data provided a visual confirmation that stocks of the hairpin mutant virus contained increased amounts of immature round particles, containing only a small percentage of mature virus forms. (Figure 4.15). By counting the spherical and brick-shaped particles, it was found that about 97% of the particles in the hairpin mutant viral stock comprised the spherical, immature form of the virus. In contrast, the WT viral stock is composed of 96-98% mature virions. These studies show that a 12-fold decrease in infectivity, and increase in defective particles, can be attributed to a defect in morphological processing of the virus.

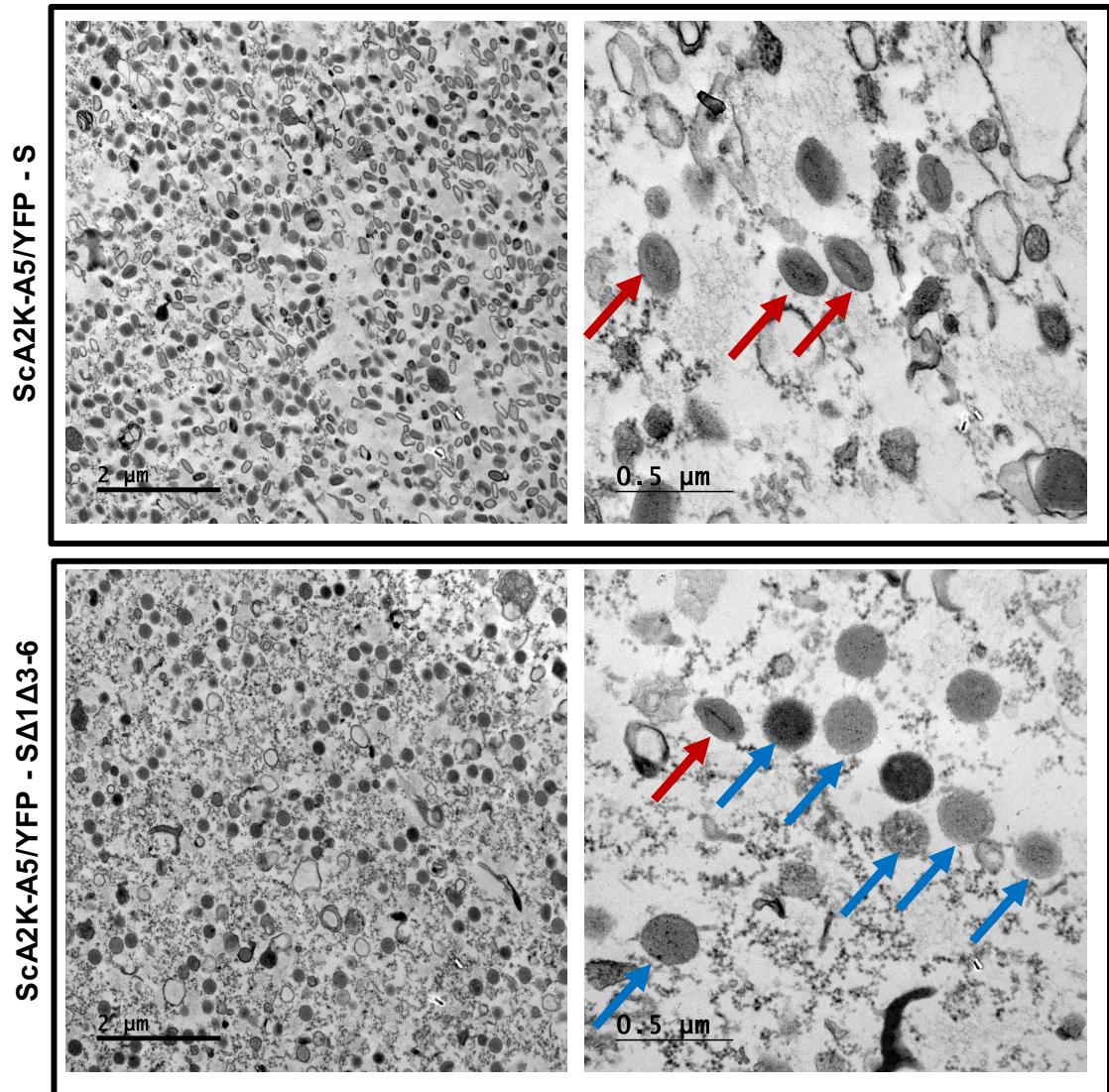


Figure 4.15. Difference in morphology between mutant viral particles compared to WT virus.

The transmission EM images were prepared using purified samples of sucrose cushioned mutant and WT viruses. The WT particles are mostly mature brick-shaped particles (red arrows) whereas the sample of mutant virus contains a significant amount of round immature particles (blue arrows). The virus stocks were prepared by Dr. Lin and the samples were processed for EM and imaged by Ms. Amidian. This figure was adapted and modified from Shenouda, M et al., 2022 (184)

Conclusions:

I have shown in this chapter that mutant viruses bearing extra-helical loop deletions do not exhibit a defect in DNA replication nor concatemer resolution. However, the harpin mutant viruses, with SΔ1Δ3-6 hairpin, do display a profound defect in viral assembly, leading to an increase in the relative proportion of defective particles produced by the virus. These defective particles have the same appearance as immature DNA-containing viral particles, there does not appear to be a defect in DNA packaging. The defect seemed to be related to a problem that arises after DNA encapsidation and which prevented its proper condensation to form mature virions. The next chapter looks at the effects these mutations on the virulence of the virus in animal models.

Chapter 5:
The effects of the hairpin end mutations on the virulence of the Sca2K-SΔ1Δ3-6 virus in animal models

Parts of this chapter of the thesis have been published as “Mira M. Shenouda, Ryan S. Noyce, Stephen Z. Lee, Jun L. Wang, Yi-Chan Lin, Nicole A. Favis, Megan A. Desaulniers, David H. Evans, The mismatched nucleotides encoded in vaccinia virus flip-and-flop hairpin telomeres serve an essential role in virion maturation. *PLoS Pathog.* **18** (2022), doi:10.1371/JOURNAL.PPAT.1010392.”

Contributions to this chapter:

MS - Development of methodology, performed experiments, writing and manuscript preparation

RN - Study supervision, conceptualization, development of methodology, technical and experimental assistance, funding acquisition, editorial revisions, manuscript preparation

NF - Technical & experimental assistance and animal support

DE - Study supervision, conceptualization, project administration, resources, editorial revisions, manuscript preparation

5. Chapter 5: The effects of the hairpin end mutations on the virulence of the ScA2K-SΔ1Δ3-6 virus in animal models

Introduction and Summary:

The last aim of my project was to look at the effects of the loop deletions within the hairpin ends on the virulence of VACV in animals. The mutant virus, with the SΔ1Δ3-6 hairpin, exhibits a growth *in vitro*, which we can attribute to a defect in virion maturation. Therefore, I expected to see a decrease in virulence in animals. In the first experiment, I used the Nu:Nu nude animal model to do a dose escalation study using a synthetic TK⁻ A2K virus bearing WR hairpin ends. The A2K virus causes a mild infection in this model with very slow progression and we did not observe weight loss as a result of the infection. This could be attributed to the fact that these animals still have intact innate cell populations as well as B-cells, sufficient to provide resistance to viral infection. For the next pilot experiment, I used SCID-NCr mice which bear defects in both B-cell and T-cell populations and again conducted a dose-escalation trial. In this experiment I also addressed a complication relating to the fact that TK mutations also attenuate poxvirus infections in animals. This was addressed by repairing the TK loci in the viruses being studied. These animals proved susceptible to infection with the J2R⁺ A2K WT virus. I then used the SCID-NCr mice to investigate the effects of loop deletion on the virulence of mutant viruses. Moreover, for the second experiment I replaced the A2K WT control with a synthetic version of the virus. The synthetic A2K virus lacks the 70bp repeats and terminates in WR hairpin sequences instead of A2K hairpin sequences. This ensured we were comparing an otherwise isogenic synthetic A2K strain with a mutant bearing SΔ1Δ3-6 hairpin ends.

Lastly, I used immune competent Balb/c mice to test whether the hairpin mutant virus, with the SΔ1Δ3-6 hairpin, could provide protection when used as a vaccine against a lethal challenge. As noted above the A2K virus strain causes a mild infection in Balb/c mice at any practical dose, whereas the VACV WR strain is lethal in an intranasal challenge at doses $\geq 10^3$ PFU.

For all the studies described below, female mice were used for ease of housing. Although there is only a very slight difference in susceptibility of female mice to VACV infection when compared to male mice (189), this could still be a limitation to our studies.

However, female mice were used here as an example to look at the difference in viral virulence and vaccine potential of the mutant virus.

5.1. Effect of extra-helical loop deletions on VACV virulence in immunocompromised mice

5.1.1. Virulence of the synthetic VACV A2K strain in Nu:Nu nude mice

The VACV A2K strain of virus is much less virulent than the WR strain in mice, so to test the effects of the hairpin deletions I elected to study A2K virulence using immunocompromised animals. The first model I tested was the Nu:Nu nude mouse, which lacks a functional T-cell population because of a spontaneous mutation in the nude locus, the *Foxn1* gene. This mutation causes a defect in the development of a the thymic epithelium (190). To test the virulence of the virus, I used escalating doses of ScA2K- Δ J2^{YFP/gpt} – S comprising 3×10^6 , 1×10^7 or 3×10^7 PFU. Three mice per group were infected *via* tail scarification. Only one mouse in the 1×10^7 dose group lost weight and was euthanized on Day 51 (Figure 5.1 – orange arrow). That mouse had developed a snout scab likely from grooming which could have affected its ability to eat. All the animals in all three groups developed a prolonged infection at the tail site that did not heal by the end of the experiment (example - Figure 5.2). However, not all animals had the same degree of severity at the infection site as shown in Figure 5.3. This showed that in Nu:Nu nude animals, although they developed a prolonged infection at the scarification site, the disease is not lethal during the experimental time course. Therefore, it is not the right animal model to detect the difference in virulence between WT and hairpin mutant virus.

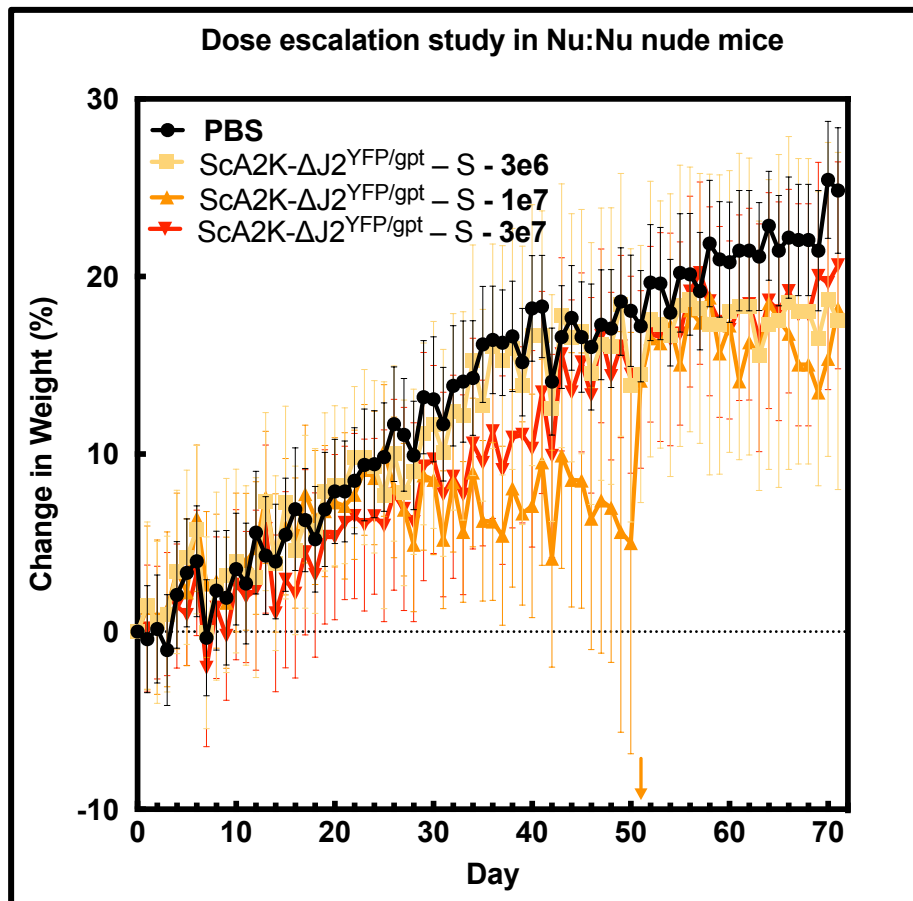


Figure 5.1. Synthetic VACV strain A2K is not lethal in Nu:Nu nude mice.

Three mice per group were infected with the ScA2K-ΔJ2^{YFP/gpt}- S virus at three different doses. PBS was used as a control (black). The viruses were administered by tail scarification and mice were monitored for weight and clinical score. The figure shows the percent change in the weights of the mice (mean and SEM) relative to day zero. One mouse was euthanized for weight loss, labored breathing and low mobility leading to a total clinical score of 7 at day 51 in the 10⁷ PFU group (orange arrow).













| Day | PBS | ScA2K- Δ J2 ^{YFP/gpt-S} (3×10^7) |
|-----|---|---|
| 7 |  |  |
| 21 |  |  |
| 35 |  |  |
| 49 |  |  |
| 56 |  |  |
| 68 |  |  |

Figure 5.2. *Nu:Nu* nude mice develop a prolonged infection at the inoculation site. The lesions at the infection site were imaged every week. Shown is a representative image from one mouse at the 3×10^7 PFU group as well as the PBS control.

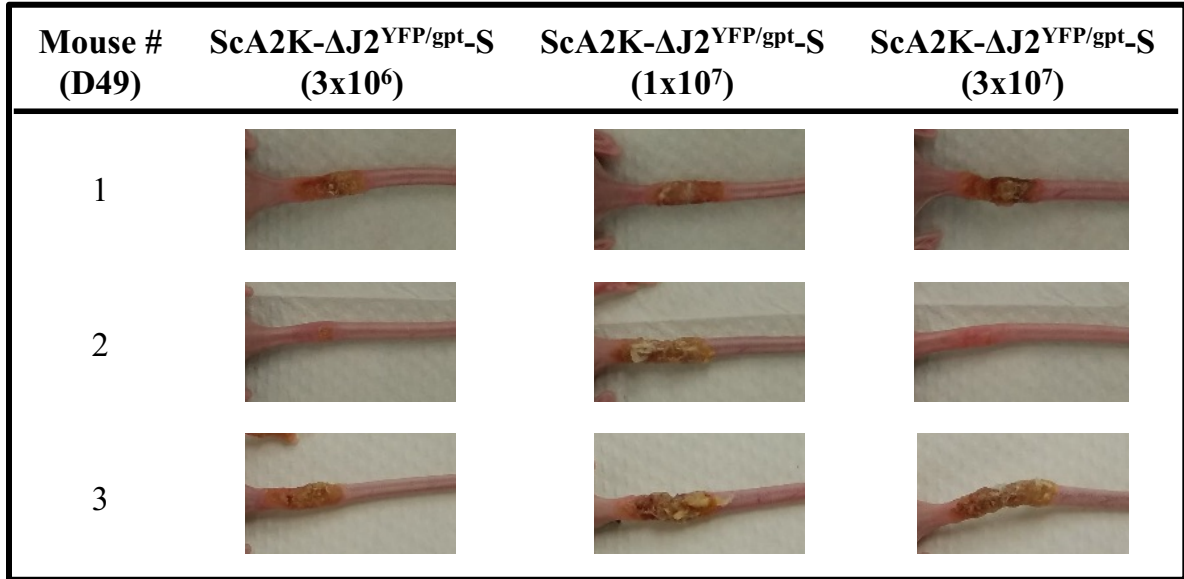


Figure 5.3. Tail lesions in different *Nu:Nu* nude mice.

The figure shows an image of the tail lesions of all the mice in all three infection groups at day 49 of the experiment. All of the mice developed lesions at the infection site, however the severity of the lesions varied greatly.

5.1.2. Virulence of mutant and WT A2K viruses in SCID-NCr Mice

For the next experiment, I performed a dose escalation trial using SCID-NCr immunocompromised mice. These bear a defect in both B and T lymphocytes due to a recessive mutation in the DNA-dependent protein kinase gene, *Prkdc^{sci/scid}* (191, 192). These animals showed an enhanced sensitivity to viral infection. In addition, I reinserted the J2R gene into the ScA2K-ΔJ2^{YFP/gpt-S}Δ1Δ3-6 synthetic mutant virus and used the WT (i.e., non-synthetic) ACAM2000 strain as a control. The mice were infected by tail scarification with the two viruses at three different doses (10⁴, 10⁵, or 10⁶ PFU) and PBS was used as a control. All the groups infected with ACAM2000 showed a decrease in weight and increase in clinical score and these mice reached end point between day 21 and day 57. In contrast the mice infected with the ScA2K-ΔJ2^{YFP/gpt-S}Δ1Δ3-6 mutant virus eventually showed a moderate weight loss (although that was not consistently seen across all mice within a group) but not enough to require euthanasia (Figure 5.4).

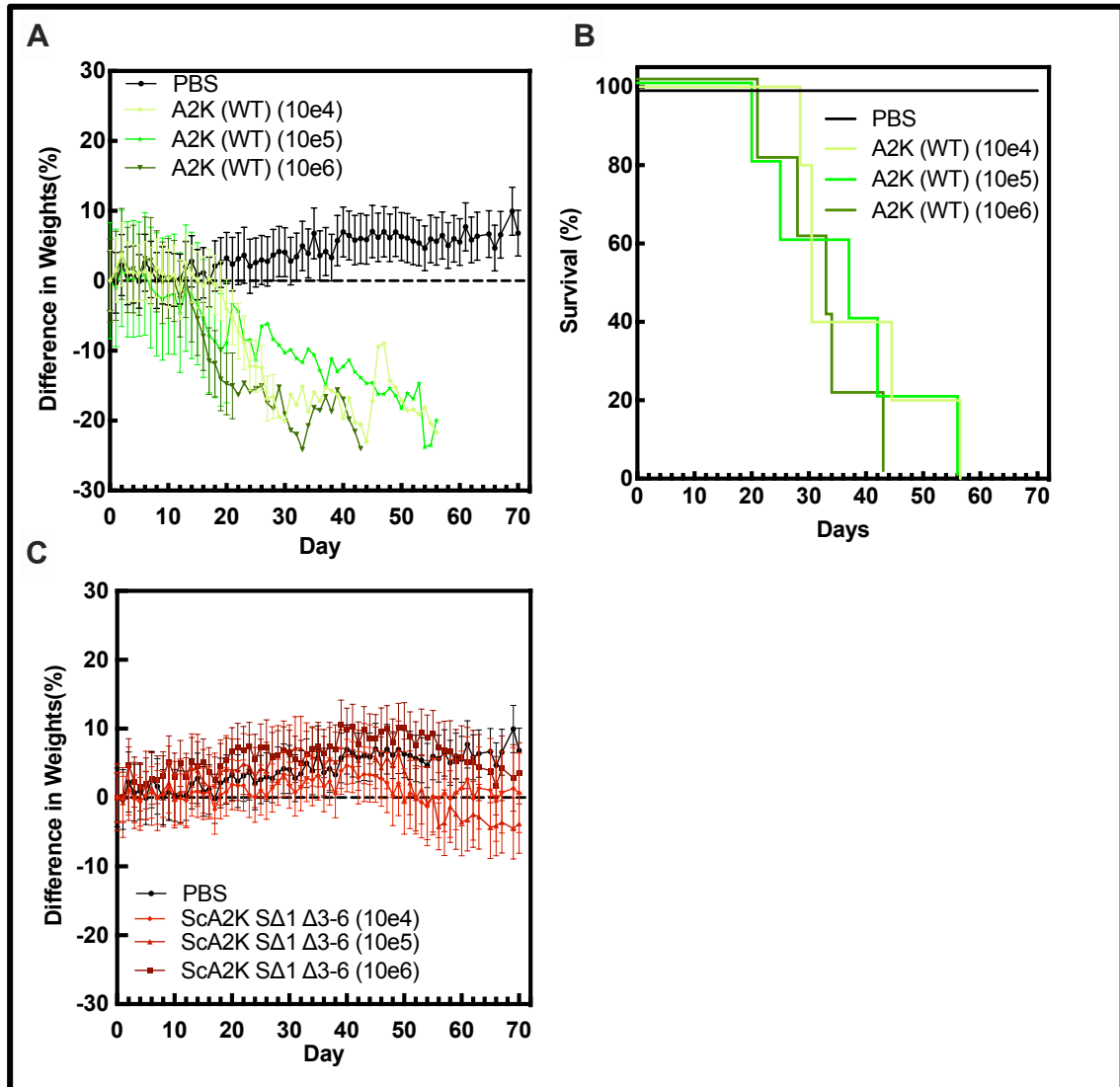


Figure 5.4. Dose escalation study comparing mutant and wildtype viruses using SCID-NCr mice.

(A) SCID-NCr female mice were infected via tail scarification with mutant (ScA2K-SΔ1Δ3-6) or WT (A2K) viruses at doses of 10⁴, 10⁵, or 10⁶ PFU. Each cohort comprised 5 mice and the animals were monitored to record weights and clinical scores. The PBS control is shown in black. The graph shows percent change in weight (mean and SEM). (B) Survival curve showing the groups shown in panel A. (C) Five SCID-NCr mice per group were infected with ScA2K-SΔ1Δ3-6 virus at three different doses. The graph shows percentage change in weight. The PBS control (black) is the same group shown in panel A but has been plotted again for reference. This figure was adapted and modified from Shenouda, M et al., 2022 (184)

To confirm that there is no difference in the viral growth *in vitro* due to reinsertion of the TK gene, I also reinserted the TK gene into the synthetic A2K strain with WT hairpin end, the ScA2K-Δ J2^{YFP/gpt}-S virus. Compared to each parent strain there was no

difference in virus growth *in vitro* between viruses with or without the $\Delta J2R$ deletion (Figure 5.5).

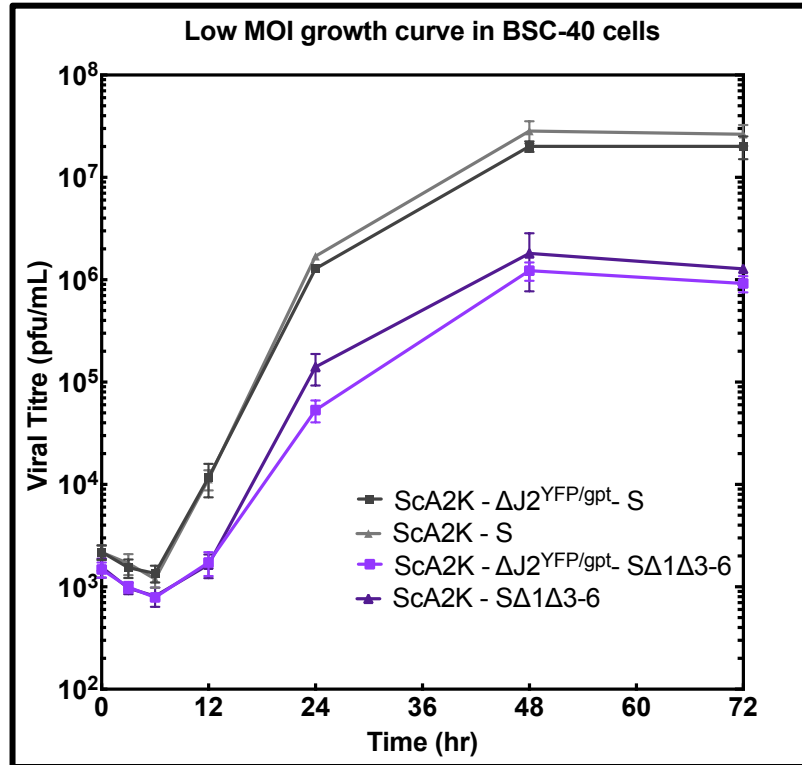


Figure 5.5. Repair of the thymidine kinase gene (*J2R*) does not alter virus growth *in vitro*.

BSC-40 cells were infected with the indicated viruses at an MOI of 0.01 PFU/cell and then the cells were harvested at different time points and frozen. After three freeze/thaw cycles the samples were titered and plotted. These data represent three independent experiments with each titre determined in triplicate.

5.1.3. Comparison of the diseases caused by synthetic A2K and hairpin mutant viruses in SCID-NCr mice

As previously mentioned, there are some genetic differences between the WT A2K strain and the synthetic viruses. These include the presence/absence of 70bp repeats, slight differences in the hairpin end sequence (the A2K hairpin is not quite the same as the WR hairpin from which the $S\Delta 1\Delta 3-6$ hairpin derives), and there are silent substitution mutations distributed across the synthetic genome. Besides the differences between the

hairpin ends, they are still not otherwise isogenic. Therefore, to properly compare the effects of the hairpin end deletions *alone* on virulence, for the last animal trial I used the synthetic A2K with WR hairpin ends and repaired J2R gene as the control. This is the ScA2K-S virus. A dose of 10^5 PFU was used in the following experiment based on the previous dose escalation study (Figure 4.5). The mice were scored for clinical signs of illness and monitored for weight loss for 70 days. The mice that were infected with the ScA2K-S hairpin virus started losing weight at around day 14 and between day 28 and day 35 all five mice within the group reached their end points and had to be euthanized. However, only one mouse in the ScA2K-S Δ 1 Δ 3-6 hairpin cohort started losing weight on day 48 and the weight loss mostly stabilized until the end of the experiment (Figure 5.6). None of the mice in the S Δ 1 Δ 3-6 group had to be euthanized by the end of the experiment. These mice did develop lesions at the infection site, and this was monitored by taking pictures once per week. All the 5 mice in the S group developed lesions that quickly deteriorated, however, only 3/5 mice from the S Δ 1 Δ 3-6 developed lesions. A picture of a tail of a mouse from each group is shown (Figure 5.7). These results showed that a mutation in just the hairpin ends of the virus could significantly attenuate the virus in susceptible mice. Moreover, only 3 out of 5 mice in the S Δ 1 Δ 3-6 group developed lesions at the infection site, suggesting that the mutant virus has a lower infectivity rate than WT. I suspect that the mice that developed lesions might well have eventually succumbed to the infection in the absence of an adaptive immune response.

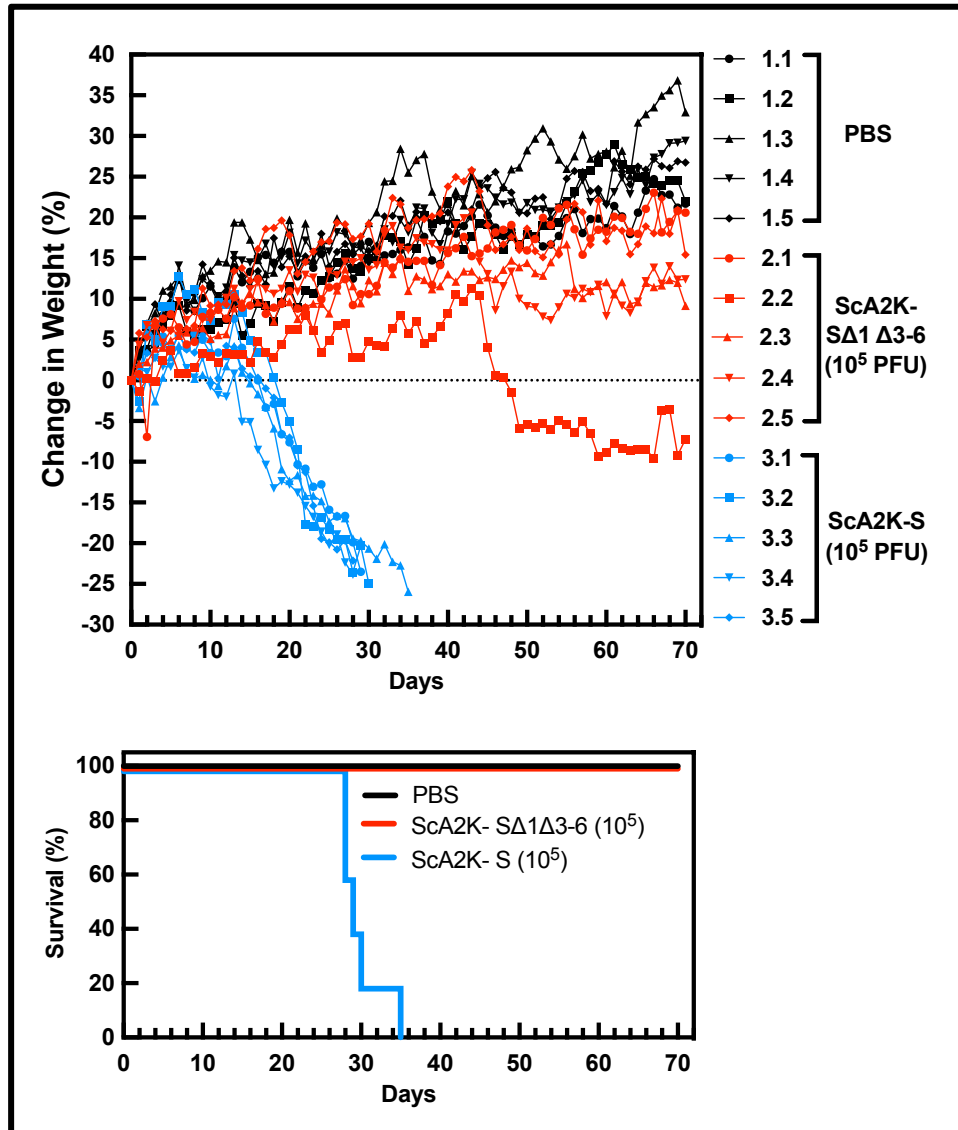


Figure 5.6. *The ScA2K-SΔ1Δ3-6 virus is less virulent in immunocompromised SCID-NCr mice.*

Groups of five female mice were infected via tail scarification with 10^5 PFU of either ScA2K-S (WT) or ScA2K-SΔ1Δ3-6 (hairpin mutant) viruses at day zero. Mice were monitored for weight loss and changes in clinical score. The PBS control is show in black. The top panel shows the percent change in weight where each line represents an individual mouse. The bottom panel shows the different survival curves for each cohort. This figure was adapted and modified from Shenouda, M et al., 2022 (184)

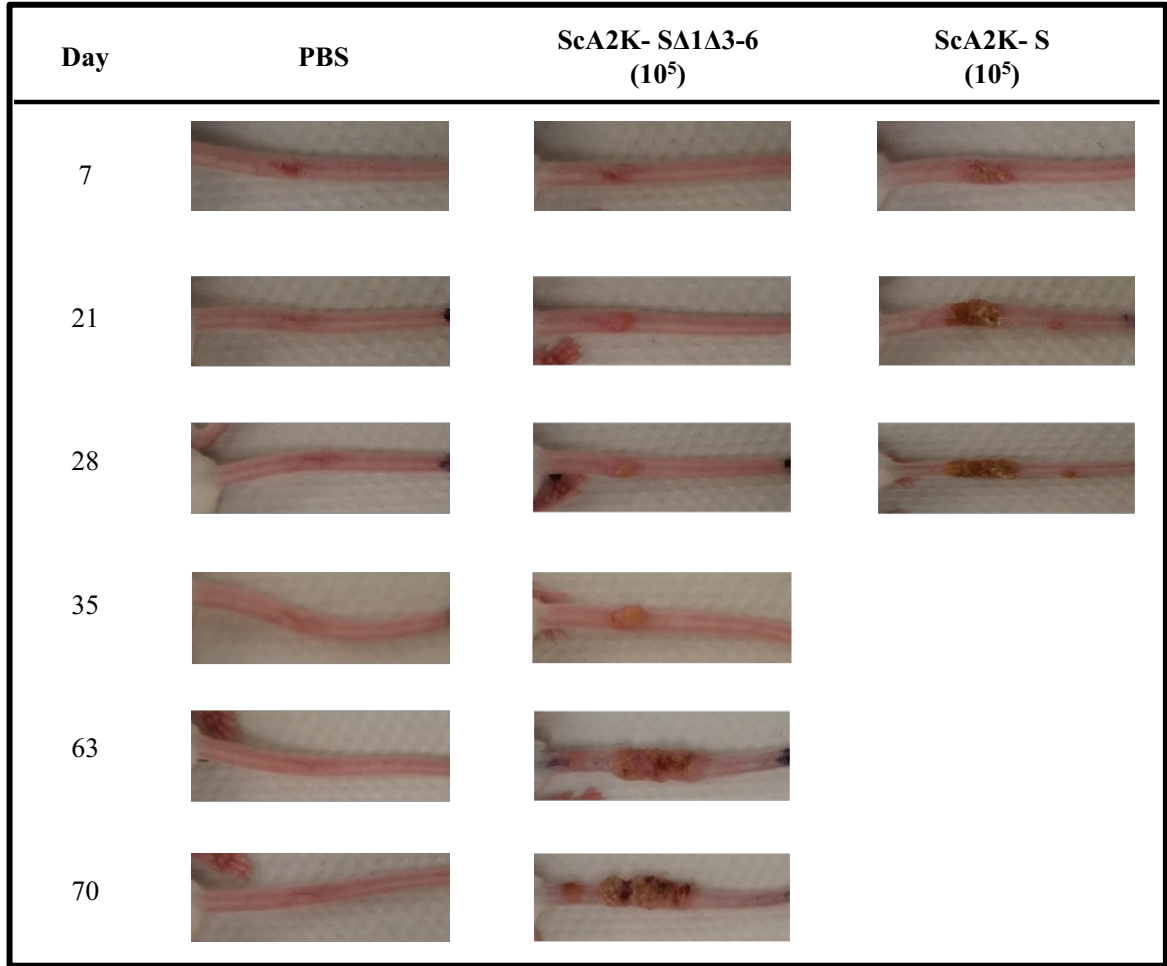


Figure 5.7. Some SCID-NCr mice developed a progressive pox lesion at the infection site.

The tail lesions were imaged once each week. Shown is a representative image from one mouse in each group. Three out of five mice infected with ScA2K-SΔ1Δ3-6 (mutant) developed a lesion at the infection site. All five mice in the ScA2K-S (WT) group developed lesions and none of these mice survived past day 35 of the experiment. This figure was adapted and modified from Shenouda, M et al., 2022 (184)

5.2. Viruses recovered from the infection site showed potential mutations in the hairpin ends

The mice infected with the mutant hairpin viruses exhibited a prolonged infection that lasted up to seventy days post-infection. Some also seem relatively healthy until partway through the experiment. This situation would permit many rounds of virus infection and growth and so provide an opportunity for more virulent mutants to arise. By isolating the viruses at the end of the study I hoped to see if the mutant telomeres are stable or whether they can revert to encoding more functional hairpins, likely encoding more mismatches. To test this question, I cultured viruses from six different tail scabs at day 70 from mutant-infected SCID-NCr mice. The mice studied exhibited different degrees of weight loss (Figure 5.8). The viruses were cultured separately and then the DNA was extracted from each pool of viruses (one pool per mouse) and sequenced. It is difficult to sequence and map hairpin ends using Illumina sequencing methods, especially using a pool of virus, as only a small number of reads are retrieved encoding the hairpin region. However, four out of the six sequences seemed to include reads that showed an insertion or deletion of nucleotides at the hairpin end (Figure 5.9). These alterations did not correlate to the severity of the disease. For example, mouse 3.2 had no apparent deletions or insertions in the telomeres but it lost about 9% body weight by day 70. Another example was mouse number 3.4 that also lost weight but acquired a duplication of sequences within the hairpin that are predicted to lead to the formation of another mismatch. This does not provide enough evidence to conclude that the mutant hairpin ends are unstable over the course of these unusually extended *in vivo* infections. Further investigations will be required to investigate hairpin stability and evolution under these conditions.

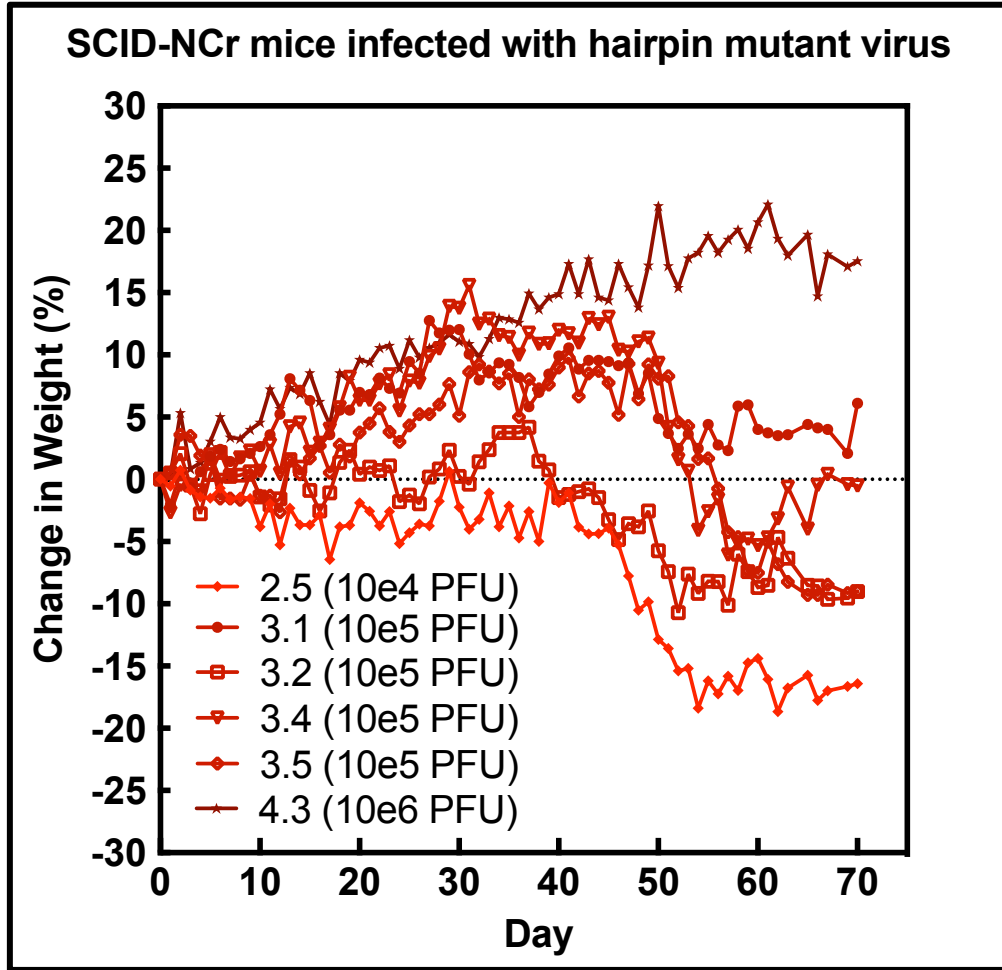


Figure 5.8. Weight change observed in individual SCID-NCr mice infected with the mutant ScA2K- Δ 1 Δ 3-6 virus.

The figure shows percentage weight change in six individual mice infected with different doses of ScA2K- Δ 1 Δ 3-6 virus. This experiment is described in section 5.1 and shown in Figure 5.4. All six mice developed a tail lesion that was collected at the end of the experiment and used to isolate viruses.

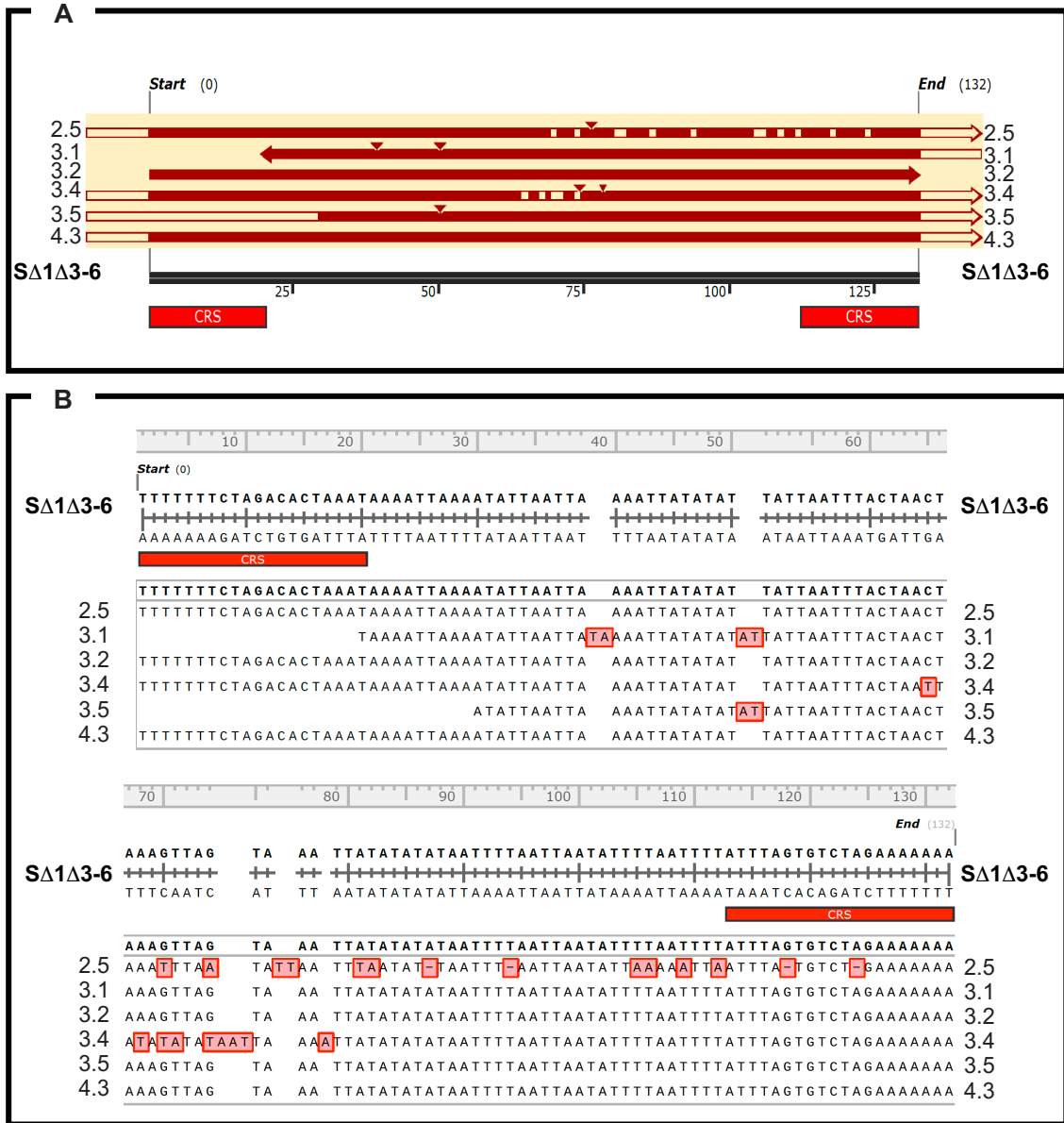


Figure 5.9. Sequence of hairpin ends of viruses isolated from mice infected with ScA2K- Δ I Δ 3-6 virus.

The viruses were isolated from the mice shown in Figure 5.8 and sequenced using Illumina sequencing. Panel (A) shows overall alignment of the hairpin ends with the original S Δ I Δ 3-6 hairpin. (B) shows the sequence alignment with the different insertions and deletions. The sequence acquired for samples 3.1 and 3.5, did not cover the whole hairpin.

5.3. The hairpin mutant virus still protects against a lethal VACV challenge in immunocompetent mice

As a final experiment I tested whether the hairpin mutant virus can protect immunocompetent mice against a lethal VACV challenge. Balb/c mice were vaccinated *via* tail scarification with 10^6 PFU of either ScA2K- S or ScA2K- S Δ 1 Δ 3-6 viruses or with PBS as a control. At day 28 post infection, the mice were challenged with 10^6 PFU of VACV strain WR, a dose that is always lethal in Balb/c mice. The mice were monitored for weight loss and clinical signs of disease. Both vaccinated groups showed only transient weight loss and recovered quickly within 2 days post-vaccination. In contrast, the PBS control mice lost weight and their clinical score increased quickly. All these animals had to be euthanized by day 6 post challenge (Figure 5.10).

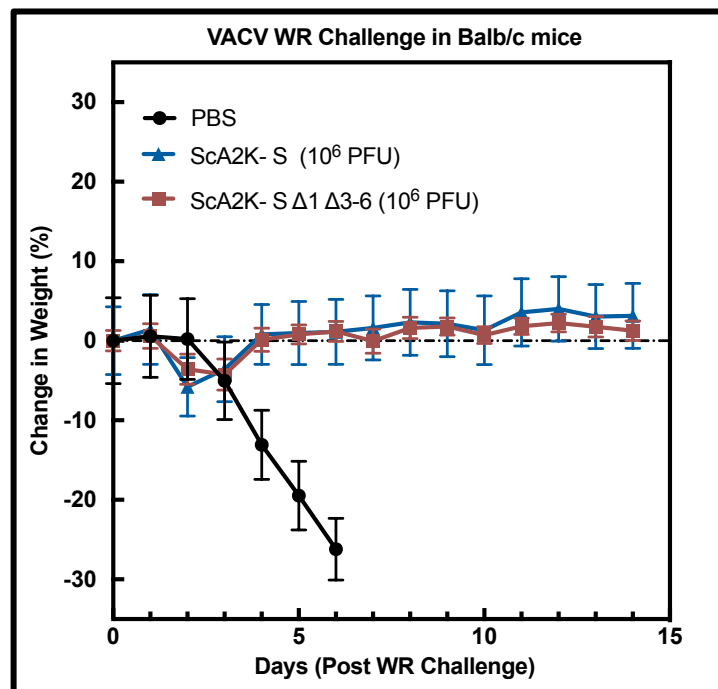


Figure 5.10. Mutant ScA2K-S Δ 1 Δ 3-6 virus protects against a lethal challenge as well as the WT ScA2K-S virus.

Group of 5 Balb/c mice were vaccinated using tail scarification with 10^6 PFU of the indicated viruses or with PBS as a control. After 28 days, the mice were challenged intranasally with 10^6 PFU of VACV strain WR (day zero in this plot). The figure shows percent change in weight after WR challenge. All the PBS control mice were euthanized by six days post-challenge. This figure was adapted and modified from Shenouda, M et al., 2022 (184)

Conclusion:

The studies described in this chapter provided us with an understanding of how hairpin mutations affect the fitness and virulence of VACV in animal models. Mutating the ~70bp hairpin end of a non-coding area within viral genome had a significant effect on its virulence. However, this did not affect the ability to protect against a lethal VACV challenge. One of the limitations of the study is that in animal models the dosing was calculated based upon the PFU, not number of particles. Based on previous studies, (Chapter 0) we know that the mutant virus has a 12-fold higher particle/ PFU ratio. Thus, in the vaccination studies the mice were infected with approximately 12-fold more particles, but the same number of infectious units. That limitation does not allow us to interpret whether the protection is due to the reduced infectivity of the virus or to the greater number of non-infectious particles. Regardless, the study shows that the mutant virus is safer to use in immunocompromised animals and can still induce a protective immune response against a lethal challenge. Further studies are needed to delineate the mechanism of protection provided by the mutant vaccine.

Chapter 6:
Discussion and future directions

6. Chapter 6: Discussion and future directions

6.1. General conclusions and key findings

My project explored the role served by the secondary structure of the hairpin ends in the poxviral life cycle. The presence of mismatches within the ends of poxvirus genomes has been known since 1982 (53), however, what purpose was served by these structures has not yet been elucidated. This dissertation discusses our findings with a particular focus on the role served by base mismatches in virion maturation.

I first showed that in order to reactivate a viral genome, we only needed to attach to each end one of the two complementary forms of the hairpins. Based on our knowledge of how Holliday junctions are resolved (92, 93), this is perhaps not too surprising a discovery. However, it showed that a single viral genome was viable even if it encoded identical, rather than “flip and flop”, forms of the hairpin on the two ends. Very likely, poxvirus stocks contain four different forms of the virus, each genome encoding some combination of the two variant ends.

I next discussed how one can mutate the hairpin ends by deleting extra-helical bases and sequentially extending the completely base-paired portions of the hairpins. The viruses recovered, and those that could not be recovered, provided insights into the importance of these mismatches. A negative correlation was observed between the number of mismatches and the yield of virus, pointing to the fact that the number of the mismatches, or the number of extra-helical loops, is in some way affecting virus replication and/or assembly. Although a negative result doesn't necessarily prove it; the fact one cannot recover a virus using a completely base paired hairpin, strongly suggested that at least some of these mismatches are essential for telomere function.

Finally, I used one of the mutant viruses, which exhibited the lowest virus yield in a low multiplicity of infection growth curve, to study the role of these mismatches within different stages of the viral life cycle (Figure 6.1). I showed that the hairpin mutant had a defect in virion maturation, producing an abundance of immature defective viral particles. Different mutants grew to different final titers and it would be worth testing whether differences in the production of immature defective particles were creating a range of different particle/PFU ratios. Finally, that defect in growth also aligned with a decrease in virulence in immunocompromised animals but when these mutant viruses were used as

vaccines, they could still provide protection against a lethal virus challenge in immunocompetent animals.

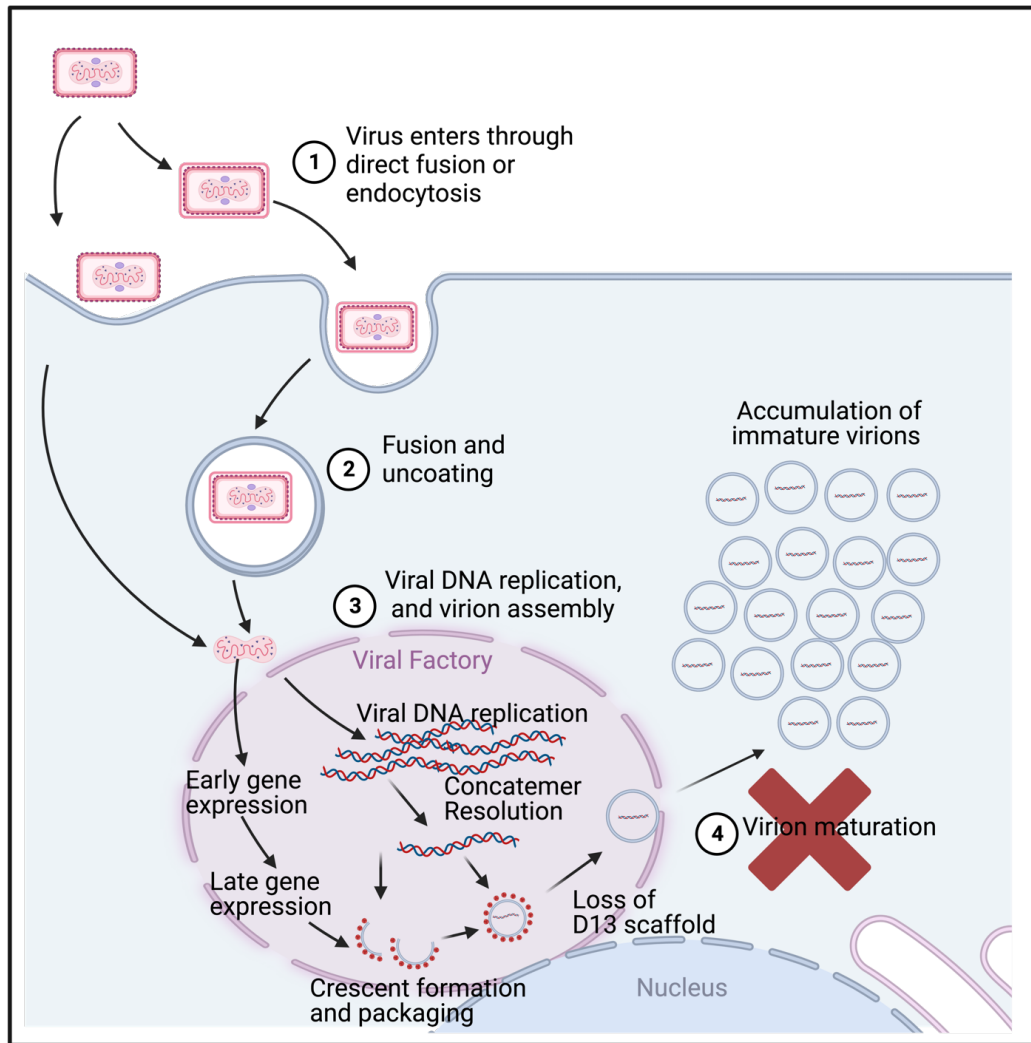


Figure 6.1: Schematic of key findings during infection with ScA2K-SΔ1Δ3-6 hairpin mutant virus.

Our investigations show that during infection with ScA2K hairpin mutant virus that lacks 5 of the 6 extra-helical hairpin loops, SΔ1Δ3-6. The results show that there is no defect in genome replication, concatemer resolution nor with immature virion assembly and DNA packaging. There is also no defect in D13 expression, scaffold ring formation nor the loss of the D13 scaffold preceding maturation. The defect is within virion maturation step which leads to the accumulation of immature defective particles that are packaged with DNA within the cytoplasm. This image was adapted from and created with BioRender.com.

6.2. Recovering reactivated virus with different hairpin ends

I approached the design of the hairpin oligonucleotides in two ways. The first was to sequentially decrease the number of extra-helical loops away from the CRS site and then away from the terminal loop. The results from these experiments suggest that the further the remaining extra-helical loops are from the terminal end, for example the S Δ 1-5 hairpin end, the less likely it is that one can recover viable virus. Even if the virus is viable this still creates a decrease in viral fitness, such as in the case of the S Δ 1-3 virus. It is also possible that fitness is affected by not only the length of the completely base paired region between the terminal loop and the first extra-helical loop, but that perhaps the total number of loops within the hairpin end is important. To address this question, we could add some more double-stranded DNA between the terminal loop and the first loop, while still retaining all the rest of the following loops and see if that affects virus recovery or fitness. That would provide insights into whether the stability of the hairpin terminal end or the number of extrahelical loops are responsible for the phenotype we see.

There are many other ways to design the hairpin oligonucleotides that might collectively provide insights into the importance of mismatch spacing and loop numbers. For example, another design would involve deleting loops numbered 2-5, especially since I could not recover viruses that have S Δ 2-6 or S Δ 1-5 hairpin ends. This could tell us if the position of certain loops or perhaps the spacing between them is important for viral replication, not just their number. In conjunction with these studies, it would also be important to test the binding affinity of the telomeric binding proteins I1 and I6 towards these different hairpin oligonucleotides. This would test whether there are correlations between the functional capacity to make a virus, versus the structural features of the hairpin element (loops, sequence, spacing), and the biochemical protein binding properties.

6.3. Hairpin stability and structure

An interesting question concerns whether the thermodynamic stability of the hairpin ends affects its role in the viral life cycle. For example, does it alter the ability to bind telomeric binding proteins or form stable cruciform structures? We hypothesized that an increase in thermal stability might affect the ability to rescue a viable virus. Indeed, we

could not recover a virus using hairpins that contained a higher CG content in the duplex portions, while still bearing all the extra-helical loops. However, this observation could also be explained if the I1 and I6 telomeric binding proteins preferentially bind to AT rich sequences. We have only done this experiment once and further studies are required to decipher the difference. Another feature of the hairpin loop that was never examined closely is the terminal loop at the hairpin end. This loop could have significant effects on the stability of the hairpin. The WR hairpin terminal loop is predicted to be a tetraloop, with four bases forming the loops. These are more stable than a “triloop” terminal hairpin composed of three bases (193). Studies have also shown that the CG closing base pair, which is found at the base of the loop in WR hairpin ends, provides higher stability than other base pairs, including GC, AT and TA pairs (193, 194). Thus, would changing that terminal loop to a triloop or pentaloop, or changing the closing base pair, change the hairpin stability and potentially viral fitness?

We also examined whether the $\Delta 1\Delta 3-6$ hairpin mutation is genetically stable. To address this question, we sequenced viruses isolated from the tail lesions of mice persistently infected with mutant viruses. These viruses are expected to have undergone multiple rounds of infection in the absence of an immune response to the virus. It is difficult to draw firm conclusions from the sequencing of these viruses, as some hairpins appeared to have drifted in sequence and some did not. Moreover, the changes we saw did not seem to correlate with the disease state in animals. However, the mutations that were detected are expected to have restored some of the mismatches and it requires further investigation to test what effect this had on the growth of these “pseudo revertant” viruses.

6.4. Interactions between the hairpin ends and telomere binding proteins

We suspect that the phenotype exhibited by our mutant viruses is due to effects on the binding to the two known DNA binding proteins I6 and I1. As previously noted (Section 1.3.5.3), inhibiting the expression of either I6 or I1 leads to an accumulation of immature particles. An I6 mutant produces aberrant IV-like particles that lack DNA, whereas an I1 mutant produces an abundance of immature virions (IMV). Infecting cells with an I1L mutant virus under non-permissive conditions produces an effect that closely resembles the phenotype seen with our hairpin mutant virus. Thus, my colleagues in our laboratory

have studied the binding of I1 protein to the different hairpin oligonucleotides that I used to construct different mutant viruses (184). Briefly, his₆-tagged I1 protein was expressed in bacteria, purified by affinity chromatography, and gel shift assays were used to monitor protein binding to fluorescently labeled DNAs. Like what has been previously described (175), this recombinant form of I1 protein bound to all forms of the hairpin oligonucleotides tested, even hairpin molecules lacking any mismatched bases. These gel-shift assays were also used to test the stability and relative affinity for binding of I1 to different hairpin ends compared to the WT S hairpin. These data showed that the I1 protein, has a greater affinity for the WT S hairpin than the SΔ1Δ3-6 form, for example (184). However, we observed similar avidity of I1 for the SΔ1-3 hairpin when compared to the WT S hairpin, even though a virus encoding SΔ1-3 hairpin ends exhibited a growth defect (184).

The interactions between I6 and the hairpin oligonucleotides used in our study have not yet been characterized as we were not able to express and purify recombinant I6 protein. However, the experiments described above showed that I1 generally bound with lower affinity to mutant hairpins, which could explain why the SΔ1Δ3-6 mutant virus exhibits a phenotype resembling an I1 mutant under non-permissive conditions. Since we have not yet tested I6 binding to the hairpin oligonucleotide, we cannot say with certainty that the phenotype exhibited by our SΔ1Δ3-6 mutant is just due to reduced binding of I1. It is noteworthy that I1 can still bind to double stranded DNA sequences in vitro, but we still couldn't recover virus with completely base-paired hairpin ends. It would be worth investigating whether the immature virions formed by our SΔ1Δ3-6 hairpin mutant still package I1 protein.

Other studies have shown that I6 binds with the highest affinity to viral hairpins, although it can still bind to non-viral hairpins bearing two base mismatches. We must assume that our SΔ1Δ3-6 hairpin ends still suffice to support the binding of I6 because preventing the expression of I6 (and thus I6 binding) produces empty virus particles, which is not the phenotype we see with this mutant virus. (In genetic terms I6 must function before I1, to package DNA, thus I6 is epistatic to I1.) Of course, it is quite possible that both I6 and I1 bind to the same hairpin end structures with one protein binding closer to the terminal loop while the other binds closer to the CRS. Given this

complexity, it seems likely that the phenotype exhibited by our S Δ 1 Δ 3-6 mutant reflects a combination of factors. The binding of I1 is of critical importance for virus maturation, but that that binding could well be altered in more subtle ways by alterations in the prior binding of I6, perhaps near the hairpin ends. Further binding and DNA foot printing studies, using different hairpin oligonucleotides and recombinant proteins, could provide further insights into the binding of these proteins to DNA and their potential interactions with other proteins.

6.5. The role of the hairpin ends in genome packaging

The exact process by which viral DNA is packaged into immature virions is not yet well understood. However, in a recent review by Greseth and Traktman (83), a model for genome encapsidation was proposed (Figure 6.2) in which the I6 protein bind to the monomeric genomes through the hairpin extrahelical bases. This protein-DNA complex then interacts with the A32 protein and then this complex interacts with the A13 transmembrane protein. This interaction causes the activation of the A32 ATPase, causing the translocation of the I6-DNA complex into the empty virion. This hypothesis suggests that the extra-helical bases might serve as a packaging signal to mark the genome for encapsidation. Since, we still do not yet know the binding affinity of our mutant hairpin oligonucleotide to the I6 protein, we cannot determine whether our observations support this hypothesis. However, our inability to recover a virus encoding completely base paired hairpin ends, could be explained by this hypothesis. The S Δ 1 Δ 3-6 mutant that we could make exhibited no defect in genome packaging, suggesting that as few as one extra-helical loop might suffice to support genome packaging.

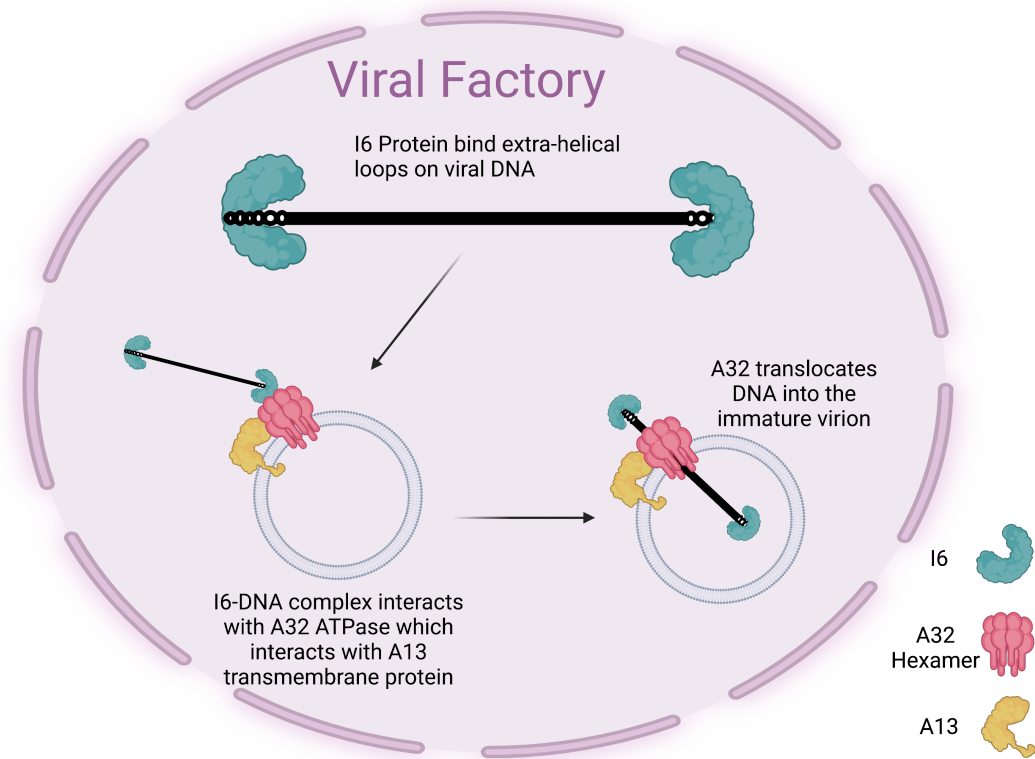


Figure 6.2: Proposed model for genome packaging.

The schematic shows a proposed model for genome encapsidation and the role of I6, A32 and A13 in the process. The figure was adapted from review by Greseth and Traktman (83). I6 protein (in green) binds to the extra-helical loops on monomeric genomes. This protein-DNA complex then interacts with the A32 protein (red) and then this complex interacts with the A13 transmembrane protein (yellow). This interaction causes the activation of the A32 ATPase, causing the translocation of the I6-DNA complex into the immature virion. This image was created with BioRender.com.

6.6. The role of the hairpin ends in virion maturation

Virion maturation involves a complex process involving the formation of lateral bodies and a core encapsidating the DNA. A critical part of that transition involves proteolytic processing of several core protein. Three main core proteins, A10 (also known as 4a), A3 (also known as 4b) and L4, have been identified where they all possess a common cleavage site that is processed by the I7 protease (152, 195, 196). That proteolysis occurs during the transition from IV to MV and thus a reduction or blockade of proteolytic processing has been used as an indicator of maturation arrest and the concomitant accumulation of immature virions. Genetic analysis has shown that I1 mutants under non-permissive conditions exhibit little to no proteolytic processing of

those three proteins (175). Moreover, the precursors of these proteins were seen to accumulate in particles obtained from an infection with an I6 mutant (*ts16-12*) under non-permissive conditions (168). Likewise, the data from our laboratory showed that only 30% of the core protein A3 (p4b to 4b) is cleaved in particles isolated from cells infected with an Δ 1 Δ 3-6 mutant virus compared to > 90% cleaved in the WT stock (184).

How mutations in the virus hairpin could possibly affect the processing of virus core proteins is not yet understood. However, it is clear that the decrease in the number of extra-helical loops, and the presumed disruption of an I1-containing complex, led to an arrest in the maturation process prior to the proteolytic processing of the core proteins and thus core condensation.

6.7. The animal models

As discussed in the Chapter 5, our mutant viruses exhibited decreased virulence in immunocompromised animal models, specifically SCID-NCr mice. The choice of this model was necessitated by the fact that aside from VACV strain WR, which was subjected to selection for virulence in mice, most other VACV strains don't produce much disease in mice even at very high doses. The susceptibility of SCID-NCr mice to the parent strain of virus, ScA2K-WT, is consistent with other data in the literature showing a progressive infection of VACV in mice inoculated by tail scarification associated with 30-40 days (197). The similarities between the two studies is not that surprising as Fisher *et al.* used the Dryvax strain of vaccinia virus (197). SCID-NCr mice lack functional T-cells and B-cells and thus even though our mutant virus is better tolerated by these mice than the ScA2K-WT parent, the hairpin mutants still produce a disease that over a considerably extended time course causes the mice to eventually succumb to the infection.

Although we have seen that the mutant hairpin virus is attenuated in immunocompromised mice, it still effective as a vaccine against a lethal viral challenge in BALB/c mice. However, because we vaccinated the mice with the same number of PFU's, without correcting for the increased particle numbers, we cannot say with certainty that the protection is dependent purely on viral growth. Non-replicating VACV, like modified vaccinia virus Ankara (MVA) or a replication defective derivative of vaccinia strain Lister (ddV-L), can also still protect against a lethal challenge with cowpox or

ectromelia viruses in mice (198, 199). However, two doses in a prime-boost immunization are needed to produce robust long-term infection with these two viruses (198, 199) whereas SΔ1Δ3-6 required only a single dose. The difference may reflect the fact that the SΔ1Δ3-6 mutant virus still produces an abundance of early and late viral antigens and some infectious progeny to further propagate the infection, whereas viruses like MVA produce an abortive infection in human cells that does not progress beyond the early stages of the virus life cycle. Interestingly, MVA can still provide protection in mice with partial immune deficiencies, such as mice lacking CD4 or CD8 T-cells (200). Therefore, it would be interesting to see if our SΔ1Δ3-6 virus can also provide protection against a lethal challenge in partially immune-deficient mice.

6.8. Hairpin ends in other DNA viruses

The mismatches found within the hairpin ends of poxviruses are not unique to poxviruses. They have also been found in other large double stranded DNA viruses such as members of the *asfarviridae* family, in African swine fever virus (201), and the *phycodnaviridae* family, in Chlorella virus (202). Interestingly, even the ends of members of the single-stranded *parvoviridae* family, minute virus of mice (203) and human B19 parvovirus (204), encode mismatches within their termini. These mismatches are essential for efficient viral replication and their removal significantly affects viral growth (203). Moreover, the sequence within the mismatches is not critical to replication (203).

Thus, the conservation of mismatched structures within the hairpin ends of these different viruses could provide some interesting insights into the evolutionary role(s) that these structures might play within these virus life cycles (205). It is interesting that these viruses share such a common feature, even though poxviruses and asfarviruses replicate in the cytoplasm while phycodnaviruses and parvoviruses in the nucleus (205). However, the evolutionary relationships between these viruses, many of which are members of the NucleoCytoplasmic Large DNA Viruses (NCLDV's or Megavirales), remains poorly understood, even though these viruses in this proposed Order share some common conserved genes (205, 206). Genome packaging is an essential and ancient aspect of the lifecycle of any virus, and it may not be surprising if future studies show that the processes used by poxviruses are conserved in other members of the Megavirales order.

6.9. Using synthetic biology to study different genomic elements within the poxvirus genome

In this dissertation, I was able to take advantage of advances in synthetic biology to study conserved elements of the virus genome. Our method for reactivating poxviruses can be used to manipulate and study features of these virus genomes that would be difficult to manipulate using conventional methods (148). For example, I showed that the tandemly repeated regions of the vaccinia virus genome are dispensable *in vitro* and the 70bp repeats are dispensable also *in vivo*. Though further studies are needed to confirm that the 125bp and 54bp repeats are also not essential for virulence *in vivo*. Furthermore, we can now easily manipulate the conserved non-repeat region 1 (NR1) between the hairpin and repeats (Figure 1.1), by removing the WR DNA duplex, and reactivating virus. Even though the CRS and neighboring DNA regions have been well studied using transfection assays, it would still be worthwhile making viruses that actually encoded some of the same mutations. This would show how the mutations that are proposed to be important, affect different aspects of viral growth (63, 69).

These methods also make it possible to precisely delete significant portions of virus and then study the effects this has on the virus. For example, the VV811 virus from the parental Copenhagen strain was constructed using molecular genetic methods which removed a block of 55 open reading frames (207). This produced a virus exhibiting a defect in viral replication (208). Our reactivation technique could be used to continue to sequentially delete different regions in the genome and examine the question of how little of a poxvirus genome is needed to still produce viable virus? It could also be used to selectively delete families of genes which collectively suppress a specific innate immune defense such as the NF- κ B signaling pathways. This is regulated by at least 18 genes (by one estimate) (209), and such a project might help uncover additional inhibitors as well as new insights into why a virus would encode so many genes with apparently overlapping functions. Perhaps most importantly, poxviruses find many uses as vaccine vectors and as cancer therapeutics. Synthetic biology offers an extraordinarily powerful tool for rapidly and precisely manipulating the genetic composition of the viruses that are used in these applications.

References

1. E. J. Lefkowitz, C. Wang, C. Upton, Poxviruses: past, present and future. *Virus Res.* **117**, 105–118 (2006).
2. S. L. Haller, C. Peng, G. McFadden, S. Rothenburg, Poxviruses and the evolution of host range and virulence. *Infection, Genetics and Evolution.* **21**, 15–40 (2014).
3. C. Gubser, S. Hué, P. Kellam, G. L. Smith, Poxvirus genomes: A phylogenetic analysis. *Journal of General Virology.* **85**, 105–117 (2004).
4. S. S. Kalter, A. R. Rodriguez, L. B. Cummins, R. L. Heberling, S. O. Foster, Experimental smallpox in chimpanzees. *Bull World Health Organ.* **57**, 637 (1979).
5. R. L. Heberling, S. S. Kalter, A. R. Rodriguez, Poxvirus infection of the baboon (*Papio cynocephalus*). *Bull World Health Organ.* **54**, 285 (1976).
6. S. J. Werden, M. M. Rahman, G. McFadden, Chapter 3 Poxvirus Host Range Genes. *Adv Virus Res.* **71**, 135–171 (2008).
7. J. H. Diaz, The Disease Ecology, Epidemiology, Clinical Manifestations, Management, Prevention, and Control of Increasing Human Infections with Animal Orthopoxviruses.
8. S. N. Shchelkunov, An Increasing Danger of Zoonotic Orthopoxvirus Infections. *PLoS Pathog.* **9**, 1–4 (2013).
9. M. A. Ruffer, A. R. Ferguson, Note on an eruption resembling that of variola in the skin of a mummy of the twentieth dynasty (1200–1100 B.C.). *J Pathol Bacteriol.* **15**, 1–3 (1911).
10. B. Mühlemann, L. Vinner, A. Margaryan, H. Wilhelmson, C. D. L. F. Castro, M. E. Allentoft, P. D. B. Damgaard, A. J. Hansen, S. H. Nielsen, L. M. Strand, J. Bill, A. Buzhilova, T. Pushkina, C. Falys, V. Khartanovich, V. Moiseyev, M. L. S. Jørkov, P. Ø. Sørensen, Y. Magnusson, I. Gustin, H. Schroeder, G. Sutter, G. L. Smith, C. Drosten, R. A. M. Fouchier, D. J. Smith, E. Willerslev, T. C. Jones, M. Sikora, Diverse variola virus (smallpox) strains were widespread in northern Europe in the Viking Age. *Science (1979).* **369** (2020), doi:10.1126/SCIENCE.AAW8977.
11. A. T. Duggan, M. F. Perdomo, D. Piombino-Mascoli, S. Marciniak, D. Poinar, M. v. Emery, J. P. Buchmann, S. Duchêne, R. Jankauskas, M. Humphreys, G. B. Golding, J. Southon, A. Devault, J. M. Rouillard, J. W. Sahl, O. Dutour, K. Hedman, A. Sajantila, G. L. Smith, E. C. Holmes, H. N. Poinar, 17th Century Variola Virus Reveals the Recent History of Smallpox. *Current Biology.* **26**, 3407–3412 (2016).
12. J. O. Wertheim, Viral Evolution: Mummy Virus Challenges Presumed History of Smallpox. *Current Biology.* **27**, R119–R120 (2017).
13. W. L. Langer, Immunization against smallpox before Jenner. *Sci Am.* **234**, 112–117 (1976).
14. *An Inquiry Into the Causes and Effects of the Variolae Vaccinae, a Disease ... - Edward Jenner - Google Books* (https://books.google.ca/books?hl=en&lr=&id=QDXShHV2z0MC&oi=fnd&pg=PA1&ots=L5gUu1v-FY&sig=lxPCZUoXznOxnKBKWq81JKNkjhc&redir_esc=y#v=onepage&q&f=false).

15. Global eradication of smallpox: WHO Global Commission for the Certification of Smallpox Eradication - PubMed, (available at <https://pubmed-ncbi-nlm-nih-gov.login.ezproxy.library.ualberta.ca/490075/>).
16. A. W. Downie, A study of the lesions produced experimentally by cowpox virus. *J Pathol Bacteriol.* **48**, 361–379 (1939).
17. A. W. Downie, The Immunological Relationship of the Virus of Spontaneous Cowpox to Vaccinia Virus. *Br J Exp Pathol.* **20**, 158 (1939).
18. A. W. Downie, Jenner's Cowpox Inoculation. *Br Med J.* **2**, 251 (1951).
19. D. Baxby, Edward Jenner, William Woodville, and the origins of vaccinia virus. *J Hist Med Allied Sci.* **34**, 134–162 (1979).
20. D. Baxby, Edward Jenner's Inquiry; a bicentenary analysis. *Vaccine.* **17**, 301–307 (1999).
21. D. Baxby, The origins of vaccinia virus. *J Infect Dis.* **136**, 453–455 (1977).
22. J. Esparza, L. Schrick, C. R. Damaso, A. Nitsche, Equination (inoculation of horsepox): An early alternative to vaccination (inoculation of cowpox) and the potential role of horsepox virus in the origin of the smallpox vaccine. *Vaccine.* **35**, 7222–7230 (2017).
23. E. R. Tulman, G. Delhon, C. L. Afonso, Z. Lu, L. Zsak, N. T. Sandybaev, U. Z. Kerembekova, V. L. Zaitsev, G. F. Kutish, D. L. Rock, Genome of horsepox virus. *J Virol.* **80**, 9244–58 (2006).
24. C. R. Damaso, Revisiting Jenner's mysteries, the role of the Beaugency lymph in the evolutionary path of ancient smallpox vaccines. *Lancet Infect Dis.* **18**, e55–e63 (2018).
25. A. Brinkmann, A. R. V. Souza, J. Esparza, A. Nitsche, C. R. Damaso, Re-assembly of nineteenth-century smallpox vaccine genomes reveals the contemporaneous use of horsepox and horsepox-related viruses in the USA. *Genome Biol.* **21** (2020), doi:10.1186/S13059-020-02202-0.
26. L. Schrick, S. H. Tausch, P. W. Dabrowski, C. R. Damaso, J. Esparza, A. Nitsche, An Early American Smallpox Vaccine Based on Horsepox. *New England Journal of Medicine.* **377**, 1491–1492 (2017).
27. A. T. Duggan, J. Klunk, A. F. Porter, A. N. Dhody, R. Hicks, G. L. Smith, M. Humphreys, A. M. McCollum, W. B. Davidson, K. Wilkins, Y. Li, A. Burke, H. Polasky, L. Flanders, D. Poinar, A. R. Raphenya, T. T. Y. Lau, B. Alcock, A. G. McArthur, G. B. Golding, E. C. Holmes, H. N. Poinar, The origins and genomic diversity of American Civil War Era smallpox vaccine strains. *Genome Biol.* **21**, 1–11 (2020).
28. A. Brinkmann, A. R. V. Souza, J. Esparza, A. Nitsche, C. R. Damaso, Re-assembly of nineteenth-century smallpox vaccine genomes reveals the contemporaneous use of horsepox and horsepox-related viruses in the USA. *Genome Biol.* **21**, 1–6 (2020).
29. L. Sánchez-Sampedro, B. Perdiguero, E. Mejías-Pérez, J. García-Arriaza, M. di Pilato, M. Esteban, The evolution of poxvirus vaccines. *Viruses.* **7**, 1726–803 (2015).
30. F. Fenner, D. A. Henderson, I. Arita, Z. Jezek, I. D. Ladnyi, Smallpox and its eradication / F. Fenner ... [et al.]. *World Health Organization* (1988), (available at <https://apps.who.int/iris/handle/10665/39485>).

31. L. Qin, N. Favis, J. Famulski, D. H. Evans, Evolution of and Evolutionary Relationships between Extant Vaccinia Virus Strains. *J Virol.* **89**, 1809–1824 (2015).
32. R. Rivers, CULTIVATION OF VACCINE VIRUS FOR JENNERIAN PROPHYLAXIS IN MAN. *J Exp Med.* **54**, 453–453 (1931).
33. C. P. Li, T. M. Rivers, CULTIVATION OF VACCINE VIRUS. *J Exp Med.* **52**, 465 (1930).
34. T. M. Rivers, S. M. Ward, R. D. Baird, AMOUNT AND DURATION OF IMMUNITY INDUCED BY INTRADERMAL INOCULATION OF CULTURED VACCINE VIRUS. *J Exp Med.* **69**, 857–866 (1939).
35. C. H. Kempe, Smallpox vaccination of eczema patients with attenuated live vaccinia virus. *Yale J Biol Med.* **41**, 1 (1968).
36. R. B. Wesley, W. C. Speers, J. M. Neff, F. L. Ruben, B. Lourie, Evaluation of two kinds of smallpox vaccine: CVI-78 and calf lymph vaccine. I. Clinical and serologic response to primary vaccination. *Pediatr Res.* **9**, 624–628 (1975).
37. W. C. Speers, R. B. Wesley, J. M. Neff, J. Goldstein, B. Lourie, Evaluation of two kinds of smallpox vaccine: CVI-78 and calf lymph vaccine: II. Clinical and serologic observations of response to revaccination with calf lymph vaccine. *Pediatr Res.* **9**, 629–632 (1975).
38. R. F. Parker, L. H. Bronson, R. H. Green, Further Studies of the Infectious Unit of Vaccinia. *J Exp Med.* **74**, 263–281 (1941).
39. J. Tartaglia, M. E. Perkus, J. Taylor, E. K. Norton, J.-C. Audonnet, W. I. Cox, S. W. Davis, J. van der Hoeven, B. Meignier, M. Riviere, B. Languet, # And, E. Paolettl, NYVAC: A Highly Attenuated Strain of Vaccinia Virus. *Virology.* **188**, 217–232 (1992).
40. L. Qin, C. Upton, B. Hazes, D. H. Evans, Genomic Analysis of the Vaccinia Virus Strain Variants Found in Dryvax Vaccine. *J Virol.* **85**, 13049 (2011).
41. R. Weltzin, J. Liu, K. v. Pugachev, G. A. Myers, B. Coughlin, P. S. Blum, R. Nichols, C. Johnson, J. Cruz, J. S. Kennedy, F. A. Ennis, T. P. Monath, Clonal vaccinia virus grown in cell culture as a new smallpox vaccine. *Nat Med.* **9**, 1125–1130 (2003).
42. T. P. Monath, J. R. Caldwell, W. Mundt, J. Fusco, C. S. Johnson, M. Buller, J. Liu, B. Gardner, G. Downing, P. S. Blum, T. Kemp, R. Nichols, R. Weltzin, ACAM2000 clonal Vero cell culture vaccinia virus (New York City Board of Health strain) - A second-generation smallpox vaccine for biological defense. *International Journal of Infectious Diseases.* **8**, 31–44 (2004).
43. R. N. Greenberg, J. S. Kennedy, ACAM2000: A newly licensed cell culture-based live vaccinia smallpox vaccine. *Expert Opin Investig Drugs.* **17**, 555–564 (2008).
44. K. A. Marriott, C. v. Parkinson, S. I. Morefield, R. Davenport, R. Nichols, T. P. Monath, Clonal vaccinia virus grown in cell culture fully protects monkeys from lethal monkeypox challenge. *Vaccine.* **26**, 581–588 (2008).
45. A. Nalca, E. E. Zumbrun, ACAM2000™: The new smallpox vaccine for United States Strategic National Stockpile. *Drug Des Devel Ther.* **4**, 71 (2010).

46. S. J. Goebel, G. P. Johnson, M. E. Perkus, S. W. Davis, J. P. Winslow, E. Paoletti, The complete DNA sequence of vaccinia virus. *Virology*. **179**, 247–266 (1990).
47. F. M. DeFilippes, Restriction enzyme mapping of vaccinia virus DNA. *J Virol*. **43**, 136–149 (1982).
48. O. Kaynarcalidan, S. Moreno Mascaraque, I. Drexler, Vaccinia Virus: From Crude Smallpox Vaccines to Elaborate Viral Vector Vaccine Design. *Biomedicines 2021, Vol. 9, Page 1780*. **9**, 1780 (2021).
49. M. Mackett, L. C. Archard, Conservation and variation in Orthopoxvirus genome structure. *Journal of General Virology*. **45**, 683–701 (1979).
50. R. Wittek, A. Menna, H. K. Müller, D. Schümperli, P. G. Boseley, R. Wyler, Inverted terminal repeats in rabbit poxvirus and vaccinia virus DNA. *J Virol*. **28**, 171 (1978).
51. C. F. Garon, E. Barbosa, B. Moss, Visualization of an inverted terminal repetition in vaccinia virus DNA. *Proc Natl Acad Sci U S A*. **75**, 4863 (1978).
52. R. Wittek, B. Moss, Tandem repeats within the inverted terminal repetition of vaccinia virus DNA. *Cell*. **21**, 277–284 (1980).
53. B. M. Baroudy, S. Venkatesan, B. Moss, Incompletely base-paired flip-flop terminal loops link the two DNA strands of the vaccinia virus genome into one uninterrupted polynucleotide chain. *Cell*. **28**, 315–24 (1982).
54. G. Pedrali-Noy, A. Weissbach, Evidence of a repetitive sequence in vaccinia virus DNA. *J Virol*. **24**, 406–407 (1977).
55. R. Wittek, B. Moss, Tandem Repeats within the Inverted Terminal Repetition of Vaccinia Virus DNA. *Cell*. **21**, 277–284 (1980).
56. B. M. Baroudy, B. Moss, Sequence homologies of diverse length tandem repetitions near ends of vaccinia virus genome suggest unequal crossing over. *Nucleic Acids Res*. **10**, 5673–5679 (1982).
57. B. Moss, E. Winters, N. Cooper, Instability and reiteration of DNA sequences within the vaccinia virus genome. *Proc Natl Acad Sci U S A*. **78**, 1614 (1981).
58. K. Zhao, R. M. Wohlhueter, Y. Li, Finishing monkeypox genomes from short reads: Assembly analysis and a neural network method. *BMC Genomics*. **17**, 527–537 (2016).
59. S. Sarker, S. R. Isberg, N. L. Milic, P. Lock, K. J. Helbig, Molecular characterization of the first saltwater crocodilepox virus genome sequences from the world’s largest living member of the Crocodylia. *Scientific Reports 2018 8:1*. **8**, 1–11 (2018).
60. N. Chen, M. I. Danila, Z. Feng, R. M. L. Buller, C. Wang, X. Han, E. J. Lefkowitz, C. Upton, The genomic sequence of ectromelia virus, the causative agent of mousepox. *Virology*. **317**, 165–186 (2003).
61. B. L. Parsons, D. J. Pickup, Tandemly repeated sequences are present at the ends of the DNA of raccoonpox virus. *Virology*. **161**, 45–53 (1987).
62. R. F. Massung, J. C. Knight, J. J. Esposito, Topography of Variola Smallpox Virus Inverted Terminal Repeats. *Virology*. **211**, 350–355 (1995).
63. A. M. DeLange, M. Reddy, D. Scraba, C. Upton, G. McFadden, Replication and resolution of cloned poxvirus telomeres in vivo generates linear minichromosomes with intact viral hairpin termini. *J Virol*. **59**, 249–59 (1986).

64. E. Winters, B. M. Baroudy, B. Moss, Molecular cloning of the terminal hairpin of vaccinia virus DNA as an imperfect palindrome in an Escherichia coli plasmid. *Gene*. **37**, 221–228 (1985).
65. M. Merchlinsky, B. Moss, Nucleotide sequence required for resolution of the concatemer junction of vaccinia virus DNA. *J Virol*. **63**, 4354–4361 (1989).
66. M. Merchlinsky, B. Moss, Resolution of vaccinia virus DNA concatemer junctions requires late-gene expression. *J Virol*. **63**, 1595–1603 (1989).
67. M. Merchlinsky, B. Moss, Resolution of linear minichromosomes with hairpin ends from circular plasmids containing vaccinia virus concatemer junctions. *Cell*. **45**, 879–884 (1986).
68. A. M. DeLange, G. McFadden, Sequence-nonspecific replication of transfected plasmid DNA in poxvirus-infected cells. *Proc Natl Acad Sci U S A*. **83**, 614–618 (1986).
69. A. M. DeLange, G. McFadden, Efficient resolution of replicated poxvirus telomeres to native hairpin structures requires two inverted symmetrical copies of a core target DNA sequence. *J Virol*. **61**, 1957–1963 (1987).
70. S. N. Shchelkunov, A. v Totmenin, P. F. Safronov, M. v Mikheev, V. v Gutorov, O. I. Ryazankina, N. A. Petrov, I. v Babkin, E. A. Uvarova, L. S. Sandakhchiev, J. R. Sisler, J. J. Esposito, I. K. Damon, P. B. Jahrling, B. Moss, Analysis of the Monkeypox Virus Genome, doi:10.1006/viro.2002.1446.
71. S. N. Shchelkunov, P. F. Safronov, A. v Totmenin, N. A. Petrov, O. I. Ryazankina, V. v Gutorov, G. J. Kotwal, The Genomic Sequence Analysis of the Left and Right Species-Specific Terminal Region of a Cowpox Virus Strain Reveals Unique Sequences and a Cluster of Intact ORFs for Immunomodulatory and Host Range Proteins (1998).
72. S. Biswas, R. S. Noyce, L. A. Babiuk, O. Lung, D. M. Bulach, T. R. Bowden, D. B. Boyle, S. Babiuk, D. H. Evans, Extended sequencing of vaccine and wild-type capripoxvirus isolates provides insights into genes modulating virulence and host range. *Transbound Emerg Dis*. **67**, 80–97 (2020).
73. T. Günther, L. Haas, M. Alawi, P. Wohlsein, J. Marks, A. Grundhoff, P. Becher, N. Fischer, Recovery of the first full-length genome sequence of a parapoxvirus directly from a clinical sample. *Scientific Reports 2017 7:1*. **7**, 1–8 (2017).
74. B. Moss, Membrane fusion during poxvirus entry. *Semin Cell Dev Biol*. **60**, 89–96 (2016).
75. B. Moss, Poxvirus Cell Entry: How Many Proteins Does it Take? *Viruses 2012, Vol. 4, Pages 688-707*. **4**, 688–707 (2012).
76. F. I. Schmidt, C. K. E. Bleck, J. Mercer, Poxvirus host cell entry. *Curr Opin Virol*. **2**, 20–27 (2012).
77. M. Law, G. G. Carter, K. L. Roberts, M. Hollinshead, G. L. Smith, Ligand-induced and nonfusogenic dissolution of a viral membrane. *Proc Natl Acad Sci U S A*. **103**, 5989–5994 (2006).
78. G. C. Carter, M. Law, M. Hollinshead, G. L. Smith, Entry of the vaccinia virus intracellular mature virion and its interactions with glycosaminoglycans. *J Gen Virol*. **86**, 1279–1290 (2005).
79. J. Mercer, A. Helenius, Vaccinia virus uses macropinocytosis and apoptotic mimicry to enter host cells. *Science (1979)*. **320**, 531–535 (2008).

80. C.-Y. Huang, T.-Y. Lu, C.-H. Bair, Y.-S. Chang, J.-K. Jwo, W. Chang, A Novel Cellular Protein, VPEF, Facilitates Vaccinia Virus Penetration into HeLa Cells through Fluid Phase Endocytosis. *J Virol.* **82**, 7988–7999 (2008).
81. F. I. Schmidt, C. K. E. Bleck, A. Helenius, J. Mercer, Vaccinia extracellular virions enter cells by macropinocytosis and acid-activated membrane rupture. *EMBO Journal.* **30**, 3647–3661 (2011).
82. A. C. Townsley, A. S. Weisberg, T. R. Wagenaar, B. Moss, Vaccinia Virus Entry into Cells via a Low-pH-Dependent Endosomal Pathway. *J Virol.* **80**, 8899 (2006).
83. M. D. Greseth, P. Traktman, The Life Cycle of the Vaccinia Virus Genome (2022), doi:10.1146/annurev-virology-091919.
84. B. Schramm, J. K. Locker, Cytoplasmic Organization of POXvirus DNA Replication. *Traffic.* **6**, 839–846 (2005).
85. N. Tolonen, L. Doglio, S. Schleich, J. Krijnse Locker, Vaccinia virus DNA replication occurs in endoplasmic reticulum-enclosed cytoplasmic mini-nuclei. *Mol Biol Cell.* **12**, 2031–2046 (2001).
86. G. C. Katsafanas, B. Moss, Colocalization of transcription and translation within cytoplasmic poxvirus factories coordinates viral expression and subjugates host functions. *Cell Host Microbe.* **2**, 221–228 (2007).
87. Q. Kieser, R. S. Noyce, M. Shenouda, Y. C. James Lin, D. H. Evans, Cytoplasmic factories, virus assembly, and DNA replication kinetics collectively constrain the formation of poxvirus recombinants. *PLoS One.* **15** (2020), doi:10.1371/JOURNAL.PONE.0228028.
88. Y.-C. J. Lin, J. Li, C. R. Irwin, H. Jenkins, L. DeLange, D. H. Evans, Vaccinia virus DNA ligase recruits cellular topoisomerase II to sites of viral replication and assembly. *J Virol.* **82**, 5922–32 (2008).
89. Y.-C. J. Lin, D. H. Evans, Vaccinia Virus Particles Mix Inefficiently, and in a Way That Would Restrict Viral Recombination, in Coinfected Cells. *J Virol.* **84**, 2432–2443 (2010).
90. P. Paszkowski, R. S. Noyce, D. H. Evans, Live-Cell Imaging of Vaccinia Virus Recombination. *PLoS Pathog.* **12**, e1005824 (2016).
91. B. Moss, Poxvirus DNA replication. *Cold Spring Harb Perspect Biol.* **5** (2013), doi:10.1101/cshperspect.a010199.
92. D. Stuart, K. Ellison, K. Graham, G. McFadden, In vitro resolution of poxvirus replicative intermediates into linear minichromosomes with hairpin termini by a virally induced Holliday junction endonuclease. *J Virol.* **66**, 1551–63 (1992).
93. A. D. Garcia, L. Aravind, E. v. Koonin, B. Moss, Bacterial-type DNA Holliday junction resolvases in eukaryotic viruses. *Proc Natl Acad Sci U S A.* **97**, 8926 (2000).
94. R. W. Moyer, R. L. Graves, The mechanism of cytoplasmic orthopoxvirus DNA replication. *Cell.* **27**, 391–401 (1981).
95. P. Dickie, A. R. Morgan, G. McFadden, Cruciform extrusion in plasmids bearing the replicative intermediate configuration of a poxvirus telomere. *J Mol Biol.* **196**, 541–558 (1987).

96. M. D. Challberg, P. T. Englund, Purification and Properties of the Deoxyribonucleic Acid Polymerase Induced by Vaccinia Virus*. *J Biol Chem.* **254**, 7812–7819 (1979).
97. P. Traktman, P. Sridhar, R. C. Condit, B. E. Roberts, Transcriptional mapping of the DNA polymerase gene of vaccinia virus. *J Virol.* **49**, 125–131 (1984).
98. M. W. Czarnecki, P. Traktman, The Vaccinia Virus DNA Polymerase and its Processivity Factor. *Virus Res.* **234**, 193 (2017).
99. W. F. McDonald, P. Traktman, Overexpression and purification of the vaccinia virus DNA polymerase. *Protein Expr Purif.* **5**, 409–421 (1994).
100. D. B. Gammon, D. H. Evans, The 3'-to-5' Exonuclease Activity of Vaccinia Virus DNA Polymerase Is Essential and Plays a Role in Promoting Virus Genetic Recombination. *J Virol.* **83**, 4236 (2009).
101. M. D. Hamilton, D. H. Evans, Enzymatic processing of replication and recombination intermediates by the vaccinia virus DNA polymerase. *Nucleic Acids Res.* **33**, 2259–2268 (2005).
102. E. Evans, N. Klemperer, R. Ghosh, P. Traktman, The vaccinia virus D5 protein, which is required for DNA replication, is a nucleic acid-independent nucleoside triphosphatase. *J Virol.* **69**, 5353–5361 (1995).
103. F. S. de Silva, W. Lewis, P. Berglund, E. v. Koonin, B. Moss, Poxvirus DNA primase. *Proc Natl Acad Sci U S A.* **104**, 18724–18729 (2007).
104. S. Kilcher, F. I. Schmidt, C. Schneider, M. Kopf, A. Helenius, J. Mercer, siRNA Screen of Early Poxvirus Genes Identifies the AAA+ ATPase D5 as the Virus Genome-Uncoating Factor. *Cell Host Microbe.* **15**, 103–112 (2014).
105. S. Hutin, W. L. Ling, A. Round, G. Effantin, S. Reich, F. Iseni, N. Tarbouriech, G. Schoehn, W. P. Burmeister, Domain Organization of Vaccinia Virus Helicase-Primase D5. *J Virol.* **90**, 4604–4613 (2016).
106. D. T. Stuart, C. Upton, M. A. Higman, E. G. Niles, G. McFadden, A poxvirus-encoded uracil DNA glycosylase is essential for virus viability. *J Virol.* **67**, 2503–2512 (1993).
107. N. Schormann, N. Zhukovskaya, G. Bedwell, M. Nuth, R. Gillilan, P. E. Prevelige, R. P. Ricciardi, S. Banerjee, D. Chattopadhyay, Poxvirus uracil-DNA glycosylase-An unusual member of the family I uracil-DNA glycosylases. *Protein Sci.* **25**, 2113–2131 (2016).
108. S. McKerr, L. HJohnston, M. Odell, S. ADuncan, K. MLaw, G. LSmith, S. William, Vaccinia DNA ligase complements *Saccharomyces cerevisiae* cdc9, localizes in cytoplasmic factories and affects virulence and virus sensitivity to DNA damaging agents. *EMBO J.* **10**, 4343–4350 (1991).
109. S. M. Err, G. L. Smith, Vaccinia virus DNA ligase is nonessential for virus replication: Recovery of plasmids from virus-infected cells. *Virology.* **180**, 625–632 (1991).
110. N. Paran, F. S. de Silva, T. G. Senkevich, B. Moss, Cellular DNA Ligase I Is Recruited to Cytoplasmic Vaccinia Virus Factories and Masks the Role of the Vaccinia Ligase in Viral DNA Replication. *Cell Host Microbe.* **6**, 563–569 (2009).
111. M. da Silva, L. Shen, V. Tcherepanov, C. Watson, C. Upton, Predicted function of the vaccinia virus G5R protein. *Bioinformatics.* **22**, 2846–2850 (2006).

112. W. F. McDonald, N. Klemperer, P. Traktman, A. York, N. York, Characterization of a Processive Form of the Vaccinia Virus DNA Polymerase compatible with processive DNA synthesis. The factors conferring processivity on a variety of viral. *Virology*. **234**, 168–175 (1997).
113. N. Klemperer, W. McDonald, K. Boyle, B. Unger, P. Traktman, The A20R protein is a stoichiometric component of the processive form of vaccinia virus DNA polymerase. *J Virol*. **75**, 12298–12307 (2001).
114. K. A. Boyle, E. S. Stanitsa, M. D. Greseth, J. K. Lindgren, P. Traktman, Evaluation of the role of the vaccinia virus uracil DNA glycosylase and A20 proteins as intrinsic components of the DNA polymerase holoenzyme. *J Biol Chem*. **286**, 24702–24713 (2011).
115. E. S. Stanitsa, L. Arps, P. Traktman, Vaccinia virus uracil DNA glycosylase interacts with the A20 protein to form a heterodimeric processivity factor for the viral DNA polymerase. *J Biol Chem*. **281**, 3439–3451 (2006).
116. K. A. Boyle, M. D. Greseth, P. Traktman, Genetic Confirmation that the H5 Protein Is Required for Vaccinia Virus DNA Replication. *J Virol*. **89**, 6312–6327 (2015).
117. N. E. Kay, T. W. Bainbridge, R. C. Condit, M. R. Bubb, R. E. Judd, B. Venkatakrisnan, R. McKenna, S. M. D’Costa, Biochemical and biophysical properties of a putative hub protein expressed by vaccinia virus. *Journal of Biological Chemistry*. **288**, 11470–11481 (2013).
118. M. D. Greseth, M. W. Czarnecki, M. S. Bluma, P. Traktman, Isolation and Characterization of vΔI3 Confirm that Vaccinia Virus SSB Plays an Essential Role in Viral Replication. *J Virol*. **92**, 1719–1736 (2018).
119. S. C. Rochester, P. Traktman, Characterization of the Single-Stranded DNA Binding Protein Encoded by the Vaccinia Virus I3 Gene. *J Virol*. **72**, 2917–2926 (1998).
120. M. D. Greseth, K. A. Boyle, M. S. Bluma, B. Unger, M. S. Wiebe, J. A. Soares-Martins, N. T. Wickramasekera, J. Wahlberg, P. Traktman, Molecular Genetic and Biochemical Characterization of the Vaccinia Virus I3 Protein, the Replicative Single-Stranded DNA Binding Protein. *J Virol*. **86**, 6197–6209 (2012).
121. M. L. Harrison, M. A. Desaulniers, R. S. Noyce, D. H. Evans, The acidic C-terminus of vaccinia virus I3 single-strand binding protein promotes proper assembly of DNA–protein complexes. *Virology*. **489**, 212–222 (2016).
122. M. Tseng, N. Palaniyar, W. Zhang, D. H. Evans, DNA binding and aggregation properties of the vaccinia virus I3L gene product. *Journal of Biological Chemistry*. **274**, 21637–21644 (1999).
123. F. S. de Silva, B. Moss, Origin-independent plasmid replication occurs in vaccinia virus cytoplasmic factories and requires all five known poxvirus replication factors. *Virol J*. **2**, 1–12 (2005).
124. S. Du, P. Traktman, Vaccinia virus DNA replication: Two hundred base pairs of telomeric sequence confer optimal replication efficiency on minichromosome templates. *Proc Natl Acad Sci U S A*. **93**, 9693–9698 (1996).

125. T. G. Senkevich, D. Bruno, C. Martens, S. F. Porcella, Y. I. Wolf, B. Moss, Mapping vaccinia virus DNA replication origins at nucleotide level by deep sequencing. *Proc Natl Acad Sci U S A.* **112**, 10908–10913 (2015).
126. H. Li, Y. Hwang, K. Perry, F. Bushman, G. D. van Duyne, Structure and Metal Binding Properties of a Poxvirus Resolvase. *J Biol Chem.* **291**, 11094 (2016).
127. X. Li, W. D. Heyer, Homologous recombination in DNA repair and DNA damage tolerance. *Cell Res.* **18**, 99–113 (2008).
128. D. H. Evans, Poxvirus Recombination. *Pathogens.* **11** (2022), doi:10.3390/PATHOGENS11080896.
129. M. R. Odom, R. Curtis Hendrickson, E. J. Lefkowitz, Poxvirus protein evolution: family wide assessment of possible horizontal gene transfer events. *Virus Res.* **144**, 233–249 (2009).
130. S. D. Ehrlich, H. Bierne, E. d'Alençon, D. Vilette, M. Petranovic, P. Noirot, B. Michel, Mechanisms of illegitimate recombination. *Gene.* **135**, 161–166 (1993).
131. G. Vallée, P. Norris, P. Paszkowski, R. S. Noyce, D. H. Evans, Vaccinia Virus Gene Acquisition through Nonhomologous Recombination. *J Virol.* **95** (2021), doi:10.1128/JVI.00318-21/SUPPL_FILE/JVI.00318-21-S0001.PDF.
132. M. J. Culyba, N. Minkah, Y. Hwang, O. M. J. Benhamou, F. D. Bushman, DNA branch nuclease activity of vaccinia A22 resolvase. *Journal of Biological Chemistry.* **282**, 34644–34652 (2007).
133. T. G. Senkevich, E. v. Koonin, B. Moss, Predicted poxvirus FEN1-like nuclease required for homologous recombination, double-strand break repair and full-size genome formation. *Proceedings of the National Academy of Sciences.* **106**, 17921–17926 (2009).
134. K. N. Kreuzer, Recombination-dependent DNA replication in phage T4. *Trends Biochem Sci.* **25**, 165–173 (2000).
135. M. M, Intramolecular homologous recombination in cells infected with temperature-sensitive mutants of vaccinia virus. *J Virol.* **63**, 2030–2035 (1989).
136. R. J. Colinas, R. C. Condit, E. Paoletti, Extrachromosomal recombination in vaccinia-infected cells requires a functional DNA polymerase participating at a level other than DNA replication. *Virus Res.* **18**, 49–70 (1990).
137. M. D. Hamilton, A. A. Nuara, D. B. Gammon, R. M. Buller, D. H. Evans, Duplex strand joining reactions catalyzed by vaccinia virus DNA polymerase. *Nucleic Acids Res.* **35**, 143–151 (2007).
138. D. O. Willer, M. J. Mann, W. Zhang, D. H. Evans, Vaccinia virus DNA polymerase promotes DNA pairing and strand-transfer reactions. *Virology.* **257**, 511–523 (1999).
139. F. Fenner, I. H. Holmes, W. K. Joklik, G. M. Woodroffe, Reactivation of Heat-inactivated Poxviruses : a General Phenomenon which includes the Fibroma–Myxoma Virus Transformation of Berry and Dedrick. *Nature 1959 183:4671.* **183**, 1340–1341 (1959).
140. W. K. Joklik, G. M. Woodroffe, I. H. Holmes, F. Fenner, The reactivation of poxviruses. I. Demonstration of the phenomenon and techniques of assay. *Virology.* **11**, 168–184 (1960).
141. F. Fenner, B. C.- Virology, undefined 1958, Genetic studies with mammalian poxviruses: I. Demonstration of recombination between two strains of vaccinia

- virus. *Elsevier* (available at <https://www.sciencedirect.com/science/article/pii/0042682258900436>).
142. L. K.-J. of the N. C. Institute, undefined 1958, Fibroma-myxoma virus transformations in different types of tissue culture. *academic.oup.com* (available at <https://academic.oup.com/jnci/article-abstract/20/4/729/1007581>).
 143. GP Berry - Proceedings of the American Philosophical Society, 1937, The transformation of the virus of rabbit fibroma (Shope) into that of infectious myxomatosis (Sanarelli). *JSTOR* (available at <https://www.jstor.org/stable/984774>).
 144. C. K. Sam, K. R. Dumbell, Expression of poxvirus DNA in coinfecting cells and marker rescue of thermosensitive mutants by subgenomic fragments of DNA. *Annales de l'Institut Pasteur / Virologie*. **132**, 135–150 (1981).
 145. F. Scheifflinger, F. Dorner, F. G. Falkner, Construction of chimeric vaccinia viruses by molecular cloning and packaging. *Proc Natl Acad Sci U S A*. **89**, 9977–9981 (1992).
 146. X.-D. Yao, D. H. Evans, High-Frequency Genetic Recombination and Reactivation of Orthopoxviruses from DNA Fragments Transfected into Leporipoxvirus-Infected Cells. *J Virol*. **77**, 7281–7290 (2003).
 147. X. D. Yao, D. H. Evans, Construction of recombinant vaccinia viruses using leporipoxvirus-catalyzed recombination and reactivation of orthopoxvirus DNA. *Methods Mol Biol*. **269**, 51–64 (2004).
 148. R. S. Noyce, S. Lederman, D. H. Evans, Construction of an infectious horsepox virus vaccine from chemically synthesized DNA fragments. *PLoS One*. **13**, e0188453 (2018).
 149. G. McFadden, A. Richard Morgan, DNA cruciform structures: Implications for telomere replication in eukaryotes and instability of long palindromic DNA sequences in prokaryotes. *J Theor Biol*. **97**, 343–349 (1982).
 150. A. D. Garcia, L. Aravind, E. v. Koonin, B. Moss, Bacterial-type DNA Holliday junction resolvases in eukaryotic viruses. *Proc Natl Acad Sci U S A*. **97**, 8926–8931 (2000).
 151. D. Stuart, K. Graham, M. Schreiber, C. Macaulay, G. McFadden, The target DNA sequence for resolution of poxvirus replicative intermediates is an active late promoter. *J Virol*. **65**, 61–70 (1991).
 152. L. Liu, T. Cooper, P. M. Howley, J. D. Hayball, From crescent to mature virion: vaccinia virus assembly and maturation. *Viruses*. **6**, 3787–808 (2014).
 153. P. Szajner, A. S. Weisberg, J. Lebowitz, J. Heuser, B. Moss, External scaffold of spherical immature poxvirus particles is made of protein trimers, forming a honeycomb lattice. *J Cell Biol*. **170**, 971–981 (2005).
 154. C. Risco, J. R. Rodríguez, C. López-Iglesias, J. L. Carrascosa, M. Esteban, D. Rodríguez, Endoplasmic reticulum-Golgi intermediate compartment membranes and vimentin filaments participate in vaccinia virus assembly. *J Virol*. **76**, 1839–1855 (2002).
 155. L. Maruri-Avidal, A. S. Weisberg, B. Moss, Direct Formation of Vaccinia Virus Membranes from the Endoplasmic Reticulum in the Absence of the Newly Characterized L2-Interacting Protein A30.5. *J Virol*. **87**, 12313 (2013).

156. A. S. Weisberg, L. Maruri-Avidal, H. Bisht, B. T. Hansen, C. L. Schwartz, E. R. Fischer, X. Meng, Y. Xiang, B. Moss, Enigmatic origin of the poxvirus membrane from the endoplasmic reticulum shown by 3D imaging of vaccinia virus assembly mutants. *Proc Natl Acad Sci U S A*. **114**, E11001–E11009 (2017).
157. B. Unger, J. Mercer, K. A. Boyle, P. Traktman, Biogenesis of the vaccinia virus membrane: genetic and ultrastructural analysis of the contributions of the A14 and A17 proteins. *J Virol*. **87**, 1083–1097 (2013).
158. T. Betakova, E. J. Wolffe, B. Moss, Regulation of vaccinia virus morphogenesis: phosphorylation of the A14L and A17L membrane proteins and C-terminal truncation of the A17L protein are dependent on the F10L kinase. *J Virol*. **73**, 3534–3543 (1999).
159. H. Bisht, A. S. Weisberg, P. Szajner, B. Moss, Assembly and disassembly of the capsid-like external scaffold of immature virions during vaccinia virus morphogenesis. *J Virol*. **83**, 9140–9150 (2009).
160. L. Maruri-Avidal, A. Domi, A. S. Weisberg, B. Moss, Participation of vaccinia virus I2 protein in the formation of crescent membranes and immature virions. *J Virol*. **85**, 2504–2511 (2011).
161. L. Maruri-Avidal, A. S. Weisberg, H. Bisht, B. Moss, Analysis of viral membranes formed in cells infected by a vaccinia virus L2-deletion mutant suggests their origin from the endoplasmic reticulum. *J Virol*. **87**, 1861–1871 (2013).
162. W. Resch, A. S. Weisberg, B. Moss, Vaccinia virus nonstructural protein encoded by the A11R gene is required for formation of the virion membrane. *J Virol*. **79**, 6598–6609 (2005).
163. X. Wu, X. Meng, B. Yan, L. Rose, J. Deng, Y. Xiang, Vaccinia virus virion membrane biogenesis protein A11 associates with viral membranes in a manner that requires the expression of another membrane biogenesis protein, A6. *J Virol*. **86**, 11276–11286 (2012).
164. P. S. Satheshkumar, A. Weisberg, B. Moss, Vaccinia virus H7 protein contributes to the formation of crescent membrane precursors of immature virions. *J Virol*. **83**, 8439–8450 (2009).
165. X. Meng, A. Embry, L. Rose, B. Yan, C. Xu, Y. Xiang, Vaccinia virus A6 is essential for virion membrane biogenesis and localization of virion membrane proteins to sites of virion assembly. *J Virol*. **86**, 5603–5613 (2012).
166. M. C. Cassetti, † Michael Merchlinsky, E. J. Wolffe, A. S. Weisberg, B. Moss, DNA Packaging Mutant: Repression of the Vaccinia Virus A32 Gene Results in Noninfectious, DNA-Deficient, Spherical, Enveloped Particles. *J Virol*. **72**, 5769–5780 (1998).
167. B. Unger, P. Traktman, Vaccinia Virus Morphogenesis: A13 Phosphoprotein Is Required for Assembly of Mature Virions. *J Virol*. **78**, 8885–8901 (2004).
168. O. Grubisha, P. Traktman, Genetic analysis of the vaccinia virus I6 telomere-binding protein uncovers a key role in genome encapsidation. *J Virol*. **77**, 10929–42 (2003).
169. C. Morgan, S. A. Ellison, H. M. Rose, D. H. Moore, Serial sections of vaccinia virus examined at one stage of development in the electron microscope. *Exp Cell Res*. **9**, 572–578 (1955).

170. M. Hollinshead, A. Vanderplasschen, G. L. Smith, D. J. Vaux, Vaccinia virus intracellular mature virions contain only one lipid membrane. *J Virol.* **73**, 1503–1517 (1999).
171. R. C. Condit, N. Moussatche, P. Traktman, In a nutshell: structure and assembly of the vaccinia virion. *Adv Virus Res.* **66**, 31–124 (2006).
172. K. L. Roberts, G. L. Smith, Vaccinia virus morphogenesis and dissemination. *Trends Microbiol.* **16**, 472–9 (2008).
173. M. Law, G. L. Smith, Antibody neutralization of the extracellular enveloped form of vaccinia virus. *Virology.* **280**, 132–142 (2001).
174. A. Vanderplasschen, E. Mathew, M. Hollinshead, R. B. Sim, G. L. Smith, Extracellular enveloped vaccinia virus is resistant to complement because of incorporation of host complement control proteins into its envelope. *Proc Natl Acad Sci U S A.* **95**, 7544–7549 (1998).
175. N. Klemperer, J. Ward, E. Evans, † And, P. Traktman, The vaccinia virus I1 protein is essential for the assembly of mature virions. *J Virol.* **71**, 9285–9294 (1997).
176. J. DeMasi, S. Du, D. Lennon, P. Traktman, Vaccinia Virus Telomeres: Interaction with the Viral I1, I6, and K4 Proteins. *J Virol.* **75**, 10090–10105 (2001).
177. E. v. Koonin, T. G. Senkevich, V. I. Chernos, Gene A32 product of vaccinia virus may be an ATPase involved in viral DNA packaging as indicated by sequence comparisons with other putative viral ATPases. *Virus Genes 1993 7:1.* **7**, 89–94 (1993).
178. L. M. Iyer, K. S. Makarova, E. v. Koonin, L. Aravind, Comparative genomics of the FtsK–HerA superfamily of pumping ATPases: implications for the origins of chromosome segregation, cell division and viral capsid packaging. *Nucleic Acids Res.* **32**, 5260–5279 (2004).
179. T. Salmons, A. Kuhn, F. Wylie, † Sibylle Schleich, J. R. Rodriguez, D. Rodriguez, M. Esteban, G. Griffiths, J. Krijnse Locker, Vaccinia virus membrane proteins p8 and p16 are cotranslationally inserted into the rough endoplasmic reticulum and retained in the intermediate compartment. *J Virol.* **71**, 7404–7420 (1997).
180. G. C. Katsafanas, B. Moss, Colocalization of transcription and translation within cytoplasmic poxvirus factories coordinates viral expression and subjugates host functions. *Cell Host Microbe.* **2**, 221–228 (2007).
181. S. E. Smallwood, M. M. Rahman, D. W. Smith, G. McFadden, *Curr Protoc Microbiol*, in press, doi:10.1002/9780471729259.MC14A01S17.
182. G. J. Kotwal, M. R. Abrahams, Growing poxviruses and determining virus titer. *Methods Mol Biol.* **269**, 101–112 (2004).
183. M. Zuker, Mfold web server for nucleic acid folding and hybridization prediction. *Nucleic Acids Res.* **31**, 3406–3415 (2003).
184. M. M. Shenouda, R. S. Noyce, S. Z. Lee, J. L. Wang, Y. C. Lin, N. A. Favis, M. A. Desaulniers, D. H. Evans, The mismatched nucleotides encoded in vaccinia virus flip-and-flop hairpin telomeres serve an essential role in virion maturation. *PLoS Pathog.* **18** (2022), doi:10.1371/JOURNAL.PPAT.1010392.

185. J. L. Baker, B. M. Ward, Development and comparison of a quantitative TaqMan-MGB real-time PCR assay to three other methods of quantifying vaccinia virions. *J Virol Methods*. **196**, 126–132 (2014).
186. A. Vanderplasschen, G. L. Smith, A novel virus binding assay using confocal microscopy: demonstration that the intracellular and extracellular vaccinia virions bind to different cellular receptors. *J Virol*. **71**, 4032–4041 (1997).
187. W. Mitsuhashi, K. Miyamoto, S. Wada, The complete genome sequence of the Alphaentomopoxvirus *Anomala cuprea* entomopoxvirus, including its terminal hairpin loop sequences, suggests a potentially unique mode of apoptosis inhibition and mode of DNA replication. *Virology*. **452–453**, 95–116 (2014).
188. J. Schindelin, I. Arganda-Carreras, E. Frise, V. Kaynig, M. Longair, T. Pietzsch, S. Preibisch, C. Rueden, S. Saalfeld, B. Schmid, J. Y. Tinevez, D. J. White, V. Hartenstein, K. Eliceiri, P. Tomancak, A. Cardona, Fiji: an open-source platform for biological-image analysis. *Nature Methods* 2012 9:7. **9**, 676–682 (2012).
189. T. L. Geurs, E. B. Hill, D. M. Lippold, A. R. French, Sex Differences in Murine Susceptibility to Systemic Viral Infections. *J Autoimmun*. **38**, J245 (2012).
190. C. C. Blackburn, C. L. Augustine, R. Li, R. P. Harvey, M. A. Malin, R. L. Boyd, J. F. A. P. Miller, G. Morahan, The nu gene acts cell-autonomously and is required for differentiation of thymic epithelial progenitors. *Proc Natl Acad Sci U S A*. **93**, 5742 (1996).
191. G. C. Bosma, R. P. Custer, M. J. Bosma, A severe combined immunodeficiency mutation in the mouse. *Nature*. **301**, 527–530 (1983).
192. G. C. Bosma, M. T. Davisson, N. R. Ruetsch, H. O. Sweet, L. D. Shultz, M. J. Bosma, The mouse mutation severe combined immune deficiency (scid) is on chromosome 16. *Immunogenetics*. **29**, 54–57 (1989).
193. J. Wang, P. Dong, W. Wu, X. Pan, X. Liang, High-throughput thermal stability assessment of DNA hairpins based on high resolution melting. *J Biomol Struct Dyn*. **36**, 1–13 (2018).
194. E. M. Moody, P. C. Bevilacqua, Thermodynamic Coupling of the Loop and Stem in Unusually Stable DNA Hairpins Closed by CG Base Pairs. *J. AM. CHEM. SOC*. **125**, 2032–2033 (2003).
195. E. M. Kane, S. Shuman, Vaccinia virus morphogenesis is blocked by a temperature-sensitive mutation in the I7 gene that encodes a virion component. *J Virol*. **67**, 2689–2698 (1993).
196. C. M. Byrd, T. C. Bolken, D. E. Hruby, The vaccinia virus I7L gene product is the core protein proteinase. *J Virol*. **76**, 8973–8976 (2002).
197. R. W. Fisher, J. L. Reed, P. J. Snoy, M. G. Mikolajczyk, M. Bray, D. E. Scott, M. C. Kennedy, Postexposure Prevention of Progressive Vaccinia in SCID Mice Treated with Vaccinia Immune Globulin. *Clin Vaccine Immunol*. **18**, 67 (2011).
198. S. Coulibaly, P. Brühl, J. Mayrhofer, K. Schmid, M. Gerencer, F. G. Falkner, The nonreplicating smallpox candidate vaccines defective vaccinia Lister (dVV-L) and modified vaccinia Ankara (MVA) elicit robust long-term protection. *Virology*. **341**, 91–101 (2005).
199. L. H. McCurdy, J. A. Rutigliano, T. R. Johnson, M. Chen, B. S. Graham, Modified Vaccinia Virus Ankara Immunization Protects against Lethal Challenge

- with Recombinant Vaccinia Virus Expressing Murine Interleukin-4. *J Virol.* **78**, 12471–12479 (2004).
200. L. S. Wyatt, P. L. Earl, L. A. Eller, B. Moss, Highly attenuated smallpox vaccine protects mice with and without immune deficiencies against pathogenic vaccinia virus challenge. *Proc Natl Acad Sci U S A.* **101**, 4590–4595 (2004).
 201. A. Gonzilez, A. Talavera, J. " M. Almendral, E. Vinuela, Hairpin loop structure of African swine fever virus DNA. *Nucleic Acids Res.* **14** (1986) (available at <https://academic.oup.com/nar/article/14/17/6835/1036080>).
 202. Y. Zhang, P. Strasser, R. Grabherr, J. L. van Etten, Hairpin loop structure at the termini of the chlorella virus PBCV-1 genome. *Virology.* **202**, 1079–1082 (1994).
 203. E. Costello, R. Sahli, B. Hirt, P. Beard, The mismatched nucleotides in the 5'-terminal hairpin of minute virus of mice are required for efficient viral DNA replication. *J Virol.* **69**, 7489–7496 (1995).
 204. N. Zhi, Z. Zádori, K. E. Brown, P. Tijssen, Construction and sequencing of an infectious clone of the human parvovirus B19. *Virology.* **318** (2004), doi:10.1016/j.virol.2003.09.011.
 205. L. M. Iyer, L. Aravind, E. v. Koonin, Common Origin of Four Diverse Families of Large Eukaryotic DNA Viruses. *J Virol.* **75**, 11720–11734 (2001).
 206. H. A. M. Mönttinen, C. Bicep, T. A. Williams, R. P. Hirt, The genomes of nucleocytoplasmic large DNA viruses: viral evolution writ large. *Microb Genom.* **7** (2021), doi:10.1099/MGEN.0.000649.
 207. M. E. Perkus, S. J. Goebel, S. W. Davis, G. P. Johnson, E. K. Norton, E. Paoletti, Deletion of 55 open reading frames from the termini of vaccinia virus. *Virology.* **180**, 406–410 (1991).
 208. K. Burles, C. R. Irwin, R. L. Burton, J. Schriewer, D. H. Evans, R. M. Buller, M. Barry, Initial characterization of Vaccinia Virus B4 suggests a role in virus spread. *Virology.* **456–457**, 108–120 (2014).
 209. J. B. Reus, E. A. Rex, D. B. Gammon, How to Inhibit Nuclear Factor-Kappa B Signaling: Lessons from Poxviruses. *Pathogens 2022, Vol. 11, Page 1061.* **11**, 1061 (2022).